# A COMPUTATIONAL FLUID DYNAMICS STUDY OF THE NEAR SURFACE WIND PATTERNS OVER A DESERT DUNE AND THE EFFECT ON SEED DISPERSION

by

Eugéne Christiaan Joubert

Thesis presented in partial fulfilment of the requirements for the degree
Master of Science in Engineering at the University of Stellenbosch
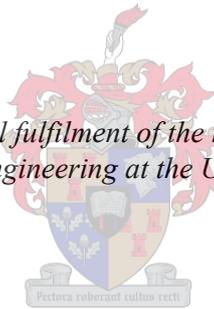
Supervisor: Prof. Thomas Michael Harms
Department of Mechanical and Mechatronic Engineering

March 2010

DECLARATION

I, Eugéne Christiaan Joubert, the undersigned, hereby declare that the work contained in this report is of my original work and I have not, in its entirety or in part, submitted it at any other university for a degree.

……………………….. ………………………..

Signature   Date

i

ACKNOWLEDGEMENTS

ABSTRACT

This project originated when a team of scientists at the Gobabeb training and research and centre observed seed accumulation sites on the slope of sand dunes in the Namib Desert. Seeds that accumulate on the slip face of a sand dune provide food for small desert creatures that in turn attract larger animals, resulting in a small ecosystem on the side of the dune. Since wind is the primary transport of seeds throughout the Namib Desert it is of interest to investigate wind patterns over the dune. In this project it is therefore desired to look at seed dynamics and deposition as a result of near surface wind patterns around a three-dimensional dune geometry using computational fluid dynamics. The project is a joint venture between the University of Stellenbosch and the University of Namibia. This document presents the South African MScEng thesis part.

The literature review shows the dominant winds in the Namib Desert to be from the south to westerly direction. Previous studies on air flow over dunes focussed on sand movement and were often limited to simplified two-dimensional geometries and steady state simulations. From these studies the basic flow features associated with dunes can be identified. Lastly, factors that influence particle dynamics around dune geometries are looked at. These particle studies mostly involve the movement of sand rather than seeds but still provide valuable insight.

The project methodology is explained and includes the equipment used, the considerations taken into account, the simplifications made as well as the procedure followed when conducting field work and simulations. A section of an actual Namibian linear dune is mapped in order to obtain a geometry for the simulations. Flow measurements are carried out with a wind mast to obtain velocity profile inlet conditions for the simulations. Furthermore, seed sampling is done by the collaborating Namibian team of which the data is used to obtain an effective seed particle model. Lastly, simulations are carried out using primarily OpenFOAM-1.5. The simulations look at general near surface wind patterns, time dependant flow features and particle movement and seed deposition around and on the linear dune.

The results show different wind profiles for different wind direction. It is also possible to see how the profile changes as the flow accelerates up the dune slope. Two-dimensional results provide the opportunity to compare results with previous studies as well as to provide the basis for looking at aspects such as differencing schemes, turbulence models and parallel computing before three-dimensional simulations are carried out. The importance of higher order differencing schemes are confirmed in the two-dimensional results. The turbulence models, however, produce very similar results. The results from the two- and three-dimensional results show typical flow features associated with dunes. Transient flow features and separation vortex structures can be identified from time dependant simulations. Furthermore, particle simulations reveal how particles tend to be trapped in the recirculation regions.

The conclusions explain how the project objectives were achieved and provide recommendations for future studies related to this project.

iii

OPSOMMING

Die projek het ontstaan toe naforsers areas van saad akumulasie op die hellings van duine in Namibë opgelet het. Hierdie akumulasie van plant materiaal verskaf die voedsel vir klein diere op die duin wat 'n klein ekosisteem tot gevolg het. Aaangesien die primêre vervoermiddel vir sade in die woestyn wind is beoog die projek om deur die wind patrone oor die duin beter te verstaan die saad verspreiding te beskryf. Die doel is dus om saad verspreiding en akumulasie te beskryf deur die wind patrone te bekyk wat die verspreiding tot gevolg het deur gebruik te maak van numeriese vloei dinamika. Die projek is 'n saamgestelde projek tussen die Universiteit van Stellenbosch en die Universiteit van Namibië. Hierdie dokument behels die Suid Afrikaanse MScIng gedeelte van die projek.

Deur die hersiening van literatuur word daar gesien dat die domineerende wind rigtings as suid tot wes beskryf kan word. Vorige studies wat verband hou met wind vloei oor duine wys dat die meeste op twee-dimensionele eenvoudige geometrië gefokus het met tyd onafhankike simulasies. Dit is egter moontlik om die resultate te gebruik om karakteristieke vloei patrone te identifiseer wat met duin wind patrone geassosieer kan word. Laastens word daar gekyk na die faktore wat partikel beweeging beïnvloed, maar hierdie studies sluit hoofsaaklik sand partikels in eerder as sade.

Die motodologie beskryf die toerusting, oorwegings en prosedures wat gevolg is tydens veld werk asook simulasies. Tydens die veld werk is 'n gedeelte van 'n Namib lineêre duin gemeet en so gebruik om 'n geometrie te maak wat vir simulasie doeleindes gebruik kan word. Daar is ook wind meetings gedoen met 'n wind mas om wind profiele vir inlaat kondisies vir die simulasies te kry. Verder het saad bestudeering die nodige data verskaf om 'n voledige saad partikel model op te stel wat in die simulasies gebruik kan word. Laastens kyk die simulasies veral na algemene vloei patrone, tyd afhanklike vloei effekte en ook partikel beweging in die vloei veld.

Die resultate wys hoe wind profiele verskil wat van verskillende rigtings af waai. Dit is ook moontlik on te wys hoe die wind profiele verander soos die wind versnel teen die duin op. Twee-dimensionele simulasies verskaf die geleentheid om te kyk na die effek van verkillende numeriese modelle, turbulensie modelle en ook multi-prosesseerder verwerking. Tydens die twee-dimensionele simulasies is die belangrikheid van hoër orde numeriese metodes besef. Die verkillende turbulensie modelle het egter klein verkille gewys. Alby die twee- en drie-dimensionele resultate wys karakteristieke vloei patrone wat met duine geasosieer kan word. Verder het tyd afhanklike simulasies gewys hoe wind patrone verander met tyd. Die partikel simulasies wys ook die beweging van partikels deur die wind en hoe dit neig om te akumuleer in die hersirkulasie gebied agter die duin.

Die gevolgtrekkings wys dat al die doelstellings bereik is en maak voorstelle vir toekomstige studies wat met hierdie studie verband hou.

TABLE OF CONTENT

LIST OF FIGURES

LIST OF TABLES

LIST OF SYMBOLS

α	Angle
ε	Turbulent kinetic energy dissipation rate
θ	Absolute temperature
κ	Von Karman constant
ν	Kinematic viscosity
ρ	Fluid density
σ_ε	Constant of the standard k-ε model
τ	Flow shear stress
τ_w	Wall shear stress
ω	Specific dissipation rate
$C_{\varepsilon 2}$	Constant of the standard k-ε model
$C_{\varepsilon 1}$	Constant of the standard k-ε model
C_μ	Constant of the standard k-ε model
$^\circ$	Degrees
g	Gravitational constant
k	Turbulent kinetic energy
k_s	Sand-grain roughness height
m	Seed particle mass
n	Sample size
Q	Second invariant of the velocity gradient tensor
R_μ	Viscosity ratio
R_{iB}	Bulk Richardson number
s	Distance of fall
t	Time duration of fall
u	Velocity (Particle fall rate)
U	Mean free-stream velocity
u^*	Friction velocity of the wall-function
u^*_{ABL}	Friction velocity of atmospheric boundary layer
u^+	Dimensionless variable for boundary layer analysis
y^+	Dimensionless variable for boundary layer analysis
y_p	Distance from the centre point to the wall of the cell adjacent to the wall
z_0	Atmospheric terrain roughness length

LIST OF ABREVIATIONS

ABL	Atmospheric boundary layer
CAE	Computer aided engineering
CFD	Computational fluid dynamics
FD	Finite difference
FE	Finite element
FV	Finite volume
GPS	Global positioning system
GUI	Graphical user interface
LES	Large eddy simulation
NRF	National Research Foundation
OpenFOAM	Open field operation and manipulation
PISO	Pressure-implicit with splitting of operators
RANS	Reynold-averaged Navier-Stokes
RNG	Renormalized group
SADC	Southern African Development Community
SD	Standard deviation
SGS	Sub-grid scale
SIMPLE	Semi-implicit method for pressure linked equations
STL	Stereolithography
VTK	The Visualisation ToolKit

1. INTRODUCTION

1.1 Project Motivation

Researchers stationed in the Namib Desert have observed how seeds and plant material collect near the crest of dune slip faces. The plant material originates primarily from grassy plants on and between the dunes. The seeds and plant material serve as food for insects. The insects then attract larger animals to form a small ecosystem. Considering the seed morphology, discussed in section 3.3.1, which shows large wing like flight appendages, it is clear that wind is the primary source of transport. However, exactly how the wind causes the seeds to collect in the specific locations is a mystery. This motivated the creation of a project to study the near surface wind patterns over a linear dune and how seeds get transported in the Namib Desert.

A further motivation for such a study was provided when rains in the Namib Desert caused grass to grow from seed collection areas. The grass presented a rare opportunity to study seed collection areas that were already covered with sand. An interesting observation was that the collection areas occurred in rows along the length of the dune, not in pools, and also at some distance up the slope rather than at the foot of the dune slope.

Dr. Joh Henschel and Prof. Thomas Harms proposed a project consisting of two teams which are sponsored by the National Research Foundation (NRF) Southern African Development Community (SADC) division. The South African team is responsible for the computational fluid dynamics (CFD) work and the Namibian team responsible for the ecological research associated with the project. The motivation to do a dual project is to promote collaboration as well as sharing of scientific data and experience between researchers.

The work conducted by the two teams forms the bases of two MSc projects. The work contained within this document represents South African MSc student's work. The South African team consists of Mr. Eugéne Joubert (author) and Prof. Thomas Harms (supervisor). The Namibian team is Ms. Annethea Muller, Dr. Joh Henschel and Dr. Martin Hipondoka.

Figure 1: Grass on dune slip face (Muller, 2008)

1

1.2   Project Description

The proposed project is the study of the near surface wind patterns over a linear dune as found near Gobabeb training and research centre in Namibia. The location of Gobabeb in Namibia can be seen in Figure 53 in Appendix A. The study aims to investigate how the wind patterns over the dune may influence where seeds are deposited. The thesis focuses principally on the educated use of CFD software to describe the wind patterns and particle movement that occurs.

In this project it is decided to simulate the air flow over the actual dune topography. This requires a three-dimensional model of the dune. Since no dune models are available a surface has to be constructed manually. The process involves collecting topography data and which is then used to create a three-dimensional surface of the actual dune.

In order to achieve inlet conditions for the simulations wind data of the atmospheric boundary layer (ABL) is needed. To gather wind data a wind-mast is used. The wind mast is 10 m long with sensors evenly distributed. Sensors on the mast include air temperature, speed and direction. The data is transmitted to a data logger, which stores the data until it can be downloaded to a computer for further processing. The wind mast can be placed in strategic positions so that the data can later be analysed.

In this report, general background for the thesis project is given as well as the motivation for the project. Furthermore, this report states the objectives set out for the project as well as explaining the approach that was followed in order to achieve the objectives set within the given time available. Lastly, this report elaborates in detail on the results achieved from the different field measurements as well as modelling and simulation results.

1.3   Project Objectives

- Perform a literature review that focuses on project related topics in the field of fluid dynamics.

- Do wind measurements for the purpose of providing inlet conditions describing the ABL.

- Conduct a three-dimensional simulation of air flow over the actual sand dune.

- Use open source software like OpenFOAM for meshing and simulations.

- Do some transient simulations of air flow over the actual dune implementing a large eddy simulation (LES) turbulence model.

- Run a number of simulations on the faculty cluster.

- Collaborate with the Namibian team by exchanging information and observation and assistance with regards to the wind patterns and seed dynamics for the benefit of both projects.

2. LITERATURE REVIEW

Previous studies are important to lay a foundation for this project as well as to provide guidelines on how to approach the problems we face in this project. In this chapter previous and current research related to the project is reviewed. The aim of this chapter is to discuss the findings of the previous studies and to explain how these studies influence the research for this project. Furthermore, the existing work may be used to support the motivation for performing this study as well as how this study is approached.

The content of the literature discussed in this chapter starts with some of the history regarding wind patterns of the Namib Desert. From there the research regarding the formation of linear dunes and the effect they have on the wind patterns is discussed. Furthermore, specific attention is paid to previous studies related to the use of CFD for environmental flows and the use of an ABL model.

2.1   Surface Winds of The Namib Desert

Understanding the dominant winds of the Namib Desert is important to the project due to the influential role they play in shaping the landscape as well as distribution of plant species. According to Lancaster *et al.* (1984) the dominant winds of the Namib Desert can be grouped into three directions. These three wind groups are seasonal specific and can be described as a northerly to westerly occurring from December to February, an easterly to north-easterly occurring from May to August and a southerly to south-south-westerly occurring from September to November. Of the three groups the winds from the westerly to south-south-westerly directions occur the most frequent and represent 16 – 40 % of all winds recorded. These winds correspond to see breezes which occur due to the high thermal contrast between the cold ocean current and warmer land surface.

From this review it is seen that the dune field experience a number of different wind directions. Studying the effect of all of these wind directions falls outside the scope of this project. It is decided to simulate only a westerly wind direction which will strike the linear dunes perpendicularly and simplify the simulation in this way. The westerly wind direction is common in the summer months and will also provide insight into the easterly wind which will result in similar flow features only in the opposite direction.

2.2   Linear Dune Research

A previous study of great relevance to the project discussed in this report was done by Livingstone (1985). Livingstone did a study on linear dunes near the Gobabeb training and research centre by looking at flow patterns as well as dune profile changes over seasons. In order to observe the change in dune profiles Livingstone had to document the vertical changes in sand surfaces relative to iron poles on the dune. In later years he used a differential global positioning system (GPS) to map the dune profiles and compare them to profiles of the same site documented from previous dates. In the study he also looked at the wind patterns with the use of smoke flares and wind anemometers.

One of the main question regarding linear dunes is why the dunes are stationary. From his studies Livingstone (1985) concluded that the wind patterns, consisting mainly of south-westerly winds in the summer and easterly winds in the winter, cause the sand to travel parallel to the dune crest. This is different to transverse dunes near the coast that experience south-westerly winds for most of the year and as a result the sand travels in a northerly direction up the coast. The sand particles at Gobabeb, however, travel all the way to the Kuiseb River, where they are flushed away by occasional floods.

A similar study on linear dunes was done by Tsoar (1978). In the study the focus was on wind patterns as well as dune profile changes due to seasonal variations in wind conditions. Tsoar (1978) specifically looked at wind pattern characteristics around linear dunes in terms of separation regions, velocity profiles and streamlines. In the study he noticed, using smoke flares, how flow that approaches the dune crest at an oblique angle forms helical streamlines on the lee side. Another observation from his study is the highly unsteady nature of the wind in the dunes and the constant movement of lee side eddies.

Although the studies done by Livingstone (1985) and Tsoar (1978) were done some time ago they are still relevant to the current study since both looked at the wind patterns around linear dunes where most other investigations regarded the more common transverse dunes. The study by Livingstone (1985) is especially relevant to the project since he looked at the dunes near the Gobabeb training and research centre where the study presented in this document was also conducted.

The work presented differs from the work done by Livingstone (1985) and Tsoar (1978) by making use of CFD. The wind is simulated over a region of the dune making it possible to visualise the near surface wind patterns over a three-dimensional area rather than one transverse section. However, the characteristics observed from the simulations may be compared to those which Livingstone (1985) and Tsoar (1978) discovered during their studies. It should be noticed that the majority of previous studies focussed on air flow over dunes and effect on sand transportation. This work takes previous research into account but at the same time focuses on how the wind transports seeds rather than sand.

2.3   Application of CFD to Environmental Flows

In the past wind characteristics were predominantly investigated by visualisation methods, full scale measurements or in some cases measurements in wind tunnels on scaled models. Since the increase in computational power in recent years, CFD is starting to have a greater impact on the discipline of fluid mechanics (Kim and Boysan, 1999). CFD is especially helpful for situations where knowledge is necessary of the flow patterns over complex geometries or places where measurements are imposing and sometimes even impossible. Despite the recent advances in CFD, modelling wind effects still present several challenges.

One such challenge is the difficulty in modelling the ABL with sufficient detail and accuracy needed for CFD simulations. To carry out environmental flow modelling sufficient knowledge of the ABL is required (Kim and Boysan, 1999). Not only is the mean wind speed data important but also the atmospheric turbulence data which relates to wind gusts in the flow stream. Turbulence data of adequate detail, needed in CFD modelling, is often difficult to obtain since

meteorological weather stations usually measure wind with only one anemometer and this data is usually averaged over time. One anemometer only gives data for a certain point in the atmosphere rather than a profile. The velocity profile data required for simulation boundary conditions is therefore often not available or insufficient.

Another major difficulty is the fact that atmospheric flows are highly three-dimensional (Kim and Boysan, 1999). The flows are also accompanied by strong streamline curvature, separation and in some places unsteadiness. The effects mentioned here are often difficult to observe when doing steady state simulations. To visualise the flow unsteadiness associated with gusts and vortices therefore require transient simulations which further increase the computational time.

Furthermore, there is the challenge of discretizing the complex topography with enough detail to include large as well as small scale flow patterns (Kim and Boysan, 1999). This large and small scale flow features are especially found in atmospheric flow environments. The large and small scale flow patterns are usually vortices of different sizes and characteristics. These vortices represent areas of high vorticity magnitude. The vorticity magnitude is usually highest in boundary layers and recirculation zones. In these regions viscous effects are especially important (Kim and Boysan, 1999). The viscous effects are important since they transport momentum energy across the flow field and therefore the mesh needs to be of sufficient resolution in these regions.

Discretizing the flow domain more finely in some areas than in others can pose some challenges when using structured meshes. Structured meshes often result in great amount of mesh being wasted in regions where small mesh resolution is not needed (Kim and Boysan, 1999). The development of CFD for unstructured meshes addresses the wasted mesh resolution problem. Unstructured meshes also make it possible to apply cells with arbitrary shape, which in turn facilitates meshing of very complex geometries.

Discretizing the computational domain involves compromising between accuracy or detail and computational resources. This compromise may sometimes be difficult to find. To address this problem unstructured meshing has an additional advantage in that it conveniently provides a framework for local mesh refinement. Local mesh refinement reduces the number of cells needed since refinement can be done only where necessary. Local mesh refinement therefore reduces the computational resources needed while maintaining accuracy and detail.

Another aspect to look at for environmental flows is to take into account the effect of eddies in the flow by using a turbulence model. The turbulent eddies cause a mixing effect on the flow since they transport energy across the flow mean stream lines. Understanding this mixing effect of turbulence is important since turbulent flows are far more common in engineering applications than laminar flows (Versteeg and Malalasekera, 2008). Some turbulence models perform better for certain flows than others. Because the flow around bluff bodies are often highly unsteady and three-dimensional makes it is difficult to choose a turbulence model that would best fit all types of flows encountered (Kim and Boysan, 1999).

Of the many turbulence models available the original k-ε model presented by Launder and Spalding (1974), also known as the standard k-ε model, is still favoured in the aerodynamic industry for its simplicity, robustness and reasonable accuracy (Mikkel and Livesey, 1995).

5

However, the conventional k-ε model has built in disadvantages due to the isotropic eddy viscosity hypothesis which form the core of the model equations. Some disadvantages include poor performance in flows where strong anisotropy is present. Other problems with the standard k-ε model are the poor performance with stagnation flows as well as the high generation of turbulent kinetic energy. The large turbulent kinetic energy in turn increases the turbulent eddy viscosity in the region of the stagnation zone which is transported downstream and has the potential to suppress flow separation (Kim and Boysan, 1999).

The disadvantages of the standard k-ε model prompted the pursuit for better alternatives. Some alternatives to the standard k-ε model include the renormalization group (RNG) and the realizable k-ε models. Kim and Boysan (1999) investigated the performance of the RNG k-ε model and realizable k-ε model relative to the standard k-ε model for bluff-body aerodynamics. Although both RNG and realizable models cannot fully resolve the overproduction of k, both have features to greatly reduce the problem. It was found that both RNG and realizable models greatly improve the results especially the realizable model.

The work done by Kim and Boysan (1999) is of interest to the project discussed in this report since it provides certain insights for environmental flow modelling especially the important aspect of turbulence modelling. It is of interest to do simulations implementing the three k-ε based turbulence models to see how they compare. From the work by Kim and Boysan (1999) the realizable k-ε model is chosen for more detailed simulations. However, the limitations of the RANS are noted and therefore it is decided that LES turbulence models will also be considered.

2.4   Large Eddy Simulation Turbulence Modelling

As mentioned in a previously section, turbulence is associated with eddies in the flow field that cause a mixing effect across the flow streamlines. These eddies occur in a range of different sizes and characteristic. Small eddies are isotropic (non-directional) and have universal behaviour. Furthermore, small scale eddies are primarily responsible for dissipating energy and can therefore be modelled successfully by a turbulent viscosity to resemble this dissipating effect.

Large eddies on the other hand are anisotropic (directional) and are responsible for transporting momentum across the flow field. Large eddies are also greatly affected by the geometry and other boundary conditions. Due to the difference in behaviour for small and large eddies, developing a general-purpose turbulence model poses a difficult task (Versteeg and Malalasekera, 2008). For example, the widely used k-ε based models, which are based on the isotropic eddy viscosity hypothesis, are not able to resolve large eddies. The necessity therefore exits for a turbulence model that is able to reproduce large eddies in the flow field.

Generally the smaller eddies are that have to be resolved, the finer the mesh has to be. Therefore, greater computational resources are necessary. Furthermore, additional complex differential equation have to be solved to include these eddies numerically. It is this high demand on computational resources that motivates the modelling of eddies as a turbulent viscosity instead of the complex differential equations. However, due to the advances in computational power and improved understanding of the behaviour different types of eddies allows for more complex turbulence models to be developed and implemented more effectively. Existing turbulence

models can be categorised into three main categories according to size to which eddies in the flow are resolved. This is depicted in Figure 2 (Bagleito, 2009).
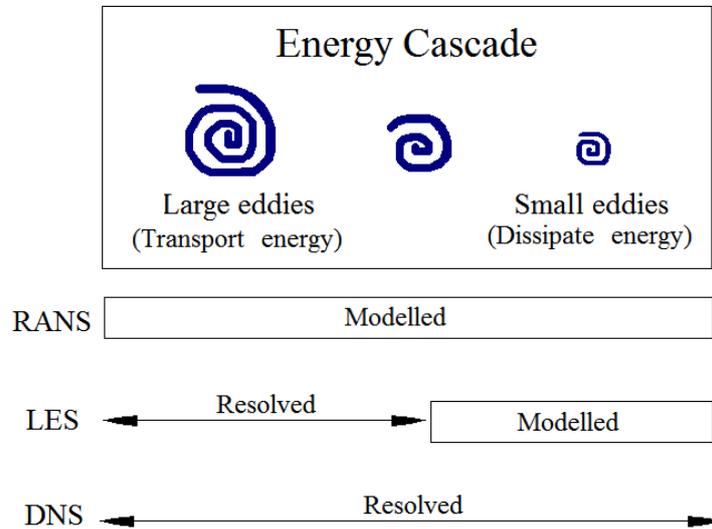
Figure 2: Turbulence modelling in relation to the energy cascade

The first category is the RANS models that model the entire spectrum of eddies as a turbulent viscosity that resembles the dissipative and transportation effects. The second group is LES turbulence models which model small scale eddies and resolves larger eddies by using filtering equations to filter out the small eddies. Lastly, direct numerical simulation (DNS) models resolves the whole spectrum of eddies.

As mentioned previously LES turbulence models were developed where the governing equations contain the effects of filtered-out small eddies on the resolved eddies. The filtered out small eddies are represented in terms of so called sub-grid-scale (SGS) stresses similar to that of the RANS models. Two popular groups of SGS models are the algebraic and differential models. An example of an algebraic model is the Smagorinsky model. The Smagorinsky model is one of the first developed SGS models and is based the assumption that the small scale eddies are in equilibrium and therefore dissipate entirely and instantaneously all the energy received from the larger resolved scale eddies (De Villiers, 2006). This assumption, however, reduces the accuracy of the Smagorisky model when flow strays from equilibrium. According to De Villiers (2006) non-equilibrium conditions commonly arise in flows associated with separation, reattachment, boundary layers and wall dominated flows. This makes the Smagorinsky SGS model ill suited for the dune simulations where separation, reattachment and boundary layer flows are expected to be present.

A simple differential model also considered is the one-equation SGS model. The one-equation SGS model is also based on the eddy-viscosity concept but solves for a transport property on which the eddy viscosity depends as well (De Villiers, 2006). This added feature of the one-equation SGS models has been shown to make it superior to algebraic models in flows associated

with unsteadiness (Fureby *et al.*, 1997). Furthermore, the one-equation models takes into account non-equilibrium effects (De Villiers, 2006) which makes it attractive for this study.

On the other hand LES also has its drawbacks. LES is still very expensive in terms of computational resources since it usually requires very fine grid resolution (Hanjalić and Kenjereš, 2008). Furthermore, LES simulations are usually transient which further increases the computational resources required.

Despite the fact that LES is an expensive turbulence model, it can be very useful for studying flow physics, vortices structures and turbulence for simple structures and low Reynolds numbers. According to Hanjalić and Kenjereš (2008) LES can be seriously considered as a complementary resource for studying wind engineering.

It can be summarised that LES poses the opportunity to study the effect of large scale eddies in the flow which is not possible with RANS turbulence models. For this reason it is of interest to this project to use LES to look at the large eddies in the flow patterns over the dunes. It is, however, noted that using LES will increase the computational resources required since the LES is associated with finer meshes as well as transient simulations. The increased computational resources therefore limited the number of LES simulations conducted.

2.5   Atmospheric Boundary Layer Modelling

In order to achieve accurate and reliable results for the atmospheric flow patterns it is important to model the ABL (Blocken *et al.*, 2007) with sufficient detail. The ABL is represented in CFD simulations by implementing fully developed flow profiles of mean wind speed and turbulence at the inlet. Fully developed flow profiles means that the flow is horizontally homogeneous and therefore no streamwise gradients exist. Therefore, the flow profiles are maintained with downstream distance.

In considering modelling the ABL as stable one thing to be kept in mind is how the hot desert surface influence the flow. Hot surfaces have a potential to destabilize the ABL due to the formation of air plumes. Since air plumes shear off irregularly, they contribute to the unsteady nature of atmospheric flows. The effect of hot air plumes should be considered for this project since on some days the Namib Desert surface could reach 70 ˚C. Considering the stability of the ABL there are a number of ways to determine the significance of this destabilising effect. One way is by using the bulk Richardson number R_{iB} with the following equation (Sharan *et al.*, 2003):

$$R_{iB} = \frac{g(\theta - \theta_0)(z - z_0)}{\theta U^2}$$
(2.1)

In equation (2.1) g is the gravitational acceleration, θ is the absolute temperature, z is the vertical distance and U the free-stream flow velocity. The $_0$ subscript refers to the location of the parameter on the ground where the flow velocity is considered zero. For stable conditions the

8

bulk Richardson number is restricted to values of $R_{iB}<0.2$ (Sharan *et al.*, 2003). From this equation it is possible to see that if the flow velocity is high, the ABL will be more stable. Furthermore, if the temperature difference is large, the flow will be more unstable.

From an investigation of the data measured from using a wind mast, discussed in section 3.2, the ABL was found to be stable even during the hottest time of the day. This is due to the relatively high wind velocities experienced in the field that overpowers the buoyancy effect of hot air plumes. Furthermore, since seed dispersion occurs specifically when the wind velocities are high and not only during the day but at night as well, this motivates modelling the ABL without simulating the effect of a heated surface temperature. This decision is supported since in numerous literature reviews considering ABL modelling no references regarding the surface temperature was found. Furthermore since the inlet conditions for the simulations are from measured data collected in the field, it is possible to say that the inlet conditions already account for buoyancy affects. The inlet conditions and measurement equipment are discussed in section 3.

In order to model an ABL that is realistic, the profiles should be representative of the roughness characteristics of the terrain upstream of the inlet. The surface roughness is accounted for by a parameter called the atmospheric terrain roughness length y_0. The surface roughness length takes into account the effect of plants and other obstacles that might be present on the terrain. This parameter is also very important for maintaining the velocity profile downstream of the inlet. The surface roughness value can be obtained or compared to the Davenport classification of aerodynamic terrain roughness length in Table 5 of Appendix B.

Since the ABL is represented by flow profiles at the inlet, equations for these profiles would be needed. Richards (1989) proposed equations that could be implemented with the k-ε based turbulence model. The equations include the mean wind speed U, turbulent kinetic energy k and the turbulence dissipation rate ε. The ABL profiles proposed by Richards (1989) are based on the Harris and Deaves (1981) model. It should be noted that the turbulent kinetic energy is constant with height. This assumption is possible since the computational domain is often lower than the ABL height (Richards and Hoxey, 1993). The profiles can be expressed by the following equations:

$$U(y) = \frac{u^*_{ABL}}{\kappa} \ln\left(\frac{y+y_0}{y_0}\right) \tag{2.2}$$

$$k(y) = \frac{u^*_{ABL}{}^2}{\sqrt{C_\mu}} \tag{2.3}$$

$$\varepsilon(y) = \frac{u^*_{ABL}{}^3}{\kappa(y+y_0)} \tag{2.4}$$

9

$$\kappa^2 = (C_{\varepsilon2} - C_{\varepsilon1})\sigma_\varepsilon \sqrt{C_\mu} \tag{2.5}$$

In the equations given above u^*_{ABL} is the ABL friction velocity, κ is the Von Karman constant and y is the vertical distance from the ground (Blocken *et al.*, 2007). Also, $C_{\varepsilon2}$, $C_{\varepsilon1}$, σ_ε and C_μ are constants of the standard k-ε model. The value for u^*_{ABL} can be determined so that for the initial simulation, a specific reference wind speed for a specific height is obtained (Briggen *et al.*, 2009). Also, the value for y_0 can be estimated by visually inspecting the terrain and then using the updated Davenport surface roughness classification as proposed by Wieringa (1992) which is provided in Table 5 in Appendix B. With some modifications the equations given above can also be used to define ABL profiles for simulations using different Reynold-averaged Navier-Stokes (RANS) turbulence models.

Based on the work conducted by Blocken *et al.* (2007) it is possible to implement a stable ABL. This can be done by applying turbulent flow profiles at the inlet boundary as presented by equations (2.2) to (2.5). The flow profiles can also be converted for use with other RANS turbulence models like the k-ω SST and the Spalart-Allmaras models should it be desired. Furthermore, it is desired to comply with the requirements mentioned in order to ensure homogenous ABL throughout the flow field.

2.6   Air Flow Over Idealized Transverse Dune

There have been numerous studies concerning air flow and sediment transport over transverse aeolian dunes. Parsons *et al.* (2004a) conducted such a study of the flow over an idealized transverse dune to address the limitations from previous studies. According to Parsons *et al.* (2004a) limitations from previous studies include technical shortcomings of wind tunnel instrumentation, lack of appropriate turbulence instrumentation, limited number of field sites for studying dune flow-form interaction and the lack of appropriate numerical models that are able to reproduce all flow features found around dunes. In addition to the numerical simulations Parsons *et al.* (2004a) carried out wind tunnel measurements over a scaled dune model.

According to Parsons *et al.* (2004a) CFD is beginning to play an increasingly important role in the studying of fluvial processes. The development of numerical models to simulate fluvial processes has provided scientists with the greater insight into the fluid processes and their significance. Parsons *et al.* (2004a) mention that CFD complements the work done in laboratories and in the field and often provides the capability to study fluid processes in places where traditional methods for measuring and observation is limited or impossible.

To simulate the flow over the idealized two-dimensional dune Parsons *et al.* (2004a) decided to implement the RNG k-ε model as proposed by Yakhot *et al.* (1992). The reason for implementing the RNG k-ε model was its good performance for simulating flows involving considerable shear. Studies by Bradbrook *et al.* (1998) have confirmed the good performance of the RNG k-ε model for re-circulating flows over a backward facing step. Furthermore, flow profiles were implemented at the inlet of the computational domain and the law-of-the-wall was

10

used on the wall boundaries. From the results Parsons *et al.* (2004a) concluded that the turbulence model performed satisfactory for the flow over the dune in general. The model was also capable of successfully reproducing the separation zone.

A number of key flow features were identified from simulation results carried out by Parsons *et al.* (2004a). Flow approaching the dune toe on the windward side experiences increasing pressure as the flow decelerates. A deceleration of approximately 20 % relative to unaffected flow is observed. From this region of high pressure the flow accelerates up the dune slope towards the crest where the maximum velocity occurs. The flow overshoots from the crest resulting in separated flow due to the rapid change in dune slope. The separation zone is characterised by recirculation, low velocity, low pressure and turbulent kinetic energy generation in the regions of high shear (velocity gradients). Furthermore, from the results it was seen that even though reattachment occurs within 3-15 dune heights, flow boundary layer recovery takes much longer (Parsons *et al.*, 2004b). Therefore, due to the limitations in computational resources it is difficult to simulate flow over a dune with complete boundary layer recovery on the lee.

The simulations conducted by Parsons *et al.* (2004a) are relevant to the project discussed in this report since they also looked at turbulent flow over a sand dune with the help of CFD. In the study a number of flow characteristics were identified that would be important to identify in the current analysis. Parsons *et al.* (2004a) chose to use the RNG k-ε turbulence model since it was reported to have good performance reproducing flows of high shear and recirculation (separation zones). Furthermore, Parsons *et al.* (2004a) complemented the model by stating that the turbulence model performed adequately in the prediction of separation.

The difficulty of doing field measurements of the flow over an actual linear dune can be expensive in terms of equipment, time and travel expenses. The dunes are often in remote locations and harsh climates, therefore, requiring specialized equipment. Even constructing a three-dimensional scale model for wind tunnel measurements could prove tedious and costly. Therefore it is decided to use CFD to gain better insight of the flow patterns over the dune. In this way the flow over the entire dune can be visualised rather than with individual locations only as suggested with traditional methods like smoke flares and wind tunnel measurements. This observation is reinforced by Parsons *et al.* (2004a) who conclude that CFD helps to provide a more complete picture of the flow field oppose to wind tunnel and field measurements alone. It should be noted that the numerical results should be verified for which field measurement data will be used. Most of these studies, however, were only investigated in two dimensions.

The difference between the work of Parsons *et al.* (2004a) and that of this project is the switch from two-dimensional to three-dimensional simulations. Also, the simulations conducted in this study involve an actual dune. Furthermore, the dunes considered in the work of Parsons *et al.* (2004a) are transverse dunes where the ones studied in this report are linear. There is also a substantial difference in dune geometries when comparing transverse and linear dunes. Firstly, linear dunes are usually larger than transverse dunes. Secondly, linear dunes are for most part stationary whereas transverse dunes are not. Lastly, it was observed that where transverse dunes have sharp angle slip-faces, linear dunes on the other hand have relatively similarly angle slopes on both sides.

2.7   Particle Transport over Dunes

A number of studies have looked at the complex relationship between the ABL and dune morphology (eg. Tsoar 1978, 1983). From literature there are a number of contributing factors that influence particle transport in the vicinity of a sand dune. One factor is streamwise flow acceleration which causes particles to be swept up and transported along the surface. Watson (1987), however, proposed that comparing shear stress at a point to the sand transport at that point would be more useful than comparing velocities alone since shear stresses are responsible for forces on the particles.

More recent studies by Wiggs *et al.* (1996), however, suggested that surface shear stresses are induced by streamwise acceleration as well as streamline curvature. Streamlines indicate the path that an air molecule will take as it moves over the geometry and therefore near surface tend to follow the shape of the geometry. For simulation of wind over a dune, concave streamlines are likely to occur at the toe of the windward slope of the dune. On the other hand convex streamlines are more likely to exist in the upper part of the dune near the crest. In Figure 3 the dune is displayed with streamline curvature and velocity profiles indicated.
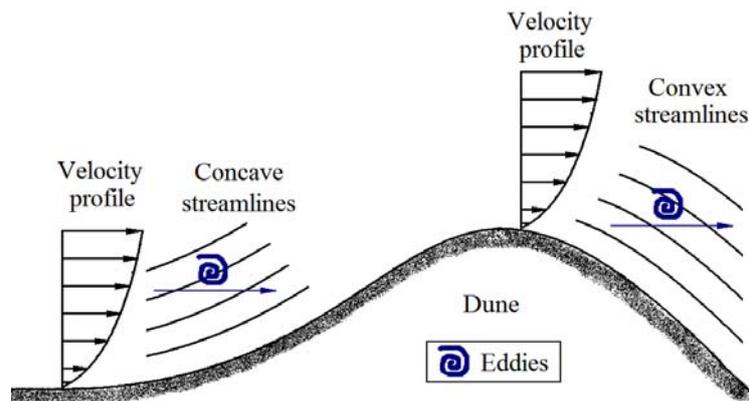
Figure 3: Effect of streamline curvature

Concave streamline suggest that the flow paths curve upward in the windward direction where convex streamlines curve downward as shown in Figure 3. Concave streamline curvature promotes unstable flow by transporting turbulent eddies from high to low velocity regions due to the curvature (Wiggs *et al.*, 1996). Similarly convex streamline curvature has the opposite effect since it moves turbulence from low to high velocity regions. Furthermore, concave streamline curvature tends to increase shear stress, τ, where convex streamline curvature decreases it. The rate of influence differs for concave and convex curvature though. The rate at which concave curvature influences the flow is delayed where the impact of flow acceleration and convex streamline curvature is instantaneous (Wiggs *et al.*, 1996).

Since concave streamline curvature occurs at the dune toe it is suspected that the shear stress would be greater in this region. Wiggs *et al.* (1996) provided evidence for this flow destabilization by doing wind tunnel measurements and observing higher turbulence intensities in the toe region. Furthermore, Wiggs *et al.* (1996) showed low turbulent mixing in the upper part

of the dune and near the crest which corresponds to convex streamline curvature. Wiggs *et al.*, (1996) concluded that curvature characteristic contribute the majority of shear stress generation in the toe region.

According to Wiggs *et al.* (1996) flow deceleration found at the dune toe is important to sand transport dynamics. Deceleration of the flow implies sand deposition. This, however, was not observed. In the study it was mentioned that sand transport rates increase progressively as the flow moves up the windward slope (Wiggs *et al.*, 1996). The sand transport reaches a maximum near the crest from where the rate of transport dramatically decreases.

The significance of streamline curvature lies in the presence of shear stresses that result from concave curvature near the toe region. The additional shear stresses have the effect of maintaining sand transport rates in spite of the flow deceleration observed. If streamline curvature would be ignored, sand deposition would be expected at the dune toe, which is not the case for field measurements with sand traps.

Finally Wiggs *et al.* (1996) proposes a new model for sand transport on the windward slope af a sand dune that includes both effects of streamwise acceleration and streamline curvature. The model presented takes concave curvature and streamwilse acceleration as increasing the shear stress and therefore sand transport rate. On the other hand convex streamline curvature and flow deceleration has the opposite effect in decreasing shear stress in the flow and therefore sand transport rates. At the toe sand transport is maintained due to the presence of shear stresses induced by concave streamline curvature. At the steepest part of the dune slope, concave curvature and flow acceleration work together to maximise erosion. Further up the slope, convex curvature and streamline deceleration occurs resulting in sand deposition at the crest. Deposition will occur until the convex curvature and flow deceleration is changed to concave curvature and flow acceleration. This causes erosion and the cycle continues.

In the work by Wiggs *et al.* (1996) particle transportation is a one of the key topics which makes it relevant to the work presented in this report. In the work the importance of streamline curvature was explained. Furthermore, a new model for sand transport was suggested incorporating both effects of streamline curvature as well as streamwise acceleration. Both streamline curvature as well as streamwise acceleration visualisation is possible in CFD. These tools make it possible to study the flow patterns and relate it to the work by Wiggs *et al.* (1996). From understanding the importance of the different flow patterns valuable insight into particle transportation could be gained when the CFD results are analysed. One observation regarding linear dunes is the low angle of both windward and lee-side slopes. This would reduce the flow deceleration at the toe and flow acceleration and streamline curvature on the windward slope further, supporting the stability of the linear dunes.

3. METHODOLOGY

In the field of CFD there are a number of numerical methods used. Of these methods the most widely known and implemented methods are the finite difference (FD), finite element (FE) and the finite volume (FV) methods. According to De Villiers (2006) the FD is known for its accuracy but is limited to simple cases because of its requirement of body fitted coordinates in some cases. The FE method maintains a high order of accuracy and is free of the limitation faced by the FD method. However, the FE method does not inherently guarantee that the conservation laws are satisfied which is of great importance in fluid dynamics.

The FV method on the other hand satisfies the conservation laws inherently due to the integral formulation and can now be employed for very complex geometries. The FV method therefore offers a desired level of compromise between flexibility and accuracy and is generally accepted to be the most widely used numerical method in fluid dynamics. For this project the FV method will be used throughout.

In this chapter the approach followed throughout the project is explained. The chapter starts with explaining the creation of the simulation domain through dune mapping as well as discretization of the simulation domain by creating a FV mesh. From there the numerical model used for simulations is explained as well as the implementation of it. Furthermore, the different simulations conducted as well as the wind measurements procedures are described. Lastly, the project limitations as well as parallel computing system and considerations are mentioned.

3.1 Simulation Domain Creation Methodology

To do simulations of the air flow over the dunes a FV mesh is needed for computations. The mesh is formed by discretizing the flow domain. Discretization in this context refers to the division of the volume into small sub-entities called control volumes. All the control volumes combined therefore represent the atmosphere flow space above the dune. The simulation domain is bounded on all sides. The bottom boundary of the volume will be the surface of an actual linear dune found at Gobabeb.

At the time of the study there were no existing dune models of sufficient accuracy and resolution to create a FV mesh from. It was decided to create a surface mesh by mapping a dune. The procedure and equipment are explained later in this section. For the purposes of this study the dune surface is assumed as stationary and unchanging. This assumption is valid since the dunes at Gobabeb have been observed to be stationary for over 50 years. Furthermore, no significant changes in the dune position could be observed for the two year duration of the study, further supporting the assumption.

Apart from the dune migration, what does occur is a slight change in the shape of the dune faces due to seasonal change in the dominant wind directions. The change in wind direction usually results in the crest being moved a meter or two while the majority of the dune stays unchanged. Since the dunes reach 100 m high at the crest, the change in the shape is small in relation to the size of the dune. It should be kept in mind that the objective of this study is not to look at the dune dynamics due to sand movement but rather the near surface wind patterns as affected by the

dune geometry and the affect this has on seed transportation. Therefore the dune is considered stationary and unchanging.

In this section the process of creating the final simulation domain is explained. The process from the site selection, equipment, dune mapping, geometry creation and manipulation is described.

3.1.1 The site location to conduct field work

For the project the field work involved creating a dune map as well as doing some field measurements of wind profiles. For the dune mapping and wind measurements a study site is needed. The study site should represent the typical dune geometry and air flow patterns found in the Namib Sand Sea to make it applicable to larger areas. Dunes found on the edge of the dune field, however, are of different shapes and sizes in comparison to the ones found deeper into the sand sea. The reason for this shape dissimilarity is due to altered wind conditions experienced on the outer edge of the sand sea. For this reason the dunes closest to the research facility were judged ill suited for the study.

The location of the site was chosen so that the air flow would represent the typical wind conditions experienced in the dune field but at the same time be close enough to the research facility so that it would be regularly accessible for equipment transport and data collection. The site chosen for the study can be seen in Figure 4. It should be noticed that the site includes one linear dune and some of the flat planes on either side. These flat planes are called interdunes. The site is approximately 1000 m long and 200 m wide.
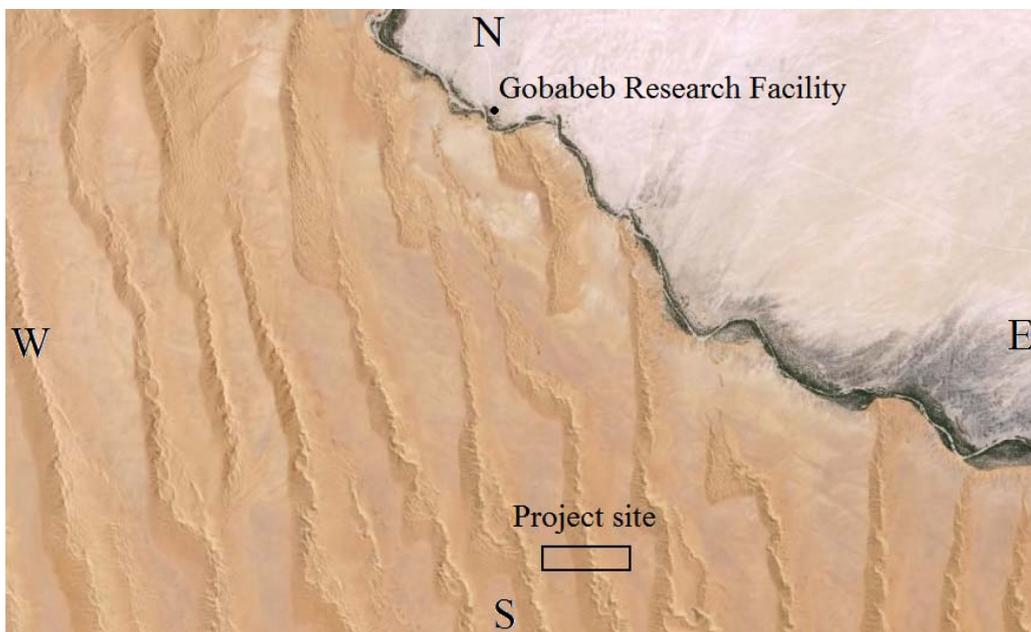
Figure 4: The outline of the project dune site (Google Earth, 2009)

It can be seen from Figure 4 and Figure 5 that the dune selected for the study has a typical linear dune shape and size. The choice of site is primarily motivated by the wind pattern expected due

15

to the size and spacing of the neighbouring dunes. The dune chosen for the project is flanked on both sides by linear dunes of approximately the same size and spacing. Therefore, the site is expected to be influenced equally from both sides. More importantly the neighbouring dunes ensure that flow patterns at the site would resemble that found even deeper into the dune field where similar sized dunes are found with similar spacing apart. The study should therefore be relevant for a larger area than if a unique dune were to be chosen such as is found on the outer perimeter of the sand sea.

Figure 5: Side view of the dune site (looking south)

Due to the sheer size of the dune and the limitation of only being able to access the dune during limited times of the day made it possible to only map a section of the dune. The region chosen for mapping was selected to include typical geometrical features observed throughout the linear dunes. In this way the applicability of the study to other areas of the Namib Desert is improved even further. A further benefit of mapping a portion of the dune that resembles similar geometrical features on the same dune is that it makes it possible to enlarge the surface model by duplication and stitching the sections together. This process is explained later in this section.

3.1.2 Dune mapping equipment

To map the dune a few processes were considered. These processes include three-dimensional surface reconstruction from satellite photos, aerial photos, existing contour maps or point clouds generated by using a differential GPS. The aerial photos and contour maps methods were rejected since at the time no up to date photos or maps with sufficient resolution were available and it would have been too expensive to get a photo taken of the site. On the other hand the differential GPS provided sufficient accuracy, appeared simple to use and was available at the Gobabeb training and research centre. Furthermore, the differential GPS has been used in the past to generate profile maps of the linear dunes (Livingstone, 1985). The differential GPS can be seen in Figure 55 in Appendix D. In Appendix D the GPS setup considerations as well as accuracy specifications are given.

The GPS takes the readings from different satellites including some for azimuth and calculates the position average as well as variance in the readings. The more satellites received, the greater the weight of the positioning. This variance reading helps the user to distinguish between readings where more satellites agreed or disagreed on the position giving the user freedom to judge the accuracy of each measurement taken. It is important to note that the position given and weight is not reflective of the actual position but rather that agreement of the different satellites.

16

Although satellites have built in errors which limit the accuracy this method was deemed sufficient for the purposes of this project. Other errors for example, the change in dune shape due to wind forces or numerical errors, may play a significantly greater role than the errors due to GPS readings.

3.1.3 Dune mapping procedure

As mentioned previously, a three-dimensional model of the actual dune surface is required in order to construct a FV mesh which will then be used for simulation purposes. The surface is constructed from a point cloud that is mapped by using a differential GPS and documenting the coordinates as well as elevation every few steps. The first task is to develop a mapping scheme. Due to the sheer size and complexity of the dune the mapping process will take long to do since the person has to walk every curve with the GPS in order to capture it. The mapping scheme is necessary to ensure sufficient accuracy and resolution while restricting the domain to allow completion within the time available in this project.

Dr. Schreve, who is an expert in surface modelling at the Department of Mechanical and Mechatronic Engineering at Stellenbosch University in South Africa, was approached to suggest a possible mapping scheme. Dr. Schreve suggested contour mapping which would support the surface generation process. From the advice received from Dr. Schreve it was decided to map the dune by doing a combination of transverse and contour sections. Transverse sections refer to mapping by walking a line perpendicular to the crest. Contours refer to walking a line parallel to the crest. To get a better idea of the mapping process there may be referred to Figure 56 in Appendix D.

During a visit to Gobabeb the dune site was studied and the different dune faces were identified and marked with posts. The posts served as a basic grid for the mapping procedure. Each dune face was mapped with the differential GPS and the data downloaded and stored on the laptop. The mapping process was repeated to improve resolution in the regions where this was considered necessary.

3.1.4 Dune surface generation

As soon as the point cloud is generated, as explained in dune mapping procedure, the points are in directional format of longitude, latitude and altitude. Longitude and latitude are given in degrees and minutes and altitude is given by meters. The data has to be converted to distances. The data conversion is done with the values in Table 1 which shows the distance of a degree, minute and second for the location of the earth where the mapping is conducted. An additional requirement is that the coordinates have to be adjusted for the degrees south from the Equator as well as the degrees east of the Greenwich line. To adjust the values they are multiplied by $\cos(\alpha)$, where α is the angle in degrees from the Equator or the Greenwich meridian.

Table 1: Coordinate conversion coefficients

Coordinate unit	Distance at equator
1 degree	111200 m
1 minute	1853 m
1 second	30.9 m

Once the data is converted to absolute distances it is also necessary to change the point cloud reference point from global to local. Global coordinates indicate the distance of the dune south of the Equator and east of the Greenwich line. Local coordinates, however, gives the dune shape arbitrarily of its position on earth. The reference frame will therefore only include the data of interest.

Following the data conversion and translation as explained in preceding paragraphs it is possible to view the point cloud in tree-dimensions with the help of a program called TerrainCAD (Sycode, 2009). Three-dimensional visualization presents the opportunity to check the quality of the point cloud. The cloud can be inspected for outlying or overlaying points. The three-dimensional feature also allows the point cloud to be compared to the actual dune. The point cloud is presented in Figure 6.
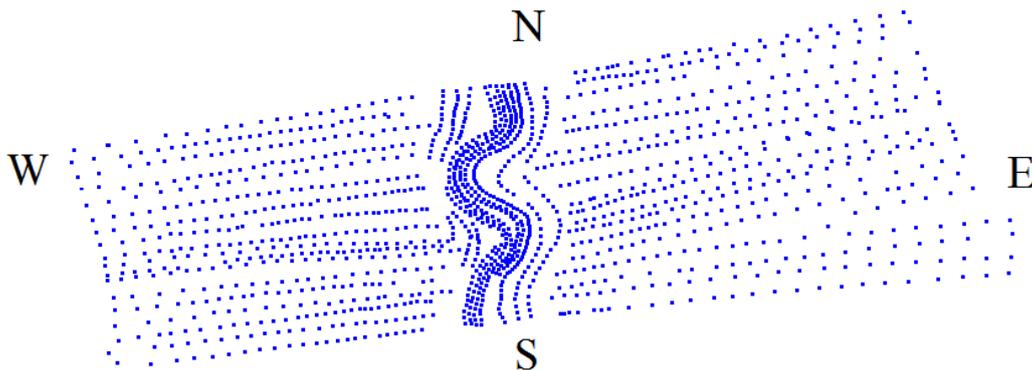
Figure 6: Point cloud of mapped dune geometry

In Figure 6 the point cloud can be seen from above. The transverse sections are visible where clear lines are formed by the points during the mapping process. Furthermore, the contour mapped section is clearly noticeable near the crest where the lines resemble the curvature of the dune faces. The point cloud density corresponds to the level of curvature in the region. The quality of the point cloud is improved by removing duplicated or overlaying points such as the areas where transverse as well as contour mapping were implemented. Further improvements include the removing of outlying points as well as points with low confidence levels.

From the point cloud a rough surface is generated. The surface is displayed in Figure 7. The sharp edges occur because of GPS errors and have to be smoothed before any mesh construction can take place. The surface that is generated consists of a number of small triangular surfaces and is stored in stereolithography (STL) format.

18
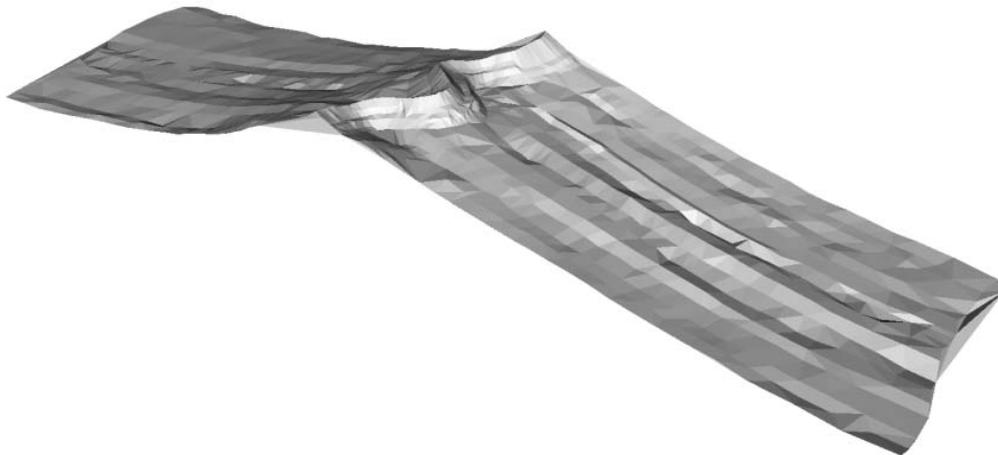
Figure 7: Dune surface constructed from point cloud

By studying the surface in Figure 7 it can be noticed how the GPS readings varied in height for the different transverse sections. This error is expected since the least accurate function of a GPS is the altitude metering capability. It calculates the altitude from satellites close to the horizon. Only a small number are usually visible at a time and within a few minutes it is very possible that one might disappear behind a mountain or other obstacle further hampering the altitude metering capability. This problem of altitude satellite reception is especially present while working in an environment with high obstacles such as the linear dunes. The result is many delays during dune mapping which is already limited by the climate in the Namib Desert. The delays restrict the size of the domain to be mapped as well as the resolution to be achieved. Even though the errors are considerable it is judged that the errors that results from the GPS and smoothing are within the acceptable accuracy for the scope of this project.

Another modification to the dune surface was to duplicate the point cloud and stitching them together. The reason for increasing the dune surface size is to make a larger simulation area available. The larger dune surface will make simulating angled wind directions possible allowing for more flow development. It is for this purpose of enlarging the dune surface by duplication that the site was selected to contain a section of dune that is typical to linear dunes and repeated throughout the Namib Desert. The duplicated point cloud can then be used to generate a surface similarly to that of the smaller cloud explained in previous paragraphs. The enlarged rough surface can be seen in Figure 57 in Appendix D.

The final dune surface is refined near the crest region to improve smoothing weights. More nodes near the crest help to include more features after refinement. The smoothing is done by shifting vertices to a more central position relative to the nodes around it. Another way to describe it is to say that the nodes are shifted so that the angle between the lines joining nodes on all sides is reduced. The peaks are flattened in this way. To prevent large features from disappearing during smoothing the mesh is smoothed mainly on flat plain areas and less near the crest. The final dune surface can be seen in Figure 8. In Figure 8 the surface can be seen with the triangulated surface mesh displayed in Gmsh (2009).

19
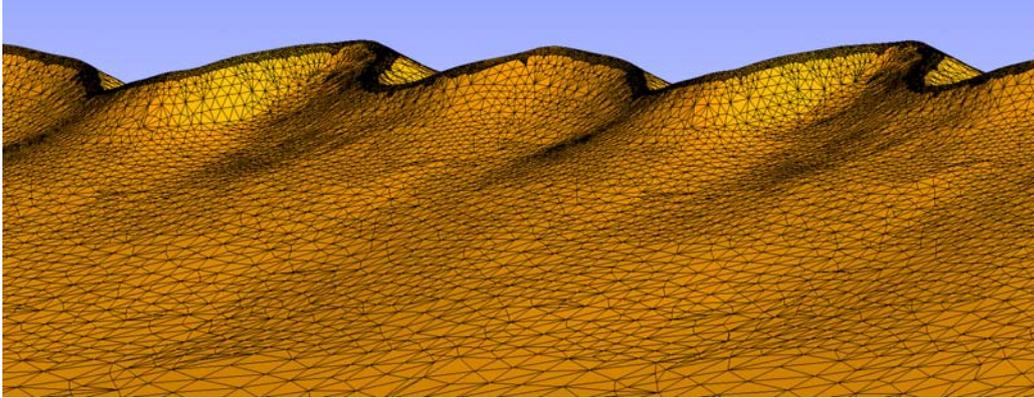
Figure 8: Final dune surface

The modelled surface can be compared to a typical linear dune in the field. This comparison can be seen in Figure 9. The comparison shows the modelled surface relates well to the actual surface as well as some in the vicinity. The general features are visible in both the model and the actual dune. The regions where the modelled dune surface differs from the actual dune is judged acceptable considering the scope of this project. This comparison supports the choice of the dune site as well as mapping and modelling techniques used.

Figure 9: Dune comparison: a) modelled dune and b) actual dune

3.1.5   Simulation domain mesh generation

The next step would be to generate the FV mesh where the flow will be calculated. To generate the mesh a number of different meshing software were considered. The open source software

20

considered includes Gmsh (2009), enGrid (enGits, 2009) and a built in automatic meshing utility in OpenFOAM-1.5 (OpenCFD, 2009). Of the volume meshing tools considered enGrid meshes are built up of tetrahedral and prism layer cells. This makes it possible to mesh very complex geometries but less attractive when considering numerical accuracies. On the other hand OpenFOAM-1.5 uses a cut hexahedral meshing tool which is also capable of meshing complex geometries but does not suffer from numerical inaccuracies as much as tetrahedral cells. It is also possible do meshing on a parallel environment with OpenFOAM-1.5 which is attractive considering the size of the domain. Therefore, of the open source meshing tools considered OpenFOAM-1.5 was chosen. The cut hexahedral meshing utility in OpenFOAM-1.5 is called snappyHexMesh (OpenCFD, 2009).

SnappyHexMesh is used to generate unstructured meshes in OpenFOAM for complex geometries. Although unstructured meshes are more costly than structured meshes on a cell by cell bases they allow for local mesh refinement as well as the use of arbitrarily shaped cells. Arbitrarily shaped cells facilitate the transition between regions of varying mesh densities which has the potential to improving computational accuracy without the penalty of global refinement (De Villiers, 2006). This means one only refines in areas where needed and so improves the accuracy while at the same time minimizing the computational resources. Furthermore, arbitrarily shaped mesh elements allow for a geometry fitted mesh which improves the comparability of the numerical results to the actual occurance in the field. Further detail as to how snappyHexMesh works is provided in Figure 58 in Appendix E.

The finished mesh consists primarily of hexahedral cells with the addition of polyhedral cells as well as boundary layer cells (prism layers) along the dune surface. Hexahedral cells are prefered since they take up greater volume than tetrahedral cells and therefore fewer are required. Furthermore, hexahedral cells have less computational faces than that of some polyhedral cells and therefore require less computational resources. Also, hexahedral cells are more accurate than tetrahedral cells.

A limitation of hexahedral cells is that they limit the geometry fitting capability of the mesh which will be better with tetrahedral or polyhedral cells. This limitation, however, is not a factor when using a cut hexahedral meshing tool since the finished mesh uses polyhedral elements to fit the geometry. The polyhedral elements serve as transition between the geometry fit and the inner structured hexahedral mesh. Furthermore, boundary layer elements are used along the dune surface. The boundary layer elements are also body fitted. The ability to use different elements is made possible with the unstructured meshing framework as explained earlier.

Another limitation of hexahedral cells is the proneness to numerical or false diffusion when flow is at an oblique angle to the cell faces. Elements with more faces are less prone to experience flux that is of such an angle to cause significant false diffusion. False diffusion is limited by refining the mesh in regions where the flow is expected to be at oblique angles to the mesh alignment such as in the boundary layer and wake. Furthermore, boundary layer cells also serve to limit false diffusion since boundary layer cells are aligned with the wall which directs the flow. The issue of false diffusion is mentioned once more in subsequent sections in the context of discretization of the governing equations.

The simulation domain represents the atmosphere above the dune where the flow takes place. The bottom surface of the atmosphere volume is the dune surface. Note that the ground surface is extended in the model to include the interdune plane. The plane allows the flow to stabilize before entering the studied area near the dune. In this way fully developed flow strikes the dune. Similarly the top boundary is positioned far away from the dune to limit interference with flow over the dune. An image of the dune surface with overlaying mesh can be seen in Figure 59 in Appendix E.

In the literature review it was shown that unstructured grids provide the framework for local mesh refinement (Kim and Boysan, 1999, De Villiers, 2006). Local refinement is possible in OpenFOAM. For the simulations, local refinement is done near the surface and recirculation zone. Refinement is done in regions where high velocity gradients are expected. In the recirculation zone and boundary layer high velocity gradients are present and therefore viscous effects are important. The viscous effects are also important in regions of high vorticity magnitude such as is generated in the boundary layer and wake. Mesh refinement is also a measure to limit false diffusion in the wake area where vortex structures produce angled flows in relation to the mesh configuration. The refined mesh also makes it possible to view more detail in these regions. The recirculation zone is of interest for the eddy and vortex structures that are expected there and sometimes only visible with sufficient grid refinement. Figure 10 shows the dune surface as well as the local refinement.

The final mesh used for all the three-dimensional simulations has a 1500 m inlet region, 2500 m outlet region, 2000 m high flow region between the interdune plain and the top boundary, Furthermore, the length of the linear dune that is included in the domain is 200 m. For comparison, the dune is approximately 85.5 m high.
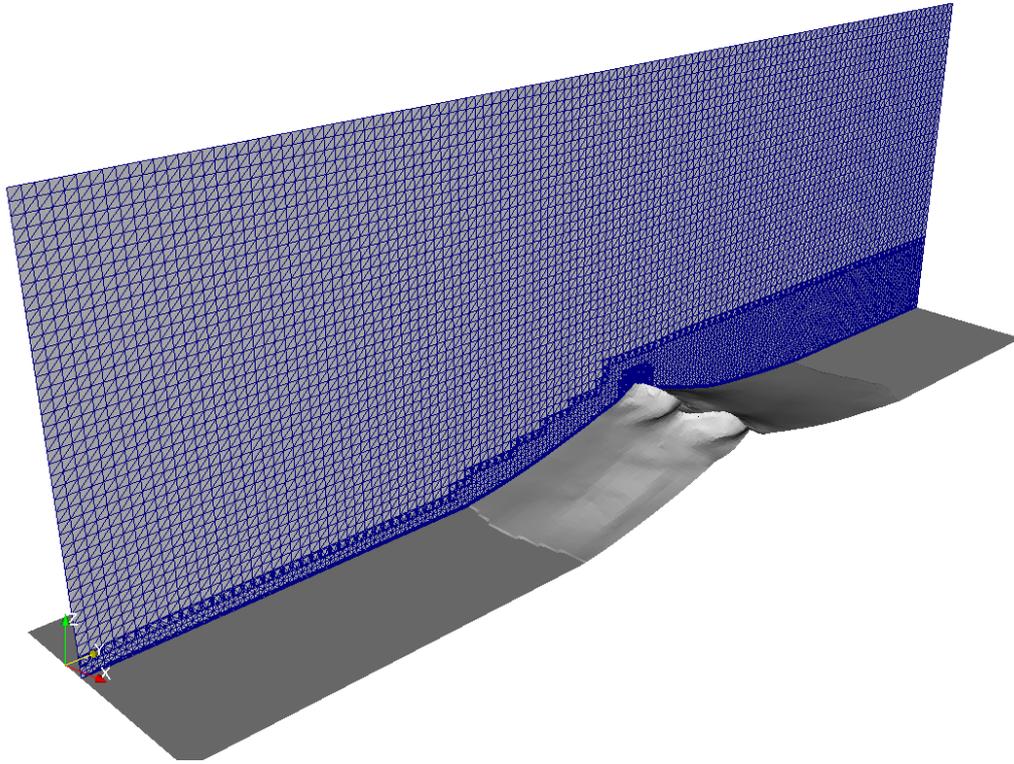
Figure 10: Volume mesh refinement

The mesh plays a key role in the simulation accuracy and time since a finer grid makes it possible to view smaller turbulent features but increases the simulation time needed. The goal is to find a balance for accuracy and simulation time. Furthermore, defining prism layers on the dune surface helps to improve boundary flow development and reduce false diffusion there. Lastly, the mesh can be checked for grid independence to see if the converged solution has enough resolution to include the underlying flow features.

3.1.6   Mesh display limitations

One important aspect to discuss is the limitation when displaying the mesh using the Visualisation ToolKit (VTK) format. The way OpenFOAM visualises CFD meshes is to convert the mesh information to VTK format and then visualise it in Paraview (2009). Paraview is open-source post-processing software that is distributed with the standard OpenFOAM software. The problem with the VTK format at the moment is that it is unable to display cells, like hexahedral and polyhedral, as a whole. What the software does is it divides the cells and then displays it as tetrahedral. For this reason hexahedral cells are shown with a diagonal through it. This makes it difficult to sometimes visually check the mesh.

Another problem arises from cell splitting. What happens is that new cells have to be generated to fill the larger hexahedral or polyhedral cells. During this cell generation slight offsets might occur that would proliferate through the mesh. The end result is a visual representation of the mesh with the addition of a feature resembling crack formation throughout the mesh.

23

However, it is important to realise that these limitations are only for the cell visualisation part of the analysis. Even though the cells appear tetrahedral, the actual cells used in the simulation are still hexahedral and polyhedral as originally generated. The VTK files generated are separate from the simulation files in OpenFOAM and could be removed or modified at any point in time without affecting the simulation model.

One way to avoid this visualization problem is to use the cellSet utility in OpenFOAM to select a set of cells. This cell set can then be transformed to VTK format and viewed in paraview. When viewing cells from the outside they appear as hexahedral and polyhedral cells but a section though it will still show diagonals. Therefore using the cellSet utility makes it possible to view cells as a whole.

Another way is to decompose the mesh in the same manner as would be done when doing parallel computations. Decomposition is the splitting of the mesh, initial conditions as well as boundary conditions among the processors available. The decomposition is controlled through a data file in which it is possible to specify the number of processors involved and the way the mesh has to be split in the three directions. During decomposition a processor boundary is made. When converting the decomposed mesh to VTK format it is possible to look at the processor boundary. Since the processor boundary is along the outside of the cells, in VTK format they are displayed as whole hexahedral and polyhedrals. Therefore the decomposition with parallel visualisation could also be used to bypass the visualisation limitation if the decomposition is done in such a way that the processor boundary falls in the position of interest. The difference between visualising the mesh in general and as cell sets can be seen in Figure 11.
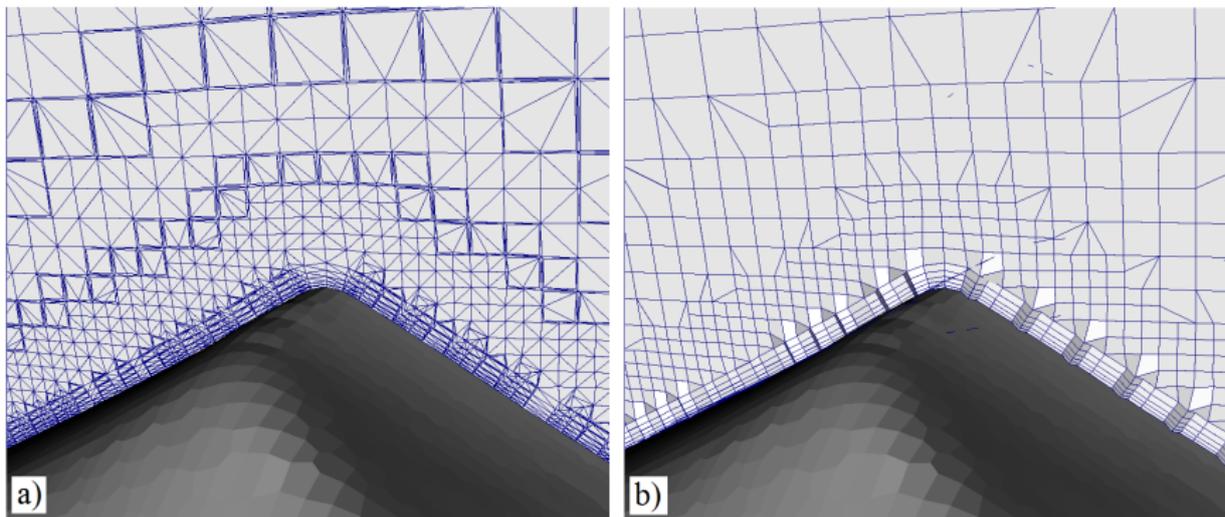
Figure 11: Mesh display error: a) tetrahedral resembling display and b) improved mesh display

Although the regular way of visualising the mesh looks unsatisfactory it is much quicker than visualising a cell set or processor boundary. Once the VTK limitation is understood it is possible to more easily identify which features are introduced by the VTK limitation and which are from the actual mesh. Therefore in this report some mesh images might be display as tetrahedral cells where in fact the majority are hexahedral and some polyhedral. Also, it should be kept in mind

24

that the meshes displayed in Figure 11 (a) and (b) are used to demonstrate the visualisation limitations and are not the final meshes used in simulations. It could also be noticed that even the improved mesh displayed in Figure 11 (b) still contains some cells that appear as tetrahedral. Tetrahedral cell appearance seems to occur between regions of different mesh densities. The actual mesh contains only hexahedral and polyhedral cells.

When meshing is completed the mesh can be checked with a utility in OpenFOAM. This utility gives the user valuable information about the quality of the mesh. The information provided includes the number of cells, boundaries as well as the amount of each type of cell which are in the mesh. Furthermore, the mesh is evaluated for orthogonality as well as skewness. An orthogonal mesh is one where the intersections of grid lines are perpendicular (Versteeg and Malalasekera, 2007). Orthogonality is calculated in OpenFOAM for control volume faces and refers to the angle that the line connecting adjacent cell centres makes with line normal to the face involved.

Nonorthogonality on the other hand may not prevent the solution from running but would certainly have an effect on the discretization schemes to be employed as well as the stability of the simulation. Furthermore, mesh nonorthogonality lessens the mesh accuracy i.e. the extent to which mesh refinement should be applied, in order to achieve grid independence, is increased. Skewness on the other hand is calculated for faces rather than cells and refers to the ratio of the distance from the face centre to the point where the line that connects the cells centres intersects the face over the length of the line connecting two cell centres. A large skewness value may results in instability errors.

3.1.7 Dune mapping limitations

There are a number of limitations that restrict the mapping detail and scope possible. Firstly, the site location, and therefore dune shape, is limited to what can be reached by vehicle within reasonable time from Gobabeb. Secondly, the time is limited by the hand in date for the thesis as well as the short visits to the Gobabeb training and research facility possible. This restricts the size of the dune to be mapped. Furthermore, the GPS accuracy is limited by the signal reception strength and satellite errors. Lastly, the mapping domain size is limited by the computational resources available. If more of the dune is mapped, more time will be needed for mesh creation, setup and simulation. Due to the larger mesh, additional computational resources will be needed to carry out the calculations.

3.2 Flow Measurement Methodology

For this project it was required to do some field measurements of the air flow over the dune. The measurement data was used for developing inlet boundary conditions. In this section the flow measurement site, equipment as well as the procedure followed are described.

3.2.1 Flow measurement locations

In order to get an acceptable representation of the flow over the dune with the equipment and time available, it was decided to do wind measurements with a wind mast on three different

locations of the dune. The wind mast referred to is discussed in section 3.2.2. The three locations where the mast was set up for wind profile measurements are indicated in Figure 12.
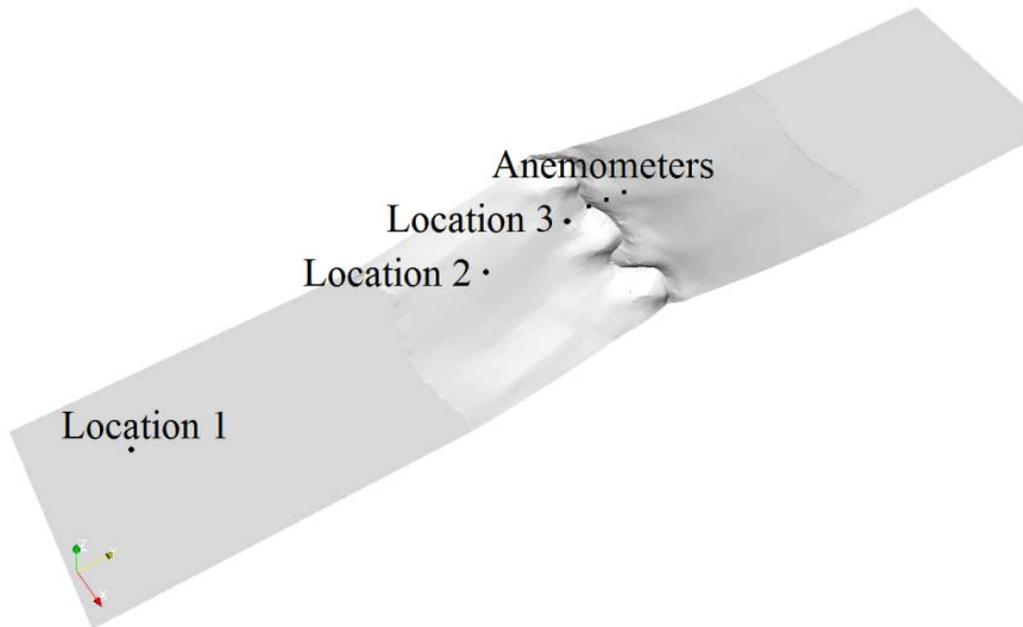
Figure 12: Wind measurement locations

The anemometers indicated on the dune in Figure 12 refer to additional wind metering equipment from an accompanying MSc project by Muller (2009). The sensors were used during the crest measurement (Location 3) of the long mast. The idea was to use these additional anemometers to measure the flow up the east slope and then compare it to the mast flow data for the same time. This gives an idea of the incoming flow and what happens to the flow as it crosses the dune crest.

The reason for placing the mast at these locations was to see if it would be possible to capture flow features noticed from previous studies as well as what is expected. The location 1, as indicated on Figure 12, is positioned in the interdune. This plane is relatively flat and is therefore modelled in this way. The measurement on the interdune is especially of importance since a large portion of the seeds in question originate from this region. The flow on the interdune is also essential for the inlet boundary condition specification. Although the neighbouring dune is not shown in Figure 12 the mast at location 1 is positioned approximately halfway between the two neighbouring dunes. The mast located on the interdune can be seen in Figure 13. The neighbouring dune is visible as well as the masts positioning half way between the two dunes.

Figure 13: Wind mast on interdune (looking west)

Location 2 is selected to see how the flow changes as it is influenced by the upward slope of the dune if a westerly wind would occur. From literature the flow near the surface should be accelerated as it moves up the slope due to the difference in high and low pressure regions that are present at the crest and toe respectively (Parsons *et al.*, 2004b). It is expected that this acceleration near the surface would fill up the velocity profile near the surface up to the highest point near the crest.

For the last point of measurement, location 3, it is decided to place the mast near the crest on the westerly face. The reason for placing the mast in this position is to measure the wind profile in this region and to compare it to the profiles of further down the slope.

3.2.2   The flow measurement equipment

As mentioned previously a wind mast is used to do flow measurements of the velocity profile. The mast is 10 m high and has four wind speed and four air temperature sensors located in pairs on different heights of the mast. Additionally the mast has one wind direction sensor. The speed and temperature sensors are located at heights of 2.5 m, 5 m, 7.5 m and 10 m above ground. The use of the mast is to measure the wind profile for the first 10 m and extrapolate for the rest. The wind mast is displayed in Figure 14.

27

Figure 14: The wind mast

The mast is tied to the ground by six individual cables. These cables are secured by ropes to a number of rods pushed deep into the sand of the dune. The secure fastening of the mast is extremely important to prevent any damage to equipment that might occur as result of high velocity gusts. Due to the remote location of the site it is very important to be protective about equipment since no spares are available in the region.

Extra securing measures proved vital during long periods of unattended measurement in the Namib Desert. It was found that the high temperatures coupled with the occasional strong easterly gusts placed a great load on the mast supports. Some of the ropes snapped while others were sheared through due to periodic wind loading causing a swaying of the mast. Temperature loading also played a role on ropes and steel cables softening the materials and so promoting shearing and loosening of secured points. However, damaged ropes and other supports did not cause damage to sensors in any way and the mast stood with a reduced number of cables stays still intact holding it upright.

The sensors that are fitted to the mast are connected to the data loggers by electrical cables. The sensor data is recorded by two data-loggers. The data-logger boxes are situated in a box at the base of the mast. These cables were initially designed for measurements in Antarctica. Each sensor had three plugs in the cable before the data logger to make assembly possible. The cables were run on the inside of the mast down to the loggers. A typical pair of sensors is displayed in Figure 15.

28

Figure 15: The wind mast sensors

The electrical cables, however, caused many problems during measurements in the Namib Desert. The main causes were sand, dust, temperature and transport of the sensors. In controlled environments the sensors would work but out in the field sand and fine dust would enter the connection points which on some occasions prevented the signal reaching the data loggers. Furthermore, high temperatures and transport damage caused some sensors to fail completely.

The decision was made to rewire all working sensors and replace broken or dysfunctional ones. Greater precautions were taken to secure sensors throughout transportation. The purpose of the rewiring was to reduce the number of connections in the system and in this way reduce the chance of sand and dust causing signal transmitting failure. During this refitting all the sensors were calibrated again to accommodate the new wiring. The modifications greatly improved the whole system reliability and robustness. The signal strength improved greatly and field measurements continued successfully.

Another problem with the equipment in the Namib Desert is the strong gusts that could damage the mast base placed on the sand. The problem does not lie in the strong winds but rather in the sand that is shifted by it. No matter how secure one fastens a mast, sand that is blown away around the base or the pins could cause the mast to fall over. On the other hand sand could pile up and cover the data-logger boxes which might cause hardware problems. To address these two concerns a plastic mesh grid was placed underneath the base of the mast to prevent it from sinking into the sand and also to prevent sand erosion around the base. Furthermore, the data-logger box was covered with plastic bags as well as canvas blanket to prevent sand penetration. The plastic and canvas layers also further improve the temperature regulation within the box.

Apart from the 10 m high wind mast a short mast is also used in the project. The short mast is used to measure the flow velocities profile in the lower part of the atmosphere as supplementary data. The reason for using the short mast to do measurements is because the lowest measurement that is possible with the long mast is at 2.5 m. The short mast uses the same sensors and data loggers as the long mast and therefore cannot be set up at the same time. The short mast is displayed in Figure 16. On the left side the temperature sensors are fitted and on right hand side

29

the wind speed sensors. The direction sensor is mounted on a separate post some distance away due to the limited space and to reduce possible flow interference.
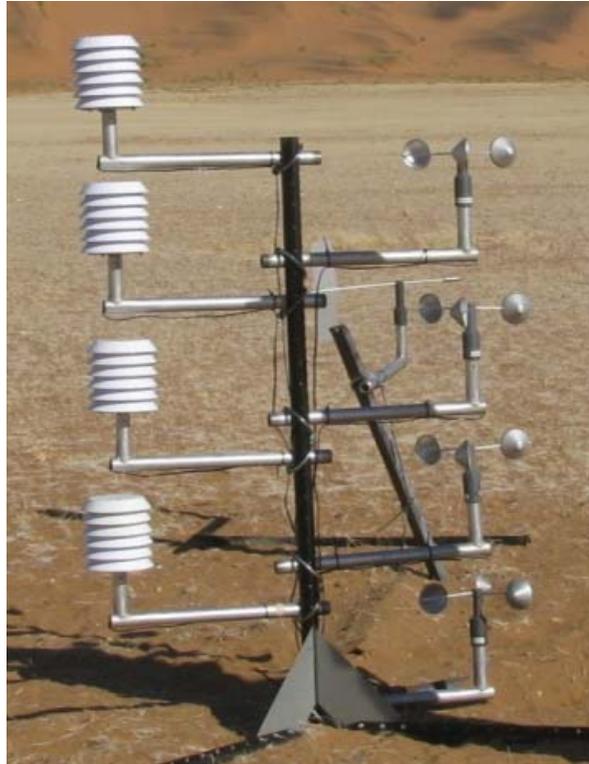
Figure 16: Short wind mast

The sensors were initially calibrated by the supplier during purchase and by previous user of the wind mast. After the rewiring of old sensors and purchase of new some sensors all sensors were recalibrated to accommodate the rewiring. The calibration parameters are given in Table 7 and Table 8 in Appendix F. In addition the mast sensors were also compared to calibrated sensors used by Muller (2009) during the field measurements as an additional check and the sensors performed adequately. Further specifications of the data loggers and sensors are provided in Table 9, Table 10, Table 11 and Table 12 in Appendix F.

3.2.3   Wind metering limitations

There are a number of aspects that limit the amount of flow measurements that can be done. For instance the measurement locations are limited to where the wind mast can be carried by persons on foot since vehicles are unable to cross some areas of the dune without causing very long term damage to the environment. Furthermore, the measurement time is limited to the seasons during which the measuring part of the study will be done. As explained in the literature review different seasons are associated with different dominating winds. This makes it difficult to compare winds with simulations since the dominant winds may not be experienced in full force during the study.

A limitation is also caused by the equipment since the mast and sensors are limited to the budget available. This encourages the use of sensors and a wind mast that is already available, and is not necessarily designed specifically for the needs of this project. Furthermore, sensor life is reduced by extreme climate and transportation conditions. Lastly, the profile measurement is limited to one mast. This makes it difficult to compare simulation data since it is impossible to measure the input and output at the same time.

3.3   Seed Particle Methodology

In order to simulate particles in the flow field a seed model is needed to quantify the interaction between the air flow and the seed particle. The seed model is defined by the drag coefficient, the mass and the diameter of the particle. In this section the seed species of interest to this study is described. Furthermore, the model used to define the seed particles for simulation purposes is presented.

3.3.1   Seed species definition and attributes

The seed selected for modelling and simulation is of the plant species named Stipagrostis sabulicola. This species is selected in collaboration with Muller (2009) due to the abundance of the plant species in the Namib Desert, making it suitable for statistical analysis, as well as the morphological properties of the seed that greatly promotes its flying ability. The seed is displayed in Figure 17. It should be noticed that the seed has three hairy flight appendages that are attached to the main seed body.

Muller (2009) examined a number of seeds and provided statistical data of the morphological features of these seeds. Each of the seeds consists of a diaspore with a flight appendage. The diaspore is part of the seed that would germinate and the flight appendage is responsible for the large sail area resulting in a drag force which in turn facilitates or promotes seed transportation.
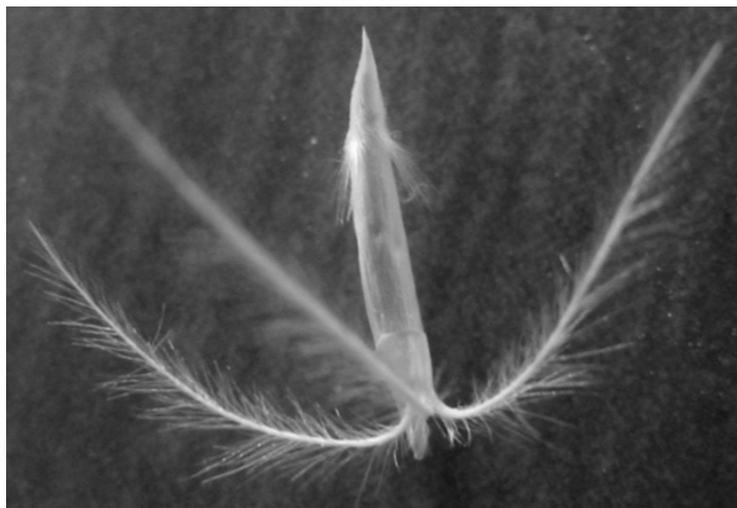
Figure 17: Stipagrostis sabulicola seed

31

The seed morphological properties as determined by Muller (2009) are given in Table 2. The mean seed mass was calculated from sample size n of 100 seeds. The individual lengths and widths are mean ± 1 standard deviation (SD).

Table 2: Seed morphological attributes

Species	Mean Mass (mg)	Length with appendage (mm)	Length without appendage (mm)	Maximum width (mm)	Appendage length (mm)
Stipagrostis sabulicola	0.562	7.08±0.67	4.6±0.48	0.9±0.15	2.48±0.57

The journey a seed takes is determined by its morphology. If the seeds are light enough the flight appendages cause the seeds to get swept up by even the slowest wind and could travel a great distance if unhindered by obstacles in its flight path. Seeds occasionally bounce or roll some distances along the surface due to periods of calm wind or sand obstacle in the particle flight path. This rolling action causes the flight appendages to break off from the main seed body. Without the flight appendages the seed has a much lower drag and will stay on the surface even with greater wind velocities. The seeds may sink beneath the sand where it would be protected from the sun and insects. Existing plants also play a role by trapping seeds that roll into them.

The seeds or other plant material like the broken off flight appendages are observed to collect near the crest on the lee-side slip face of the dune. It is this plant material that attracts insects and then small animals like lizards to form a small ecosystem. This ecosystem was also mentioned in section 1.1.

In addition to the measuring of the morphological attributes of the seeds drop tests were also conducted to determine the fall rate of the seeds in air. The drop tests were conducted in still air in a laboratory at room temperature. The drop tests consisted of dropping a number of seed samples over a distance and measuring the time of the fall. Due to the small size and large flight appendages the seeds reach terminal velocity very close to the start of the drop. It is therefore sufficient to assume the fall rate calculated over the 2 m drop is equal to the terminal velocity. The terminal velocity is determined as 0.57 ± 0.09 m/s (Muller, 2009).

3.3.2   Modelling the seed as a spherical particle

To model a seed particle that physically resembles an actual seed morphology would be very difficult and is therefore judged to be outside the scope for this project. To simplify the model the seed is modelled as a sphere particle with equivalent mass, drag and effective diameter. The particle drag is determined in a similar manner to that used by Combrinck (2008). Since the drag coefficient and the particle radius are unknown an iterative process is required where an initial condition for the drag is first chosen.

Later the drag is corrected using an alternative equation provided by Flemmer and Banks (1986) which is based on the Reynolds number of the particle moving at terminal velocity through air. This correlation is chosen since it has been proven to be superior to other similar approximations

(Flemmer and Banks, 1986). This finding is supported by the calculations done by Combrinck (2008) who determined the drag coefficients for particles experimentally as well as analytically with various approximations. The results from Combrinck (2008) showed the least difference with the Flemmer and Banks (1986) approximation.

The final drag was calculated iteratively by using Matlab R2007b software. The drag and particle diameter converge relatively quickly (5 iterations) with a final residual smaller than 0.001. Therefore the seed can be modelled as a spherical particle with the specifications given in Table 3.

Table 3: Seed model specifications

Drag coefficient, C_D	Effective diameter, d (mm)	Mass, m (mg)
0.64	7.5	0.562

3.4   Computational Fluid Dynamics Methodology

In previous sections the simulation domain generation, field measurements and particle modelling methodologies were explained. The focus of this section is to explain the simulation aspects involved in this project. The simulation aspects include the software used, simulation route, the numerical model as well as the model boundary conditions.

3.4.1   Software used for simulations

Computational fluid dynamic software packages are ever evolving and require large resources to develop. Due to the amount of time and money that is invested in the development of software packages, licences are becoming increasingly expensive to purchase, especially for smaller computer aided engineering (CAE) companies. Furthermore, due to the demand for more computational resources and the lack of computer processor development to keep up with the demand, more focus is set on the implementation of parallel computing. This involves more processors and more cores per processor to handle the computational load. However, each core used requires a licence which makes it very expensive to do simulations on a cluster using commercial CFD software. A demand therefore exists for software that can be implemented on a parallel environment to handle the increasing computational loads while at the same time being more affordable than commercial CFD packages.

As mentioned in preceding chapters the software chosen for the vast majority of simulations in this project is called OpenFOAM. OpenFOAM is an open source CFD toolbox operating on Linux systems which makes it ideal for the large scale simulations on a parallel environment as planned for the project. The software was recommended by Dr. Meiring Beyers who works for RWDI, an international company who specialises in atmospheric flow modelling around buildings. His recommendation motivated the use of OpenFOAM in this project in order to gain experience with the software as well as to lay the foundation for future studies in the local CFD group. Being open source not only means that there are no licensing cost involved but also that one has access to the source code behind the solvers utilities and boundary conditions which

makes it ideal for educational purposes. The software is especially attractive as an educational tool for CFD since it is possible to see how the governing equations are discretized and implemented in the code. The availability of a computer cluster at the University combined with the use of OpenFOAM further increases the possibilities for computational fluid dynamic studies.

Another benefit of OpenFOAM is that it was programmed in C++ in such a way to allow users to implement their own solvers, utilities, turbulence models and boundary conditions into the code with the prerequisite of some knowledge of the code (OpenCFD, 2009). This ability to add one's own code contributes to the development of the code since users from around the world can exchange code, improve it and so stimulate growth of the code in general. Furthermore, creating one's own code makes it attractive for industries who do not want to pay for a code that has many features that might not be needed but have to be paid for. OpenFOAM provides the combined benefits that it could be specialized for a specific industry while being affordable at the same time. OpenFOAM has also proven itself against other commercial codes on benchmark simulations and has been shown to perform well, further increasing its appeal to industrial companies. Some companies that have been reported to use OpenFOAM are Audi, ABB Corporate Research, BAE Systems, Mitsubishi, Shell Oil, Toyota and Volkswagen to name a few (Jasak, 2009).

OpenFOAM is able to handle unstructured FV meshes and has an automatic mesher capable of meshing very complex geometries. This meshing tool has already been discussed in more detail in section 3.1.5. Moreover, OpenFOAM has an impressive list of turbulence models, solvers, utilities and boundary conditions readily available to be used to set up a simulation.

In order to be able to use OpenFOAM effectively the author participated in three training courses including two user training courses and one more advanced programming training. This training proved vital for gaining insight into the workings of the software and provided the platform from which effective simulations could be conducted.

3.4.2   Simulation route

A difficulty with OpenFOAM is that it is less user friendly than commercial packages that spend a lot of money on developing complex graphical user interfaces (GUI). To become familiar with the software initially it was decided to approach the final objective by first doing simplified simulations and increasing the scope and complexity as the project moves on. The route followed can be divided into four categories according to the FV mesh used. These categories include:

a.   Two-dimensional no dune simulations

b.   Two-dimensional simplified dune geometry simulations

c.   Three-dimensional simplified dune geometry simulations

d.   Three-dimensional actual dune geometry simulations

The first simulation category is the two-dimensional no dune simulations. This category involves two-dimensional flow over a flat plate for velocity profile development primarily. This

34

simulation is very simple and gave the opportunity to become familiar with the software boundary implementation and solution controls. OpenFOAM has a solver specifically suited for such a simulation called boundaryFoam. The simulation mesh is a single stack of cells with cyclic boundaries on both sides of the vertical column. The bottom surface is a wall boundary to represent the no slip condition on the surface.

The next category includes all two-dimensional simulations over simplified dune geometries. This category is included since it is still simpler than full three-dimensional simulation and provides the opportunity to identify flow features that result from flow across a dune profile. From the literature review it could be seen that most dune studies have focused on two-dimensional flow patterns over a dune (Parsons *et al.*, 2004 a and b). It is therefore convenient to set up similar simulations for comparison with literature. Further benefits of doing the two-dimensional simulations are that fewer resources are required. This provides the opportunity to look at the effect of different discretization schemes, turbulence models and parallel performance within reasonable time that would aid in the full three-dimensional simulations.

The third category includes simulation of flow over a simple three-dimensional dune. The reason for this simulation is to see the difference between the two-dimensional and three-dimensional flow without using a complex geometry. It is also desired to look at flow approach angles with these simulations to see what flow features result in the lee side recirculation zone. The flow features observed for the actual three-dimensional dune simulations may then be better understood.

The fourth category involves the full three-dimensional actual dune simulations. For these simulations the mapped dune geometry was used. The inlets are provided by the velocity profile measurements in the field. This is explained later in more detail in section 4.1.

3.4.3   Numerical model

With the help of the FV mesh as well as the wind and particle data it is possible to define the numerical model. The numerical model forms the basis from which the computational fluid dynamic software calculations are made. The numerical model includes the governing equations in a solver, discretized in order to be applied to the control volumes that make up the FV mesh. Other aspects discussed that are related to the numerical model include the applied turbulence models, time controls, interpolation schemes, relaxation factors, boundary conditions, wall functions and SGS model for the LES simulations.

Differencing schemes

Discretization, as explained in the section 3.1, refers to the division of the domain into small sub-entities know as control volumes. The governing equations are also discretized and solved for the values at the centres of the control volumes. In order to calculate the flux between control volumes in a FV mesh some values are needed at cell faces. To calculate these values differencing schemes are used. The differencing scheme has a great effect on the stability and accuracy of the simulation.

35

Two of the most common differencing methods in use are the upwind and central differencing discretization schemes. Upwind differencing assumes the value of a certain parameter is the same as that at the cell centre upwind of the face. Upwind differencing has been shown to be only first order accurate on the basis of the Taylor series truncation error and therefore suffers from false diffusion (Versteeg and Malalasekera, 2008). False diffusion is the effect where the transport properties appear smeared in areas where the flow is unaligned with the grid patterns. One way to counter false diffusion is by grid refinement. However, the extent to which grid refinement is necessary usually tends to be very computationally expensive. The advantage of upwind differencing is that it is stable (bounded) and simple to extend to multi-dimensional problems.

Central differencing on the other hand calculates the value of a parameter in question by interpolating from the two cells up- and downwind of the control volume interface. Central differencing has been shown to be second order accurate and is far less prone to false diffusion than upwind differencing (Versteeg and Malalasekera, 2008). The problem with the central differencing scheme is that it is less stable than the upwind differencing scheme. While this is countered by the "deferred correction" and "flux blending" implementations, central differencing has also been shown to result in unrealistic flow features when the convection term strongly dominates the rest of the system (De Villiers, 2006).

For the steady state simulations in this project an upwind interpolation scheme is selected to interpolate the face values to the cell centre for preliminary simulations. Although the upwind differencing scheme is only first order accurate and may introduce false diffusion in regions where flow is highly skew to the computational grid it is still preferred to initialise the flow field. The reason it is chosen to initialise the flow field is to ensure simulation stability.

To lessen the errors introduced by the upwind differencing scheme the grid is constructed of hexahedral and polyhedral rather than tetrahedral cells. Hexahedral and especially polyhedral cells are less susceptible to false diffusion than tetrahedral cells due to the increased likeliness of smaller angles between flow directions and face normals. This is further supported by the fact that all the polyhedral and prism layer cells are situated near and along the geometry surface where the flow is forced to change direction. Furthermore, fewer cells are necessary when using a combination of hexahedral and polyhedral compared to tetrahedral cells and therefore allows more refinement possibility in regions where false diffusion is to be expected. The mesh refinement limits the degree of false diffusion.

Since upwind differencing errors have been reported to be intolerable, for this project second order accuracy is desired for final results to reduce dispersion and dissipation errors. Therefore higher order differencing schemes are employed once the flow is sufficiently initialized as explained previously. To ensure the stable convergence of the solution while maintaining a higher accuracy, blended schemes are considered. Blended schemes use a blending coefficient to specify the degree to which a combination of upwind and central differencing is to be employed.

A number of blended schemes are available in OpenFOAM. Of these schemes Blended, GAMMA, Limitedlinear and SFCD were investigated. All the schemes provided similar results but the GAMMA blending scheme was selected for majority of the simulations. GAMMA switching/blending scheme was first introduced by Jasak (1999) and uses central differencing in

36

the bulk of the solution but then switches to a blend of upwind and central differencing to stabilize the equations when the interpolation tends to unboundedness (De Villiers, 2006). The GAMMA scheme therefore provides the desired degree of accuracy since it makes use of central differencing while maintaining a degree of stability by employing blending where needed. A detailed list of the different discretization schemes and the corresponding terms are given in Table 15 in Appendix J and Table 17 in Appendix K.

Solver algorithms

Solvers used in this project can be separated into time dependent and time independent categories. The steady state solver implements the semi-implicit method for pressure linked equations (SIMPLE) algorithm. The SIMPLE algorithm was first introduced by Patankar and Spalding (1972). The SIMPLE algorithm is used to link pressure and momentum equations. The algorithm involves the iterative calculation of the velocity and pressure fields until continuity and mass momentum errors are adequately small i.e. smaller than 0.01 % of the inlet flux. Continuity is monitored each iteration on a local as well as global scale. This ensures that continuity is preserved throughout the simulation process.

In more depth the SIMPLE algorithm is a method where the pressure and velocity fields are initially guessed and then corrected. During the first step the guessed pressure and velocities are used in solving the discrete momentum equations. During the second step the pressure and velocity corrections are calculated. Then the pressure and velocity corrections are added to guessed pressure and velocities to give the correct pressure and velocity fields during the third step. The fourth and final step is where all other discretized transport equations are solved. After step four, convergence is checked. If the values have converged and the residuals have sufficiently reduced the process can stop. If not the newly calculated corrected pressure and velocity field are used as the initial guess and the process starts again from step one (Versteeg and Malalasekera, 2008).

For transient simulations and more specifically the LES simulations in this project the pressure implicit with splitting of operators (PISO) algorithm is used. The PISO algorithm was first introduced by Issa (1986). The PISO algorithm is similar to the SIMPLE algorithm but has an added pressure corrector step to enhance it (Versteeg and Malalasekera, 2008).

Turbulence modelling

Turbulence models are used in CFD to compensate for the lack of sufficient mesh refinement that is needed to resolve small scale eddies in the flow field. As explained in the literature review this lack of mesh refinement is brought on by the lack of computational power and time limitations. The computational resources needed in this project are especially high due to the large flow domain as the high mesh resolution associated with atmospheric flows. Therefore turbulence models are implemented in all simulations in this project.

The turbulence models used for steady state simulations include three high Reynolds number RANS turbulence models. The high Reynolds number RANS turbulence models implemented include the standard k-ε model, the RNG k-ε model and the realizable k-ε model. These models are chosen for their simplicity, robustness, accuracy and well documented performance as well as

37

shortcomings. The RNG k-ε model for instance has been shown to perform well for flow over a backward facing step (Bradbrook *et al.*, 1998). The realizable k-ε model is especially of interest since it seems to be preferred by a large part of the computational fluid dynamic community and has been reported to perform well in the calculation of the recirculation zone were the standard k-ε falls short (Kim and Boysan, 1999). The realizable k-ε model is therefore chosen to produce the final results of the steady state simulations. The standard and RNG k-ε models are included for comparison purposes.

For the transient simulations LES turbulence models are implemented. LES turbulence modelling is used to account for the effect of large eddies in the flow field which is often not detected in the RANS models. In the literature review it was found that LES turbulence modelling is more computationally expensive than the RANS models but less expensive than DNS and therefore provides an added accuracy while maintaining a reasonable computational requirements. From the literature review it was also found that LES turbulence models use filtering functions to filter out the small eddies which will be modelled with a SGS model. This SGS models considered in this project are the Smagorinsky algebraic model and the one-equation differential model. The one-equation type model is chosen for all the sub-grid turbulence modelling in LES simulations due to the fact that it accounts for non-equilibrium effects which is especially useful for more complex flow arrangements where the Smagorinsky model falls short (De Villiers, 2006). The choice is further motivated by the comparative study by Fureby *et al.* (1997) who found that the one-equation SGS model performed well in fully developed channel flows.

Near-wall treatment

In considering the near wall treatment there are low Reynolds number and high Reynolds number approaches. Turbulence models for both low and high Reynolds number approaches are available in OpenFOAM. The low Reynolds number approach calculates the flow up to the wall and to do so effectively requires a very fine mesh resolution in the wall region. In some cases up to ten prism layers are recommended. This refinement requirement makes the low Reynolds number approach computationally expensive and is therefore rejected for this project.

High Reynolds number turbulence models on the other hand use wall functions to approximate the near wall flow by analytically calculating the boundary layer in the near wall region from equations fitted to extensive experimental data. These equations are depicted in Figure 18 which is also known as the law-of-the-wall. The wall functions help to calculate the flow near the wall more effeciently than local refinement would allow. The wall functions, however, were not adapted for rough surfaces since the majority of the dune surface could be regarded as smooth. Wall functions are used throughout the simulations in this project to reduce the computational load since less refinement is required near the walls.
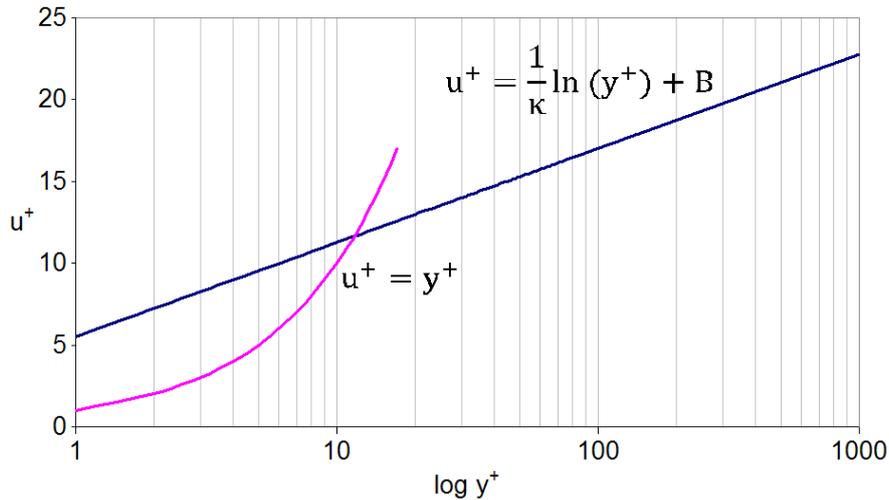
Figure 18: Near wall velocity distribution (law-of-the-wall)

There are three main regions to identify in the law-of-the-wall. The first is the viscous or linear sub-layer that fits the measured data up to a y^+ value of 10. In the linear sub-layer flow is dominated by viscous stresses. The second region is the logarithmic layer which is situated at y^+ values between 30 and 500 after which the law-of-the-wall becomes increasingly inaccurate as the data diverges from the fitted equation. In the logarithmic layer turbulent stresses dominate the flow. Lastly, a buffer layer can be identified as the region where the viscous sub-layer transitions to the logarithmic layer. This happens approximately between a y^+ value of 10 and 30. Therefore to implement high Reynolds number flows wall functions using law-of-the-wall correctly requires the centre of the first cell adjacent to the wall to fall within the logarithmic layer. The y^+ values, to stay within the logarithmic region, should therefore be between 30 and 500 effectively.

It should, however, be kept in mind that the application of the wall functions are relevant for flat plate boundary layer definition and tend to break down in flows associated with high pressure gradients and non-equilibrium. In this project the geometry of the dune can be modelled in this way since the surface can be considered as a flat plate throughout the whole of the dune. The only deviation from flat plate theory is in the region of the crest where a rapid change in the surface occurs.

Under relaxation

Under-relaxation factors are a tool used to improve convergence of steady state solutions. The under-relaxation factors specify the degree to which the new value of a variable is made up of the corrected variable during the SIMPLE algorithm and the previous value of that parameter. The under-relaxation factors are especially important in this project due to the unsteady nature of atmospheric flow modelling and are used throughout with the only exception being the time dependant simulations. Under-relaxation is employed to the pressure, velocity, turbulent kinetic energy and turbulent dissipation rate. The values range from 0.01 to 0.03 for the steady three-dimensional simulations.

39

Lagrangian partical solvers

To simulate the particles in the flow field a new solver had to be developed. In OpenFOAM-1.6 a compressible version of a Lagrangian particle solver is available but for this project an incompressible version is required. The way the solver works is to track Lagrangian particles as they are transported in a flow field. The flow field in this case is a single time step from a previously calculated flow field. The flow therefore stays constant while the particles are tracked. This method has its drawbacks since flow around the dune is highly unsteady. The ideal would be to implement the particles in a transient LES solver but this task is judged outside the scope of this project since it would require deeper understanding of the C++ programming and OpenFOAM libraries. Despite the drawbacks of using a single time step to track the particles the results would still provide valuable information towards the transportation and distribution of particles in the flow field.

The particle tracking solver developed requires a dictionary that specifies the particle properties as well as the injection properties. The particle properties required are the particle mass, effective density and drag model. In this project a sphere drag model is chosen to calculate the drag and therefore body forces on the particles that would influence their movement. In the particle properties dictionary the gravitational constant is also defined in the negative z direction. Furthermore, the wall interaction method is selected. The wall interaction is set so that the particles bounce and roll when coming in contact with the wall. The wall interaction is selected to resemble particle characteristics as observed in the field. The particle properties are investigated in section 3.3.

Fluid specification

The fluid used in the numerical model is air at 20 ˚C. Therefore the kinematic viscosity, ν, is $1.5 \cdot 10^{-5}$ m²/s. The flow model is Newtonian, turbulent and incompressible. The simulations consist of steady state as well as transient cases. The model under-relaxation factors are implemented for steady state simulations and need to be small enough to improve convergence and therefore stability of the simulation.

3.4.4   Model boundary conditions

The simulation models implemented in this project can be described by four different boundary conditions. The four boundary conditions include inlet, outlet, wall and symmetry. Each of these boundary conditions can be described in terms of the more common fixed value (Dirichlet) and fixed gradient (Neumann) boundary conditions. Fixed value boundary conditions specify the value of a variable φ at the boundary. On the other hand fixed gradient boundary conditions define the normal gradient of the variable φ at the boundary. The boundary conditions can be summarised in Table 4 as follows:

Table 4: Boundary conditions

	Velocity	Pressure
Inlet	$\overline{\boldsymbol{u}} = \boldsymbol{U}(x,y,z)$	$\dfrac{\partial p}{\partial n_b} = 0$
Outlet	$\dfrac{\partial \overline{\boldsymbol{u}}}{\partial n_b} = (0,0,0)$	$\overline{p} = p_{out}$
Wall	$\overline{\boldsymbol{u}} = (0,0,0)$	$\dfrac{\partial p}{\partial n_b} = 0$
Symmetry	$\overline{\boldsymbol{u_n}} = (0,0,0)$ $\dfrac{\partial \overline{\boldsymbol{u}}}{\partial n_b} = (0,0,0)$	$\dfrac{\partial p}{\partial n_b} = 0$

In order to simulate the effect of flow upstream of the inlet it is decided to implement a velocity profile at the inlet boundary that represents an equilibrium ABL correlated with measurements in the field. The implementation of the ABL profile improves the stability of the flow in the region where the inlet and ground boundaries meet. This is because the ABL profile starts from a zero velocity at the wall where the alternative block inlet profile starts from a high velocity.

The high velocity produced by a block profile inlet near the wall is forced to stagnate in a very short distance due to the no-slip condition. This rapid stagnation causes unrealistic flow features in this region which may cause convergence problems. Even if the inlet is positioned far upstream of the geometry the unrealistic flow features may still propagate through the flow field and affect the accuracy of results downstream.

Due to the drawbacks of the block profile a measured velocity profile is therefore implemented at the inlet boundary as a fixed value. The knowledge of the flow velocity, dune height, air density and viscosity make it possible to calculate the general Reynolds number for the simulation. With the very low viscosity the Reynolds number tends to be greater than 100 000 which relates to fully turbulent flow conditions. The inlet boundary is therefore set as turbulent where the turbulent kinetic energy k and turbulent dissipation rate ε are also specified. The ABL functions to be implemented can be described by the Von Karman constant κ, surface roughness z_0 and friction velocity u*$_{ABL}$. These values are obtained from the wind data as described in section 4.2.3 and then implemented into equations (2.2), (2.3) and (2.4). The Von Karman constant κ can be calculated by inserting the k-ε model coefficients into equation (2.5). The Von Karman constant is calculated to be 0.433.

The velocity profile generated from the wind mast data is discussed later in section 4.1.3. In section 4.1.3 the velocity profiles are examined and the one chosen for implementation on the inlet boundary is mentioned. All the boundaries are placed as far from the dune surface as would be allowed by the computational capacity available. This reduces the effect of inlet or outlet disturbances on the flow region of interest. By placing the top boundary far from the dune surface the possibility funnelling effect on the flow is reduced.

41

42

3.5   Parallel computing

Due to the size and complexity of the computational domain a large amount of computational resources are required to complete the simulations of this project within reasonable time. The project therefore makes use of the Rhasatsha computer cluster at Stellenbosch University. The cluster CPU comprises 168 cores each with 2.83 GHz processing capacity. The total memory is 363 Gb giving approximately 2 Gb per core.   Furthermore, the cluster has a theoretical performance of 2 Tflops.

4. RESULTS AND DISCUSSIONS

4.1 Flow Measurements Results

As explained in section 3.2 flow measurements were conducted to capture wind data that could be used for input data for simulations as well as for verification purposes. In this section the measured data is presented, analysed and discussed. The goal is to better understand the wind characteristics while taking into account the various objects in the region as well as the limitations of the wind measurement equipment.

It should be noted that only one mast is available for measurements at any one time. The data on the different locations are not for the same period and is therefore subject to time varying weather conditions. The interdune measurements are from 6 May to 8 June, the slope measurements are from 17 June to 1 July and the crest measurements are from 1 to 9 July during 2009. More time was spent on the interdune measurements to get more data for inlet conditions and in so doing improve confidence in the inlet boundary conditions.

4.1.1 Wind speed, direction, frequency distributions

The interdune wind data is displayed in Figure 19 with the help of a wind rosette plotting software (Lakes Environmental, 2009). From this data it can be seen that the primary wind directions were south (19 %), south-south-west (31.2 %) and south-west (11.3 %) during the measurement period. This means 61.5 % of the wind came from a direction between south-west and south resulting in a relatively concentrated directional spread of the wind. Considering the wind class frequency distribution shown in Figure 19 a normal distribution around the wind class of 2.1 - 3.6 m/s is observed. Very few periods of calm wind speed were recorded in this time period. This means that the wind never ceased for a whole period of 10 minutes.
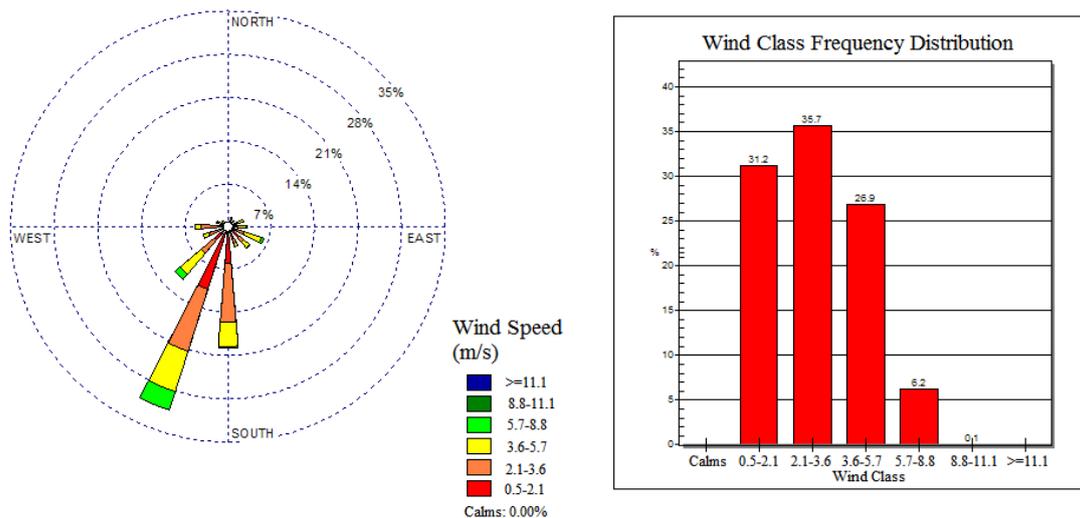
Figure 19: Wind data for interdune (location 1)

43

This wind data shows a dominant south-south-westerly wind which corresponds well with what is documented in literature by Lancaster *et al.* (1984). However, it should be noticed that this south-south-westerly wind was measured during the winter months rather than the spring as is reported by Lancaster *et al.* (1984). It is also seen that a small amount of westerly winds were observed. It is from these westerly winds that the inlet data will be obtained. It should be remembered at this time that a westerly wind is chosen for simplification purposes. The wind rosette for slope and crest measurements (locations 2 and 3 respectively) are provided in Appendix H.

4.1.2   Wind speed and direct variation for different times of the day

The wind speed can also be analysed over a one day cycle. The data is from the interdune measurements. This will give an indication of the most likely speed to occur at a certain time of the day and therefore show if it will be necessary to simulate different wind profiles for different times of the day. It may also provide information for the effects of land and sea breezes.

The speed distribution over a one day cycle is displayed in Figure 20. Figure 20 shows the wind speed varying 2.75 m/s for most of the day. From 14:00 in the afternoon the wind speed increases to a maximum of 4.5 m/s around 18:00 and then decreasing again to 2.75 m/s at 22:00 in the evening. From this data it can be seen that the wind is more or less constant for most of the day showing that there are no regular times when the wind dies down. The simulation of the time dependant inlet wind profile is therefore not necessary since the speed difference is not so significant.
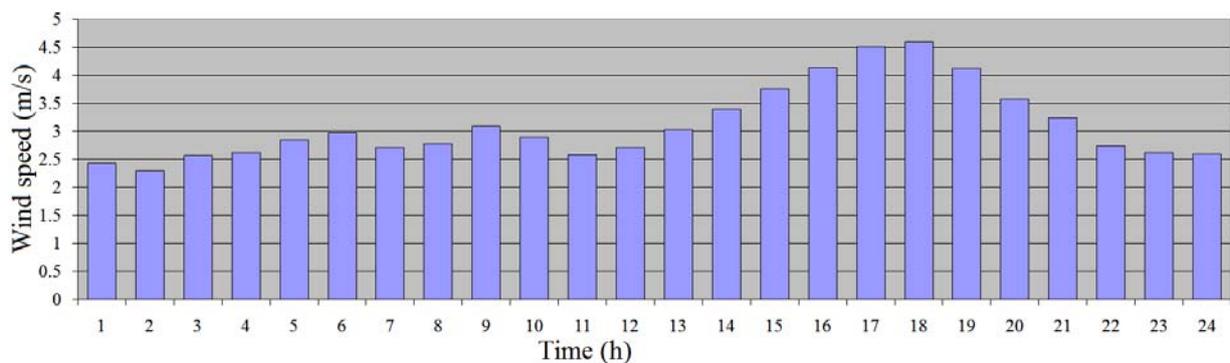
Figure 20: Average wind speed over a one day cycle

Another aspect to consider is the wind directional variation over a one day cycle. This can be seen in Figure 21. The 0° indicates north, 90° is east, 180° is south and 270° is west. The wind direction varies mostly around the southerly direction. At 11:00 in the morning the wind tends to a south-south-easterly direction and around 16:00 in the afternoon the wind tends more to a south-easterly direction.

44
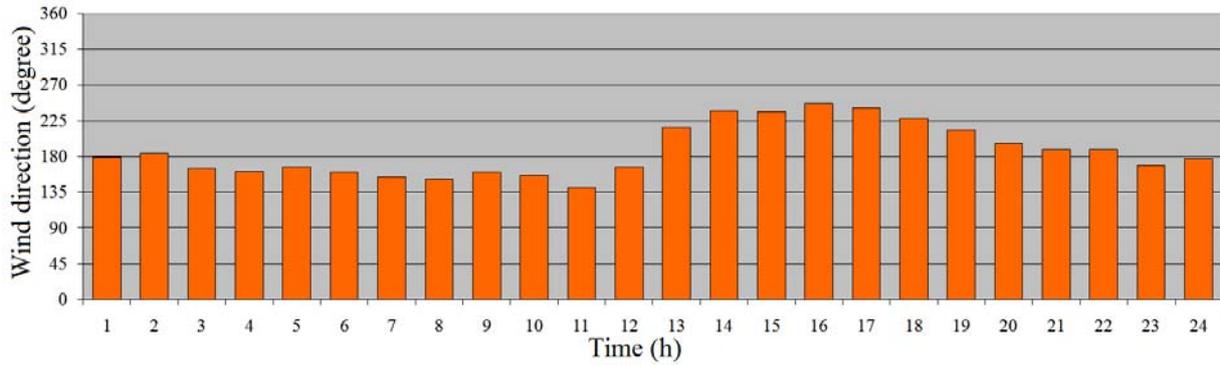
Figure 21: Average wind direction over a one day cycle

4.1.3   Wind profile generation and analysis

One problem with the wind data displayed in section 4.1.2 is the fact that it was averaged. Averaging wind data gives rise to the possibility of being misleading. If wind data in reality consists of high velocities and low velocities but few medium velocities, averaging the data will give many medium velocities, which is not representative of the actual wind occurring in the field. The same errors could be introduced by averaging the direction data over the measuring time period.

In this section the goal is to look at the different velocity profiles measured on the interdune location. Velocity profiles are formed due to the surface friction that decelerates the flow. The effect is then transported higher up with the help of viscous stresses in the flow. The profiles are categorised according to direction. Because the profiles were selected for their direction, the averaging errors are limited.

In this section velocity profiles are generated using the wind data measured in the field. A velocity profile with the shape of equation (2.2) is fitted to the selected data using the least squares method. Once the data is fitted and the values of b and m are known, the friction velocity u^*_{ABL} and surface roughness height z_0 can be calculated with the help of equations (4.1), (4.2) and (4.3). It is also possible to add weights to the data points and in this way influencing the curve fitting according to confidence levels of the corresponding data point. The surface roughness height and the friction velocity are used in the simulations for the inlet boundary condition by implementing it in equations (2.2), (2.3) and (2.4) for the k-ε turbulence model.

$$z = bm^u \tag{4.1}$$

$$z_0 = b \tag{4.2}$$

$$u^*_{ABL} = \frac{\kappa}{\ln(m)} \tag{4.3}$$

Figure 22 shows the velocity profile fitted to the measured data with Matlab 7.5.0 (R2007b) software. The data for the four lower points represent the short mast data while the four higher points represent the long mast. Both were positioned on the interdune. The profile shown is of a westerly wind direction. Analysing the profile higher up than the 12 m as displayed in Figure 22 reveals little change in speed, giving a flat appearance to the velocity part of the profile. Furthermore, the profile appears relatively square, relating to little flow development. The square shape is characteristic of a turbulent flow.
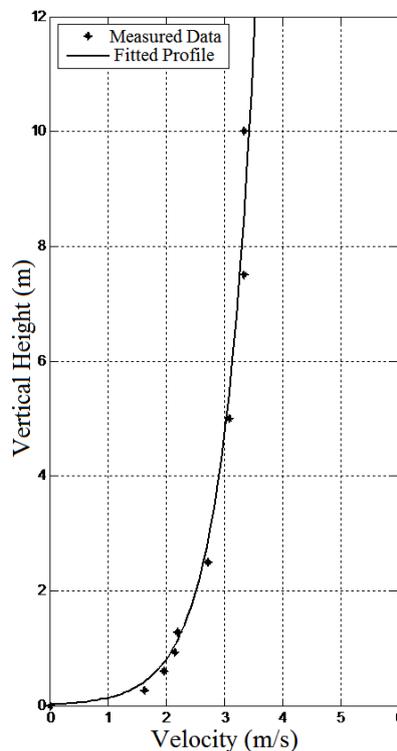
Figure 22: Velocity profile showing measured data along with fitted profile

Valuable information can be gained by analysing the various velocity profiles. Figure 23 shows the normalized velocity profiles for the different wind directions. In Figure 23 it can be seen that the velocity profiles for all the wind directions show very similar flow development with the exception of the south wind. The similarity in the east and west wind profiles supports the positioning of the wind mast on the interdune as well as the choice of study site. This is because the dunes are orientated from north to south and the mast was placed approximately halfway between the dunes. For a representation of the mast positioning on the interdune please refer to Figure 12 and Figure 13.
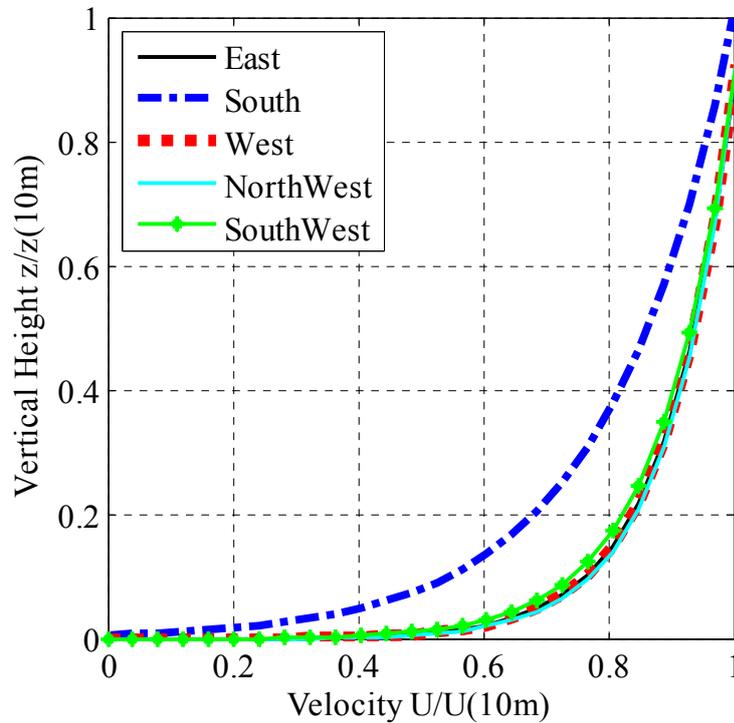
Figure 23: Velocity profiles for different wind directions on the interdune

In Figure 23 it can be seen that south wind profile shows a more developed boundary layer than that of the east and west winds. The boundary layer development is recognised by how high the effects of surface friction have been transported across the flow by viscous stresses. In other words the south wind profile is slower than the west and east wind profiles in the near surface region. The flow is more developed since it is noticeable that the low velocity has had time to spread to higher flow stream due to viscous effects. This makes sense since the south wind has the whole interdune to develop without any significant dunes in its path while the east and west winds have only a short distance with large dunes on both sides.

The next part of the wind analysis is to compare the west wind profiles. This will give an idea of what happens to the velocity profile as it moves up the dune slope. When considering the profile data the mast placement as displayed in Figure 12 should be kept in mind. In Figure 24 it can be seen that the wind profile on the interdune is fairly well developed. The profile becomes squarer as the wind near the surface is forced to accelerate up the slope.
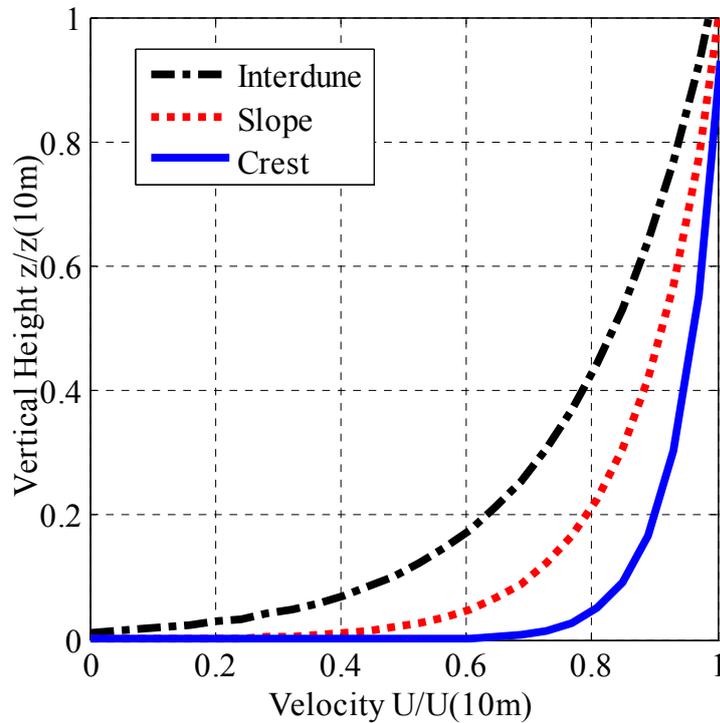
Figure 24: Wind profile for different positions on the dune

It would be very time consuming to simulate all the wind directions observed in the field. Therefore it is decided to select one or two profiles from the ones studied and implement them in the simulation inlet boundary. From all the velocity profiles the west wind profile is selected for the simulations purposes. The reason why the west wind is selected is because it has been shown to have the same shape as that of the east and south-west winds which makes it representative of a wider range of wind condition. The west wind would also give a good indication of what would happen when the wind strikes the dune perpendicularly. From the simulation it would be possible to study the profile shape as it moves up the dune slope in a similar manner as have been done in this section. The simulation may be verified in this way.

4.2 Computational Fluid Dynamics Simulation Results

In this section the results for the two-dimensional simple dune simulations and three-dimensional actual dune simulations are discussed. The results for the flow over a flat plate as well as the flow over a simple three-dimensional dune are not discussed since it was only done to supplement the other simulations.

4.2.1 Steady flow over a simple two-dimensional dune

In chapter 3 the approach and reasoning behind the two-dimensional simulations were explained. Working with unfamiliar software with highly complex and unstable flow patterns necessitates

48

the reduction of some of the variables involved. By restricting the flow to two dimensions greatly simplifies the implementation of boundary conditions making it easier to learn the software. Furthermore, the computational resources are significantly reduced meaning quicker results and greater opportunities for implementation of various turbulence models and discretization schemes. Another motivation for conducting two-dimensional simulations is to identify simple flow features associated with flow over a low hill and then to compare it to the studies previously documented. In this section the results from these simulations are explained as well as how the results were obtained.

The mesh generation involves creating a two-dimensional mesh that provides the simple dune shape. Since OpenFOAM-1.5 uses unstructured meshes it is possible to apply grid refinement only to the areas that require high resolution. In the literature review it was seen that these areas of refinement are usually necessary in regions of high vorticity magnitude and the vorticity magnitude is usually high in boundary layer as well as wake regions (Kim and Boysan, 1999). Refinement along the boundary layer is increased until y^+ values progress to the desired range. Furthermore, refinement in the recirculation region is applied to capture the smaller recirculation patterns. The two-dimensional mesh is displayed in Figure 25 with a magnification around the dune region. The reason why the dune appears so flat is because it is in reality a lot wider than it is high. The dune is approximately 10 times as wide as it is high.
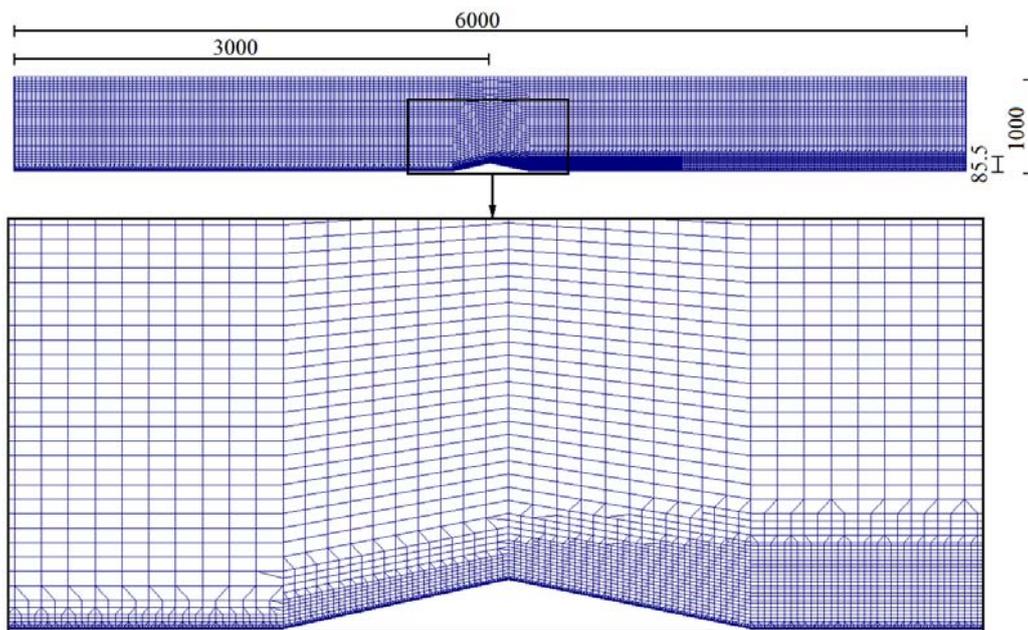
Figure 25: Two-dimensional mesh displaying refinement around the dune

It should also be mentioned that the inlet region is extended far from the dune to allow for flow stabilisation. This allows the ABL profile to stabilize and turbulent inlet noise to dissipate reducing effect on the results. The ABL turbulent inlet is taken from the measured velocity profiles in the field. The dune surface boundary is a no-slip surface with wall functions. The upper atmosphere boundary is modelled as a symmetry plane. This is a reasonable approximation since even though the velocity profile is not completely flat, it is flat enough at the

height of the boundary to have negligible effects on the flow field and therefore the results. For the purpose of explaining the results the whole mesh will not be displayed but rather a close-up view of the dune and suspected recirculation region.

Some stability problems were encountered with the mesh due to the presence of high skewness characteristics especially in the boundary layer cells near the crest region. This problem was reduced by refining the mesh in the flow direction but came at the cost of added computational requirements. Although not explicitly displayed at this point, the simulation results presented subsequently all conform to convergence and y^+ requirements. The simulation requirements such as convergence, y^+ and grid independence are discussed in more detail in section 4.2.2 and 4.2.3 for the three-dimensional simulations.

By analysing the pressure field in Figure 26 a high pressure can be identified at the toe of the windward slope. A low pressure can be identified at the crest. The high pressure zone at the dune toe results from the flow stagnation in the region due to the dune geometry in the flow path. The low pressure region near the crest corresponds to the separation in that area as well as the rapid expansion in local flow area. It is important to keep in mind that the pressures displayed in this report are represented in the kinematic form (P/ρ), as it was used in OpenFOAM by the incompressible solver. The pressure is displayed relative to a zero pressure outlet boundary.
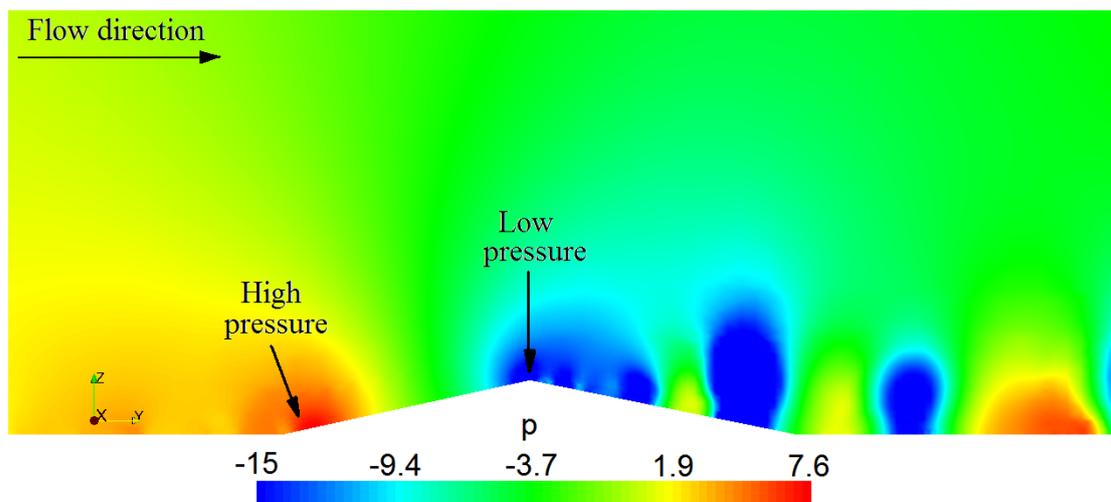
Figure 26: Relative pressure field over a simple two-dimensional dune

Another way of explaining the pressure zones is to observe a flow particle moving near the surface. As this particle is obstructed by the dune toe it is forced to slow down and change direction. The particles heap up in front of the dune and the pressure increases. Furthermore, the only way to justify the sudden decrease in velocity of the oncoming flow from the mathematical point of view is to have an adverse (increasing) pressure gradient. This explanation relates to the flow in a lid driven cavity where the flow is forced to move by the lid but also to stop where the moving lid and wall meet. This causes the pressure to increase in the corner.

The pressure increase at the dune toe region was also investigated in more detail by looking at pressure coefficient and total (stagnation) pressure plots. The pressure coefficients showed that the static pressure increase was more or less 15 % of what would have occurred if the free-stream stagnated at the dune toe. The total pressures showed that the static pressure increase and velocity decrease at the dune toe cancelled one another out. Both the pressure coefficients and total pressures supported the flow fields predicted. These are not included here due to space limitations.

The velocity magnitude plot in Figure 27 shows a low velocity at the dune toe and lee-side eddies. High velocities are observed at the crest as well as at the top of recirculating vortex structures. The low velocity at the toe corresponds to the presence of a high pressure region and the high velocity at the crest relates to a low pressure region that is present near the crest. High acceleration corresponds to the pressure gradient between the high and low pressure zones.

The velocity magnitude compares well to a previous study by Parsons *et al.* (2004) (not detailed here due to space limitations). The big difference in the two flow fields occurs in the recirculation zone where the second order scheme used in this project produces more flow features than observed from the first order upwind differencing scheme used by Parsons *et al.* (2004). It should be noticed that first order upwinding scheme is only used to stabilize the initial flow simulations. The comparison of the results for the two differencing schemes is discussed later in this section. The upwind scheme results compare very well to that of Parsons *et al.* (2004) who used a first order differencing scheme in their work as well.
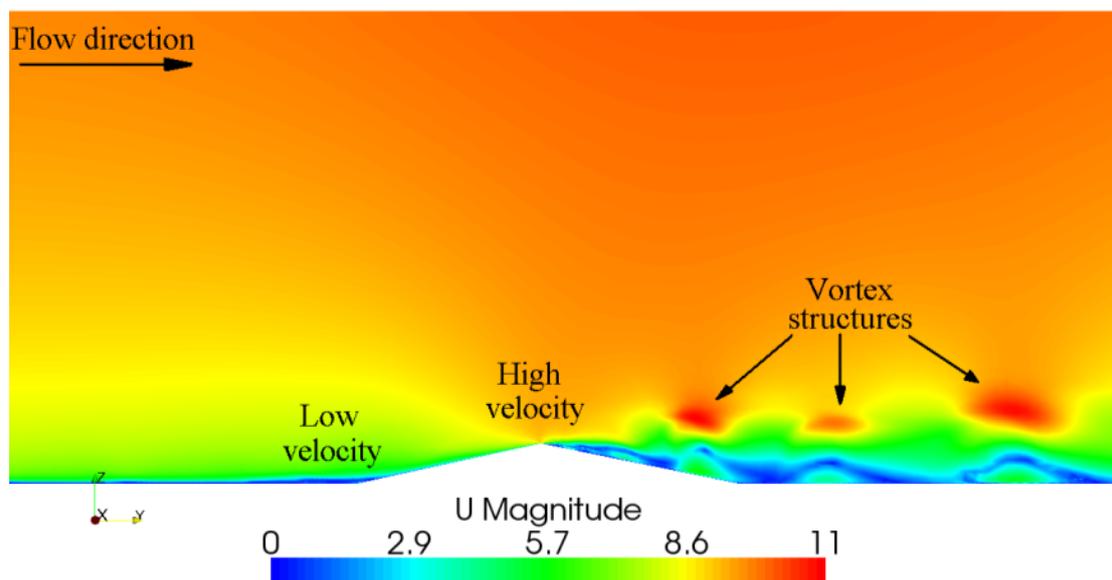
Figure 27: Velocity magnitude over a simple two-dimensional dune

It can also be seen that the vertical spread of velocity magnitude becomes less as one moves up the windward slope. This means that the distance between the high and low velocities, vertically, are greater on the windward interdune than on the slope. The spread of the velocity magnitude vertically may be better understood when considering the velocity profiles which will be done

51

next. For the moment it should just be noted that the thinner the spread, the more square the velocity profiles. This simply means the nearer the high velocity comes to the surface indicates flow acceleration especially near the surface so that the lower part of the profile if filled up. This was also observed with field measurements as explained in section 4.1.3.

In Figure 28 selected velocity vector profiles and stream lines are shown. From Figure 28 five recirculation zones are identified. The larger ones are on the lee-side which is expected. One smaller one occurs at the dune toe region of the windward slope. This recirculation zone, however, is not observed in the field. It is suspected that this recirculation zone occurs due to the sharp corner at the toe which resulted from the simplified dune geometry. This recirculation zone does provide some relevant information since it is very possible that a sudden change in wind direction could cause a flow to occur up a slip face resulting in a similar recirculation zone. The low velocity recirculation would initially encourage particle deposition. When the corner is filled up deposition will stop and be replaced by erosion along the rest of the windward slope.
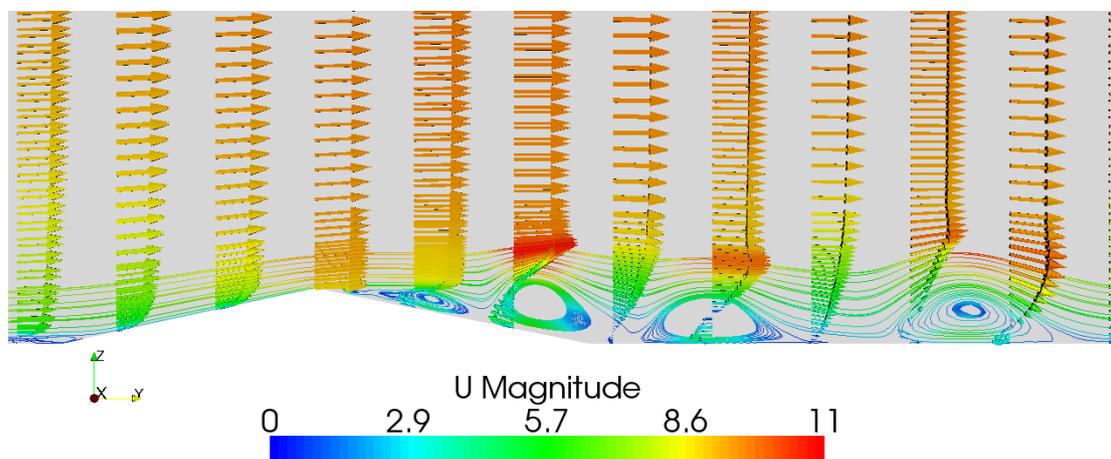
Figure 28: Flow field over a simple two-dimensional dune showing velocity profiles as well as recirculation zone with streamlines

A similar process is described by Wiggs *et al.* (1996) where the effect of streamline curvature on particle transport is investigated in addition to the traditional streamwise acceleration. Similar to the findings of Wiggs *et al.* (1996), the areas where streamlines converge are associated with high velocity and low pressure. This can be seen around the crest region. Furthermore, Wiggs *et al.* (1996) explains that the toe region will experience deposition of particles until the recirculation disappears. Although low velocities will still be present, any further deposition will be prevented by the concave curvature of streamlines that would increase the surface shear stresses. Along the windward slope erosion is expected due to increased surface stresses that result from streamwise acceleration as well as concave streamline curvature. The convex streamline curvature along with streamwise deceleration promotes deposition in the lee-side of the dune as particles in the flow field looses momentum and drops to the dune surface. The particles would be swept up again by recirculation flow towards the crest. The transport of particles in the recirculation zone is promoted by concave streamline curvature towards the crest as well as slight acceleration up the lee-side slope. This slight acceleration is also noted by Wiggs *et al.* (1996).

52

The streamlines show clear separation on the lee side. The exact point of separation and reattachment can be located by plotting the surface shear stress. Where the shear stress is close to zero separation or reattachment occurs. One way to look at separation is to consider a point along the surface where the flow from up- and downstream flow to the same point. The downstream component originates from low velocity recirculation. At this point the flow moves away from the wall which is called separation. This separation point results in the low pressure zone near the crest. Similarly a point where flow is towards the surface and then spreads out in up- and downstream components is called a reattachment point.

For a particle to become airborne it needs to be swept up by high shear stresses on the surface. The altitude the seed particle will ultimately achieve would depend on the vertical velocities it experienced during its flight, the mass as well as the fight appendages that creates the particle drag. Sand particles are small, dense and relatively round, giving them a small drag and they therefore need a relatively high shear stress to be swept up and high velocity winds to keep them up. Even with high winds sand particles seldom get transported high in the air but rather bounce along the surface. The particles of interest in this project are not sand but rather plant seeds. The seeds have wing appendices to improve their lift. The seeds require very little wind to be transported and would be greatly affected by the vertical components of the flow. The vertical components of the flow are shown in Figure 29.
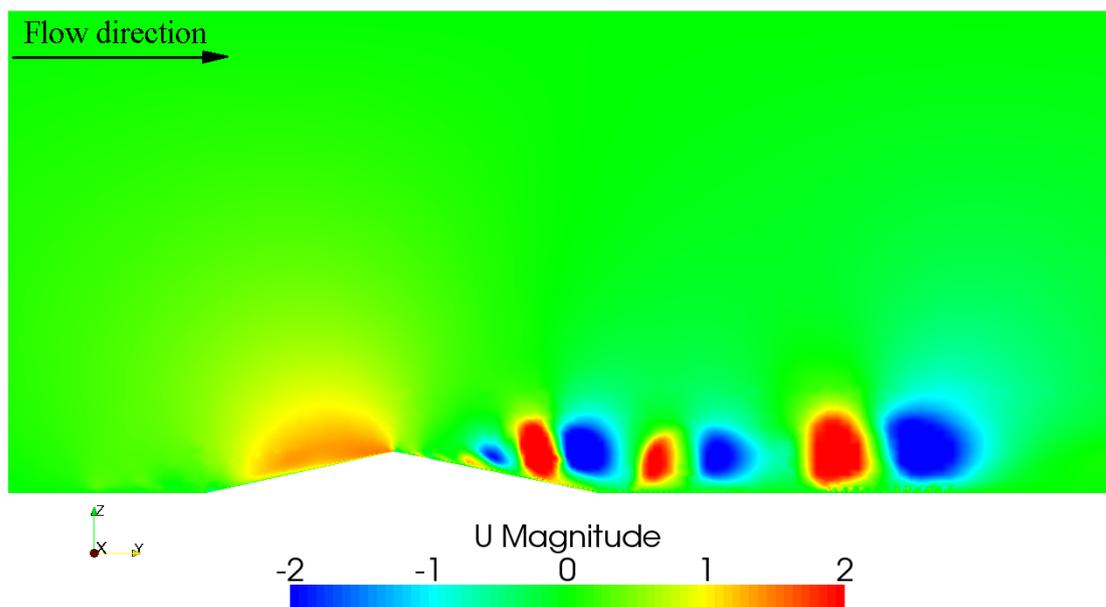
Figure 29: Vertical velocity magnitude over a simple two-dimensional dune

Figure 29 shows upward velocity components along the windward slope due to the shape of the dune geometry. In the lee-side velocity components correspond to vortex structures that are present. Each vortex has an upward component on its windward side and a downward component on its lee-side. The regions give insight to where a particle will be lifted or forces down if already airborne. From Figure 29 the particle would be lifted up rapidly on the windward slope as it nears the crest. Once over the crest, a down force would be experienced. If

53

the particle drops to the surface the upward velocities would promote further transport back towards the dune. Since a recirculation zones exits on the lee side, the particles in this region are expected to be transported back towards the dune crest. The particles might be caught up in the recirculation or might come to rest in regions where the velocities are too low to facilitate transportation.

The results from the two-dimensional simulations have been shown to compare well to previous studies by Wiggs *et al.* (1996) and Parsons *et al.* (2004) but a detailed discussion is omitted at this point due to space limitations.

The two-dimensional simulations provide the ideal opportunity to investigate the effect of various computational fluid dynamic models such as differencing schemes and turbulence models. At first upwind differencing schemes were considered to ensure stable solutions. Second order differencing scheme were implemented for the final results. A comparison of upwind and central differencing schemes is shown in Figure 30.
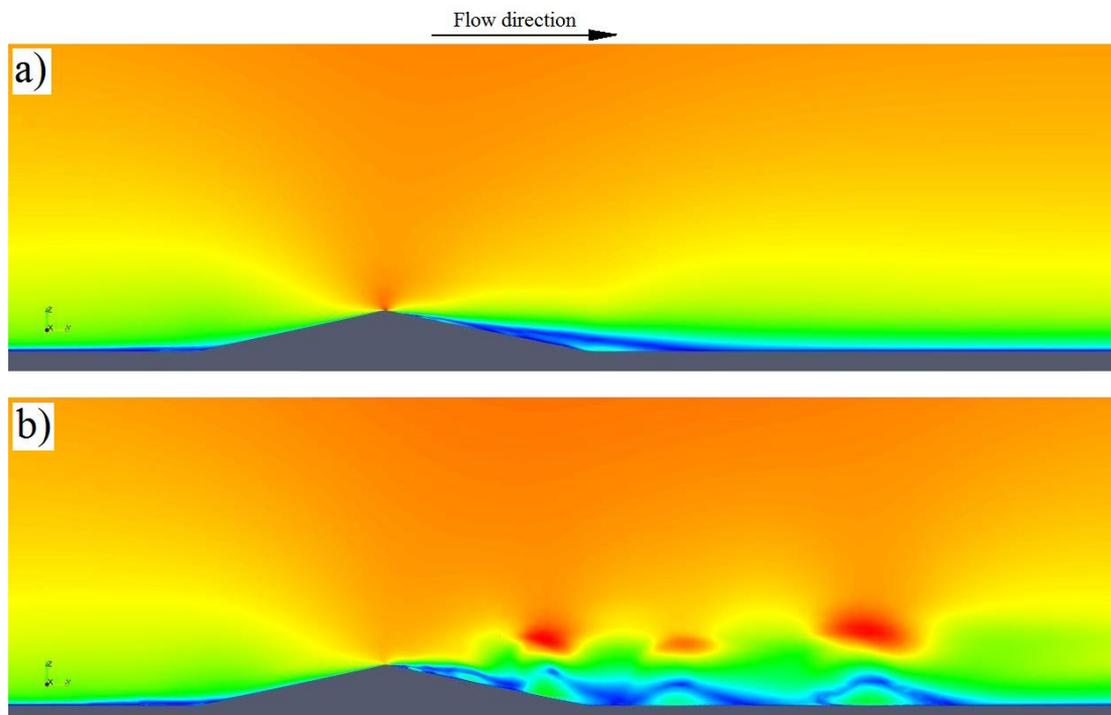
Figure 30: Velocity magnitude display used to compare differencing scheme orders of accuracy: a) first order differencing and b) second order differencing

From Figure 30 the comparison of the differencing scheme shows the velocity magnitude fields of the two simulations. As explained in section 3.4.3, the GAMMA differencing scheme is a blending/switching scheme where central differencing is used for the bulk of the flow but which switches to a blended scheme where flow tends to cause unboundedness. The two solutions compare well in the bulk flow where the velocity magnitude is almost identical. Both solutions have a low velocity zone at the dune toe on the windward side and a high velocity at the crest.

54

However, a significant difference is visible in the recirculation zone. More complex flow structures are detected by the higher order differencing schemes. Upwind differencing shows one clear recirculation zone while the higher order scheme shows a number of vortex structures. The vortex structures result in higher velocities higher in the atmosphere as well as along the surface. The high velocities correspond to the outer perimeter of vortex structures while low velocities occur at the centre. Because of the rolling action of the vortex structures energy is transported from the high to the low velocity regions near the surface. The results show that for the upwind differencing scheme grid convergence was not achieved.

The difference in flow produced by the differencing schemes will result in different seed distribution patterns. Higher velocities in the upper atmosphere due to large vortex structures may propel particles far from the dune. The presence of low velocity zones between the vortex structures may cause particles in this area to drop to the surface. Furthermore, increased velocity near the surface may result in particle transportation towards the dune.

The major differences observed between the two schemes motivate the use of a second order differencing scheme for all simulations. To maintain a degree of stability, second order differencing is used rather than any higher order scheme since the stability gained is preferred to the small increase in accuracy provided by third and fourth order accuracy differencing schemes. Furthermore, since this steady state simulation struggled to converge, it is concluded that the flow features for this geometry appear to be inherently unsteady. This motivates carrying out time dependant simulations. The results for the time dependant simulations are discussed in section 4.2.3.

In the computational methodology it was mentioned that different turbulence models are considered for the two-dimensional simulations. The models that were implemented include the standard k-ε model, the RNG k-ε model and the realizable k-ε model. The results given above are from the realizable turbulence model since it is more generally accepted in the CFD community due to its ability to more accurately reproduce the flow in areas where the standard k-ε model is insufficient (i.e. recirculation flow).

However, it was decided to investigate the effect of the different turbulence models and to compare the results. It is difficult to compare the results due to the unsteady nature of the flow. Still, the results can be seen in Figure 31 and show very little difference for the three models. The standard k-ε model and the RNG k-ε model show almost identical results. The most significant dissimilarity occurs in recirculation zones where the standard k-ε model and the RNG k-ε model predict an extra recirculation zone further away from the dune. Because of the additional recirculation zone found in the standard k-ε model and the RNG k-ε model, the reattachment point is predicted further from the dune, which translates to a larger recirculation zone.

55
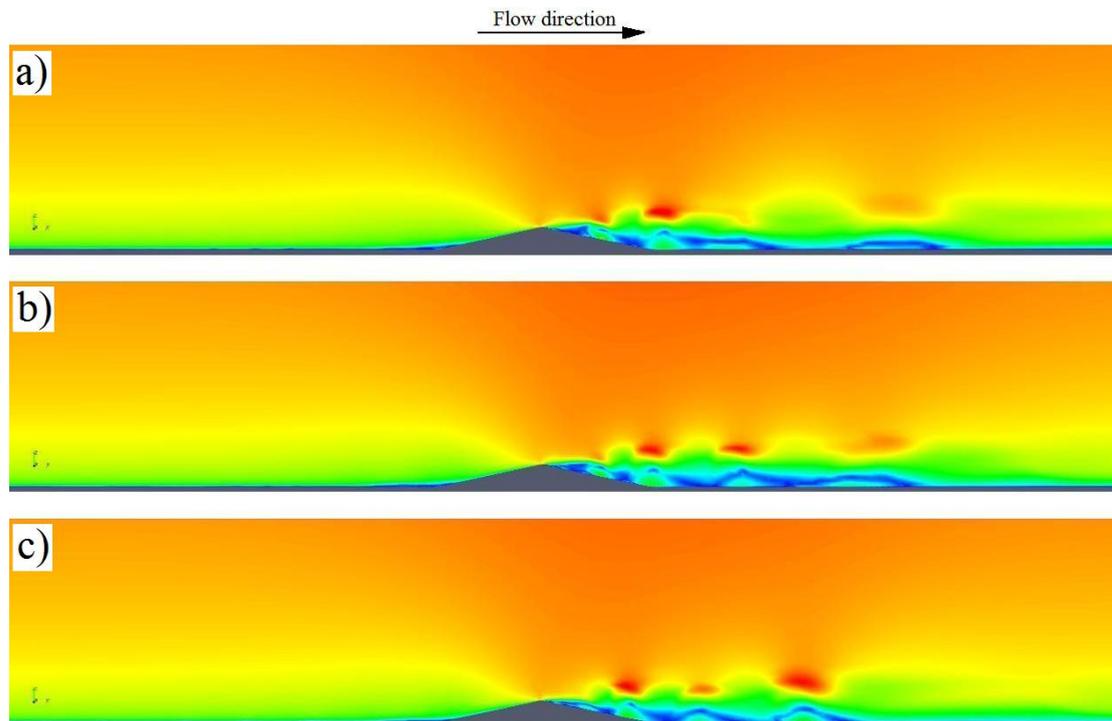
Figure 31: Turbulence model comparison: a) standard k- ε, b) RNG k- ε and c) realizable k- ε

4.2.2   Steady flow over an actual three-dimensional dune

The two-dimensional simulations provided valuable insight with regard to the flow features associated with the cross-section of the dune. Furthermore, the two-dimensional simulations also presented the opportunity to investigate the difference between first and second order differencing schemes as well as different RANS turbulence models. However, the actual dune is a much more complex geometry and through observations in the field the flow features, even with steady wind conditions, appeared highly unsteady and three-dimensional beyond the crest of the dune. Furthermore, this observation was confirmed in literature by Kim and Boysan (1999) who mentioned the unsteady and three-dimensional nature of environmental flow patterns. It is therefore considered important to investigate the near surface wind patterns over the actual dune geometry as mapped in the field.

In this section the flow is once more analysed at a steady state to investigate the average flow features that result from the dune geometry. The transient or unsteady nature of the flow will be looked at in the next section. Furthermore, from the two-dimensional simulations it was established that a second order differencing scheme is necessary. The realizable turbulence model is chosen to reproduce the effect of turbulent flow features.

In order to have a degree of confidence in the results without the help of extensive experimental results to validate them, makes it important to have a number of checks to which the simulation must agree. The first check is to make sure convergence is achieved. This is done by checking the residuals of the simulation which gives an idea of the errors in the different governing

56

equations over time. The errors in the governing equations should be low but also unchanging for convergence to be achieved. The residuals are displayed in Figure 32. From Figure 32 it can be seen that the residuals have reduced significantly and it appears to be unchanging, therefore motivating simulation convergence has been achieved. As an additional convergence check the relative pressure at various points along the dune was monitored. All the points showed initial oscillation and then clear convergence which further motivates that solution convergence has been achieved. In Figure 67 the relative pressure showing convergence over the initial part of the simulation can be seen in Appendix J.
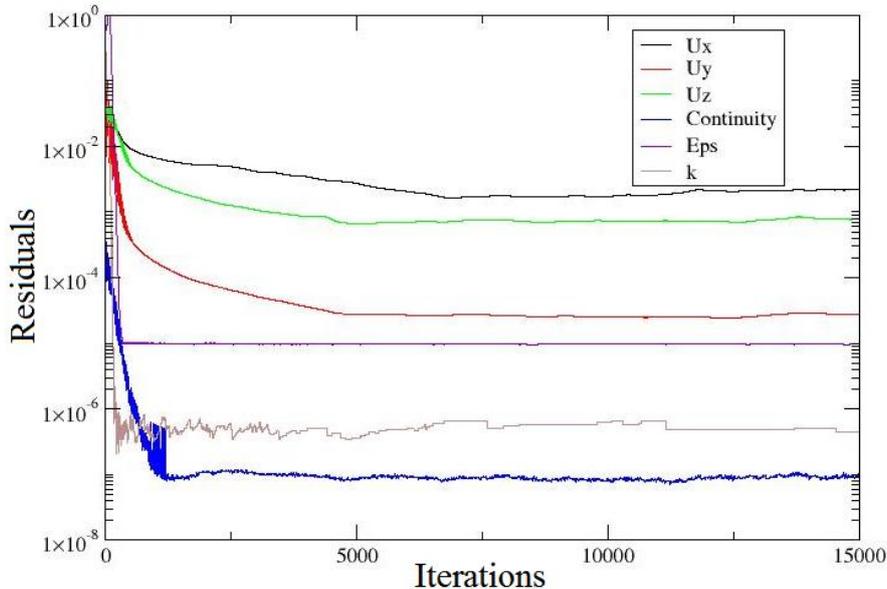
Figure 32: Three-dimensional RANS simulation residuals

Convergence means that the solution for the specific mesh has been achieved. It, however, does not mean that the solution will be the same for a different mesh. To make sure the solution is independent of the mesh, grid independence has to be achieved. Grid independence is obtained when the solution stays the same while a finer mesh is used. Testing for grid independence is difficult for this project since it requires refinement of the mesh which is associated with significant increase in the computational load. Since the mesh used already consists of approximately 7 million cells, refinement will result in an impossible load for the computational resources to handle.

It is decided to adjust the refinement of the mesh in the wake region to see if the flow field shows significant changes. Similar refinement was conducted in work done by Kim and Boysan (1999) which showed a decrease in the extent of the recirculation zone. It is therefore decided to refine the recirculation region in order to see if grid independence has been achieved. The different meshes can be seen in Figure 33. The flow results from these meshes are displayed in Figure 34.

57
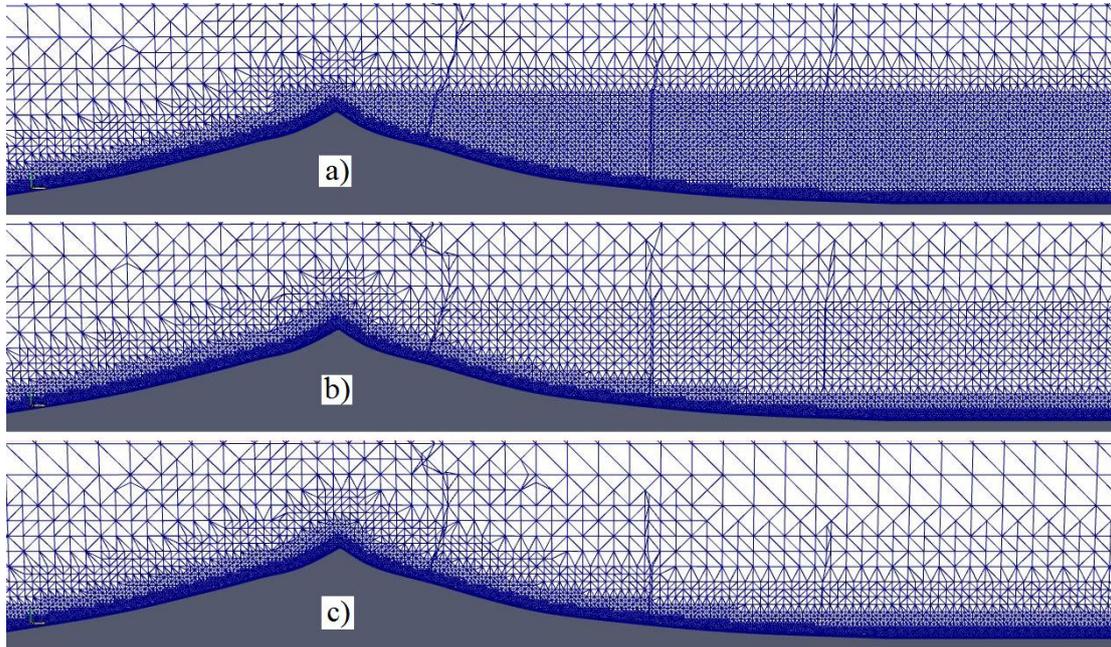
Figure 33: Grid independence meshes: a) fine, b) medium and c) coarse mesh
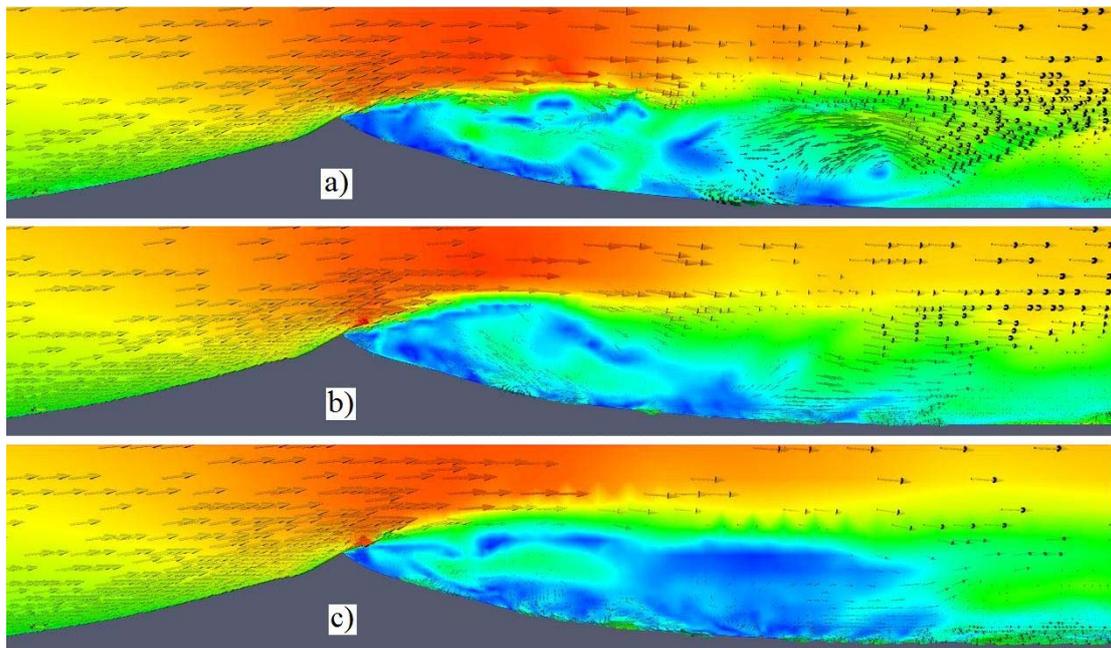
Figure 34: Grid independence flow results: a) fine, b) medium and c) coarse mesh

The results from the three meshes show very similar flow features especially in the bulk flow. Some differences that are observed in the recirculation region include smaller eddies as well as a finer velocity spread between the low and high velocity regions for the refined meshes. The overall recirculation region appears to be of similar size for all the meshes since reattachment

58

occurs in more or less the same area. Since the flow for these steady state simulations appeared very unsteady during simulation the change in flow features are attributed more to the unsteady flow than to a change in mesh. This unsteady characteristic means if more simulation iterations were conducted, the local flow features are expected to change again but the global flow remains steady. As an additional grid independence check the velocity profile is checked on the lee-side of the dune which includes the refinement area. The velocity profiles are shown with Figure 69 in Appendix J. The comparison shows decreasing difference in the profiles with increasing mesh refinement. Therefore since the reattachment point is relatively at the same distance from the dune crest and the velocity profile shows convergence with increasing mesh density it is accepted that grid independence is achieved at this point.

Since wall functions are used it is important to achieve the necessary range of y^+ values for which the wall functions are valid. High Reynolds number turbulence models that are used require the first cell centre adjacent to the wall to be placed within the logarithmic part of the boundary layer which relates to a y^+ value within the range of 30 to 500.

The wall function requirement is difficult to achieve due to the range of velocity magnitude that is experienced over the dune. Very low velocities at the windward toe region as well as just past the crest on the lee-side slope produce very low y^+ values in these regions. On the other hand, very high velocities at the crest produce high y^+ values. The difficulty lies therein to create a boundary layer mesh so that the y^+ values are within range throughout the entire flow domain. Just by looking at the crest region the short transition from high to low velocities due to separation makes it almost impossible to create a boundary layer that suits both. Since the majority of the domain lies within the acceptable range and the flat plate theory is less applicable at the high curvature regions of the crest motivates the acceptance of the mesh even though the y^+ values are at the outer extreme of the allowed range. The y^+ values of the simulation can be seen in Figure 35.
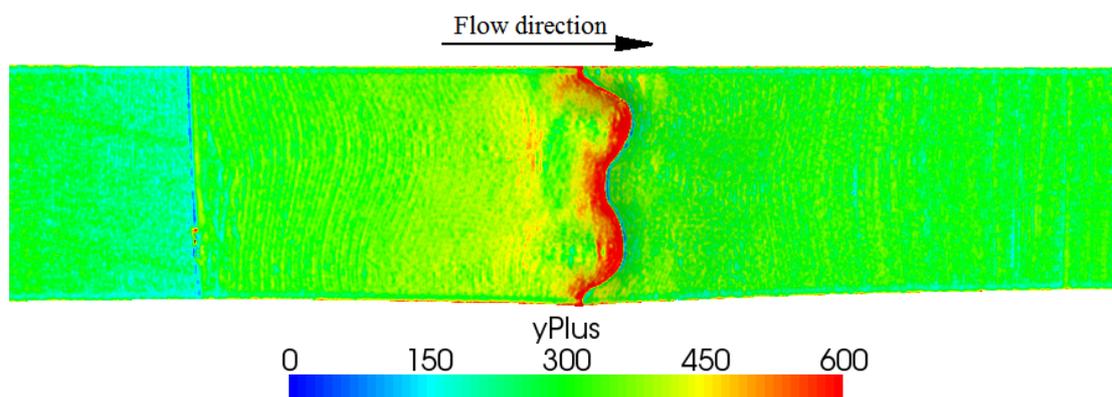
Figure 35: Three-dimensional RANS simulation y^+ values

It should be mentioned at this point that the importance of achieving convergence, grid independence and the appropriate y^+ values are taken very seriously. If more time was available these validation requirements would receive even more attention. However, due to the limitations in time and computational capacity the results presented here, even though not perfect,

59

are accepted for the educational purposes of this study. Now that an acceptable foundation with regards to the validity and computational accuracy of the simulation results is laid, the discussion of the final mesh may be presented and various flow features may be explained.

The final mesh is displayed in Figure 36. Again the boundaries are placed far from the flow domain in order to limit the effect on the flow area in consideration. Also, the grid refinement in different areas as well as the prism layer extending over the crest region should be noticed. Prism layers are extremely important for a number of reasons all of which are related to the accuracy of modelling the boundary layer and improving the near wall treatment. Due to the importance of prism layers on the flow the crest region is smoothed a little to facilitate prism layer meshing even though the boundary layer theory is less relevant in this high curvature region.

The prism layers next to the wall are fine to reduce the y^+ values. In Figure 36 it can also be seen how the layers grow towards the bulk mesh. The final layer ratio is at least 50 %. The expansion ratio as well as the final layer ratio was observed to have a significant effect on the stability of the simulation. A large final layer ratio, which relates to a mesh where the final boundary layer cells are much smaller than the first bulk mesh cell, caused instabilities due to high skewness that resulted.
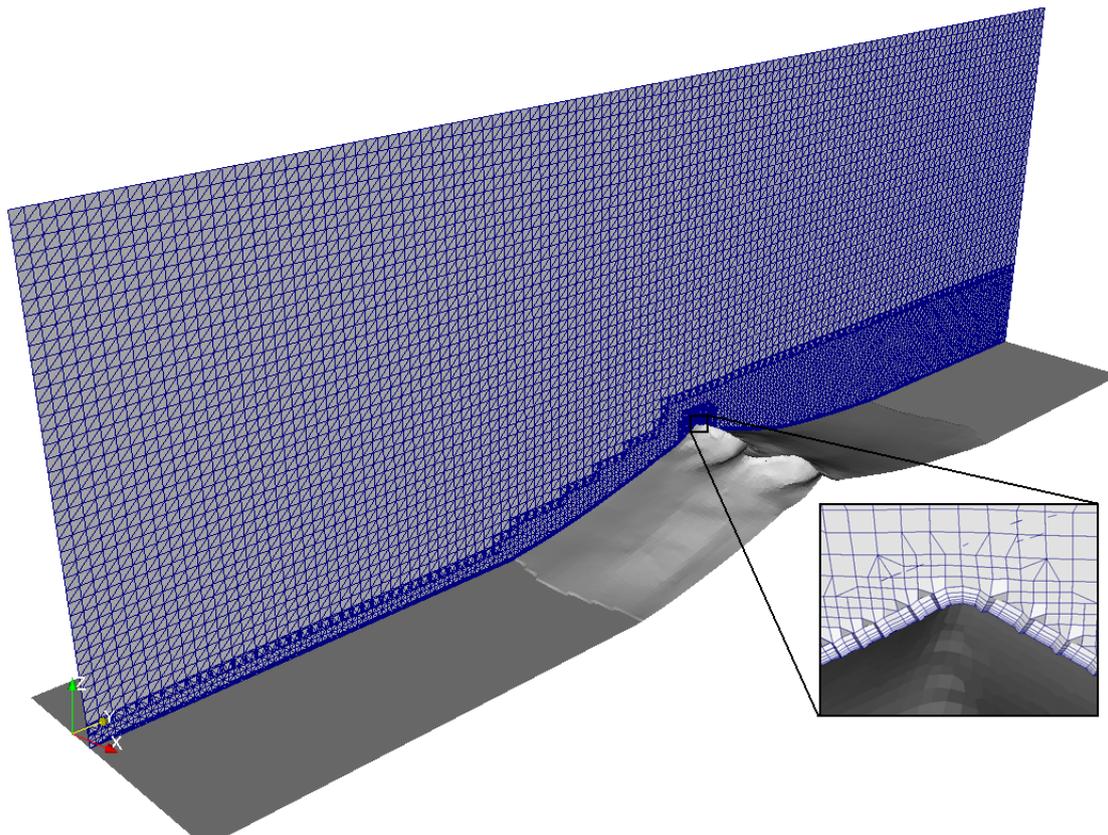
Figure 36: Three-dimensional actual dune mesh

60

In earlier simulations it was observed that the meshing of prism layers for a sharp crest would stop on the windward slope near the crest and restart again on the lee-side slope. The effect on the flow in this region caused a sudden diffusive point at the crest due to a sudden increase in cell size along the wall. The point is referred to as diffusive since low velocity is forces into the high velocity bulk flow which results in some deceleration. Another problem caused by the sudden increase in cell size is extremely large y^+ values in a region where the y^+ values are already quite large with prism layers present. This diffusive point is considered to deteriorate the accuracy in the crest region. These factors motivates the decision to smooth the crest a little to facilitate prism layer meshing. The effect of the absence of prism layers at the crest is shown in Figure 37.
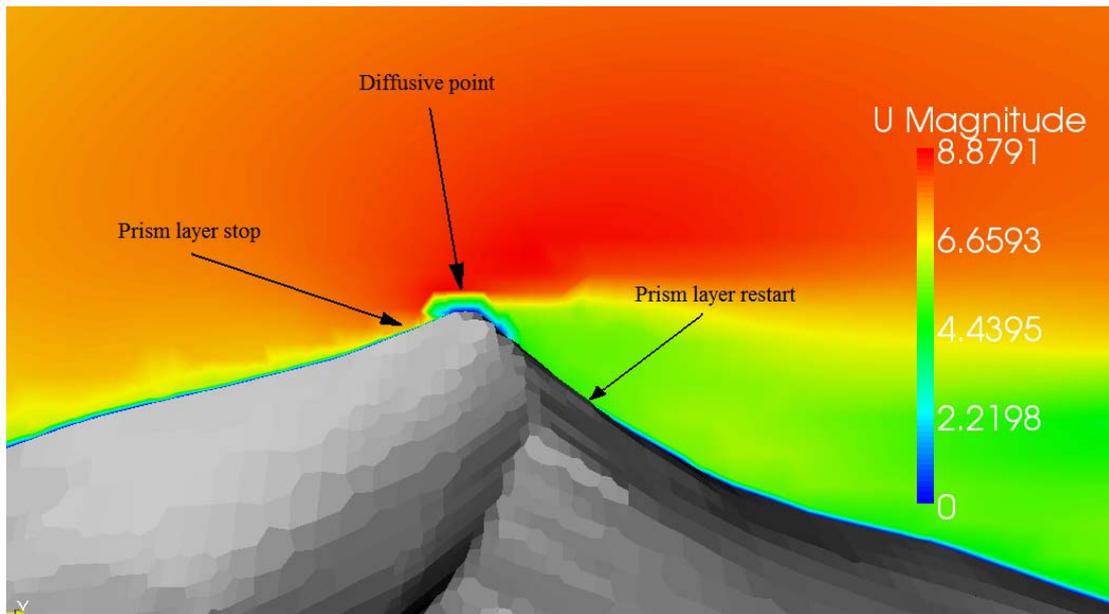
Figure 37: Diffusive point caused by sudden increase in cell size due to the absence of prism layers at the crest

Another motivation for smoothing the crest region a little before meshing is that it would have been done by the meshing software to some degree anyway. For the OpenFOAM-1.5 version the meshing tool SnappyHexMes is unable to do feature line meshing. This means that it would not be able to mesh the crest line exactly. It is only possible to approach the feature line by applying extreme refinement and even then the crest will have characteristic jagged edges. But the extent to which crest refinement is possible is limited by the computational resources available. The end result is an irregular crest edge which makes prism layer meshing in the area very difficult.

Furthermore, smoother crest edges are common in the Namib Desert. It may not always be visible from a distance but closer inspection show a number of dunes occasionally experience wind conditions that produce rounded crest edges where in some cases the crest radius is significantly larger than the one modelled. In Figure 38 (a) the rounded crest shape is visible. Even in cases where the crest has a clear edge line similar to that of Figure 38 (b) the effective radius is also large. It is therefore considered applicable, since it is observed to occur in the field, and favourable, since it improves the simulation accuracy, to smooth the crest edge and in so doing improve prism layer meshing over the crest.

61
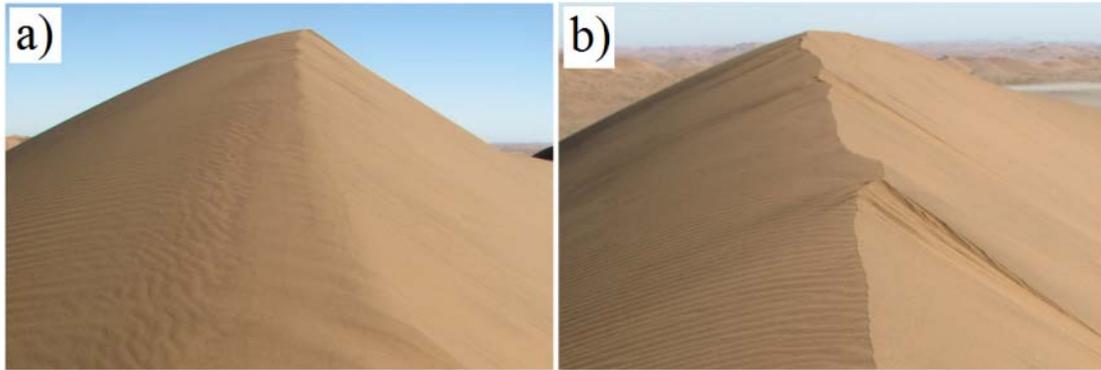
Figure 38: Dune crest shape: a) rounded and b) sharp edge crest

The flow field results discussion is started similarly to that of the two-dimensional simulations with the pressure field which is displayed in Figure 39. The pressure field show a high pressure at the dune toe, a low pressure at the crest extending to the lee-side and a higher pressure again at the lee-side of the dune. The position of the pressure zones compare very well with two-dimensional simulations results as well as literature. The magnitude of the pressure field differs considerably but this is strictly due to the different inlet flow conditions. The three-dimensional simulations results displayed in this section are based on a much slower velocity inlet condition than that of the two-dimensional results shown in Figure 26 and therefore the pressure extremes are also less.

The velocity field is displayed in Figure 40 and again shows a resemblance to the two-dimensional simulations. There exists a low velocity zone at the toe on the windward side, a high velocity at the crest and a low velocity recirculation zone on the lee-side. There is, however, a considerable difference between the vortex structures when comparing the two- and three-dimensional simulation results of Figure 27 and Figure 40 respectively. Where on the one hand the two-dimensional results in Figure 27 show clearly identifiable vortex structures in the recirculation region on the other hand the three-dimensional results of Figure 40 show more complex flow structures. With further investigation it is observed that vortex structures are greatly influenced by the three-dimensional shape of the dune.
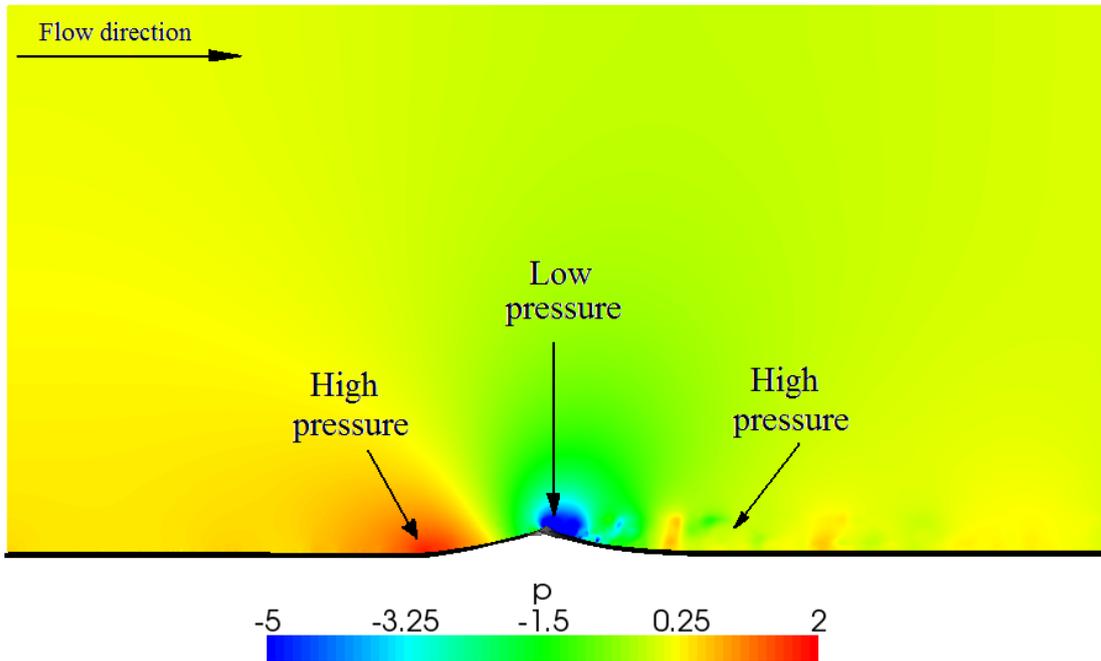
Figure 39: Relative pressure field over a tree-dimensional actual dune geometry
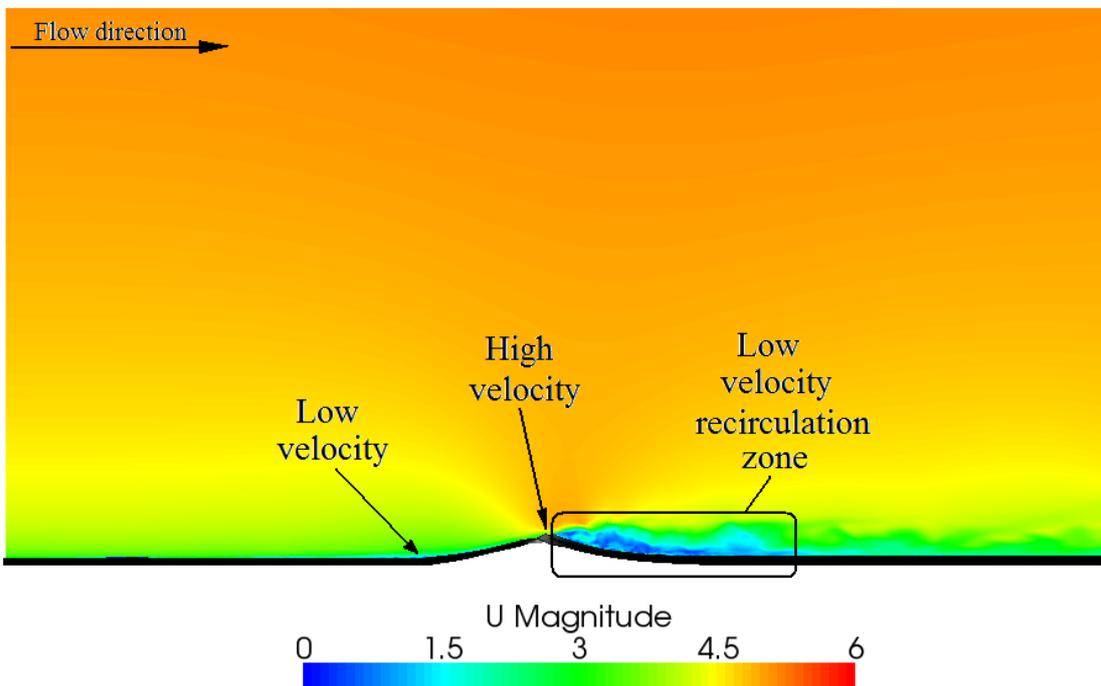
Figure 40: Velocity magnitude of flow over a actual three-dimensional dune geometry

Form Figure 40 it is clear that the approach flow is stable and fully developed. This confirms the use of the equilibrium ABL inlet conditions as well as the placement of the inlet condition so far

63

away from the dune. Furthermore, the free-stream velocity is the same all along the top boundary. This shows that the flow is unhindered by the boundary which supports the placement of the boundary so high above the dune surface. From the pressure and velocity magnitude results it is concluded that the boundaries placement is far enough to prevent influence on the flow region and therefore the mesh boundary configuration is considered acceptable. Note that a symmetry top boundary, as a less severe condition, was given preference to enforcing constant velocity and turbulent properties at the top boundary.

The first flow characteristic can be identified as a result of the curvature of the dune. Please refer to Figure 41. Flow approaching the dune at a right angle to the general dune direction will cross the dune crest first at the leading crest edge. Once the flow crosses the dune separation occurs and a recirculation zone is formed. Continuing further away from the crest the flow reattaches again. The difference in recirculation zone areas, however, causes cross flow to occur.
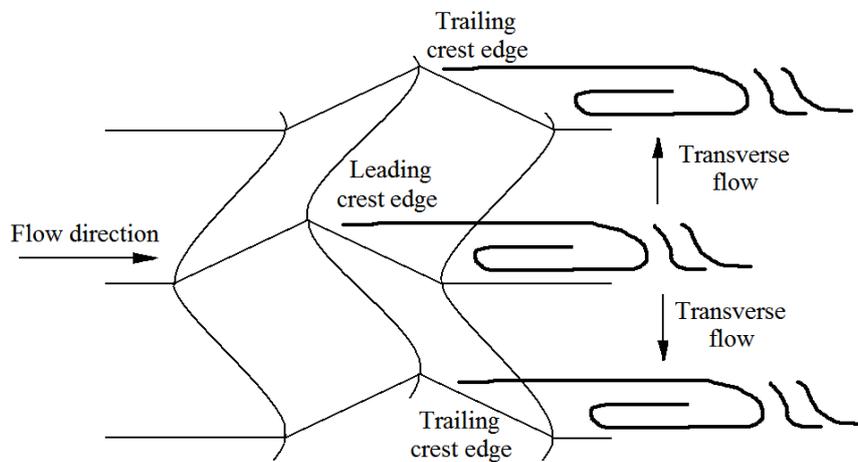
Figure 41: Effect of crest line curvature on resurculating flow

Another way to explain this cross flow is to consider the different pressure zones again. Considering the pressure zones that result because of the flow over the dune as in Figure 39 and the fact that these pressure zones will be misaligned due to the curvature of the crest line will result in cross flow to occur. A low pressure exists in the recirculating vortex as was seen in the two-dimensional simulation results. At the reattachment point and further away from the recirculation zone, however, a higher pressure region is present. Because the flow is driven by the pressure zones the effect of the low pressure zone in the vortex structures behind the trailing crest edge is therefore to draw air from the leading crest edge vortex and reattachment point. In the process the leading edge vortex may reduced in size. This draught of air disturbs the vortex structure and reattachment flow and form spiral shaped mixing of the flow moving away from the dune.

A second flow characteristic that can be identified is a helix vortex structure that is formed perpendicular to the flow due to the angle at which the flow crosses the crest line. This helix vortex can be seen in Figure 42. The rolling motion of the vortex is formed by the perpendicular component of the flow with respect to the crest line that causes separation and then a rolling

64

motion. This vortex then forms a helix due to the parallel flow component with respect to the crest line that causes the rolling vortex to be offset parallel to the crest line.
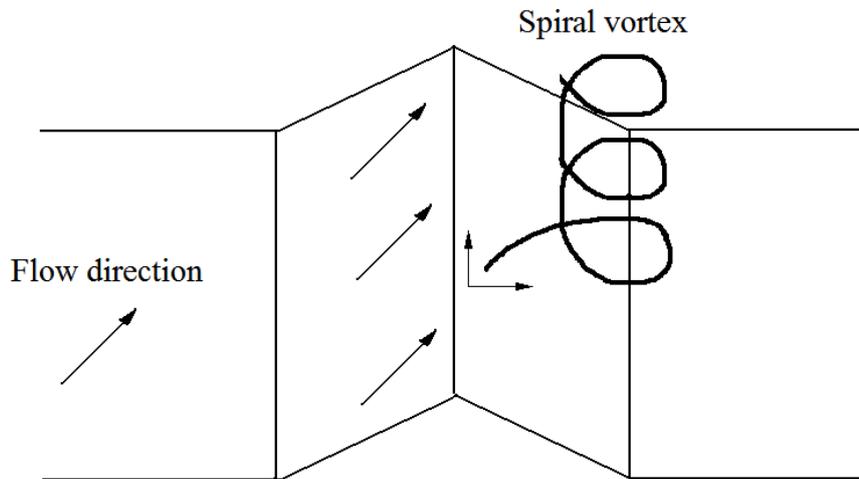
Figure 42: Effect of oblique approach flow on recirculation zone

A similar helix shaped flow feature was observed by Tsoar (1978) using smoke flares during an approach flow at and oblique angle to the crest line. The helix or spiral shaped vortex structure can occur in regions where the approach flow is at an oblique angle to the crest line or in other words regions where the crest line is at an oblique angle to the approach flow. Even with a perfectly perpendicular approach flow angle there are many regions where the crest line is at an oblique angle to the approach flow due to the snake like curvature of the crest line of the dune. In the dune model used in this study the helix vortex may occur in the regions between the leading and trailing crest edge curves during a perpendicular approach flow as considered in this study.

Considering the wall shear stress magnitude displayed in Figure 43 a number of valuable information with regards to the flow features as well as particle transport can be identified. The wall shear stress magnitude scale has been modified to increase the contrast between high and low velocity regions to aid with the feature identification process. The first thing to mention is that the wall shear stress is directly related to the velocity. High wall shear relates to high velocity regions and low wall shear stress relates to low velocity regions. The first thing that should be noticed is the difference between the windward and lee-side. The windward side appears predictable and orderly where on the other hand the lee-side appears very confusing and unstructured. It is possible to identify the flow acceleration up the windward slope, high velocity region at the crest and low velocity on the lee-side of the dune. On the windward side it is also possible to identify the depressions near the crest region that causes low wall shear stress magnitude just before the crest. Furthermore, it is possible to identify different flow acceleration rates up different regions of the dune due to the three-dimensional shape of the approach slope.
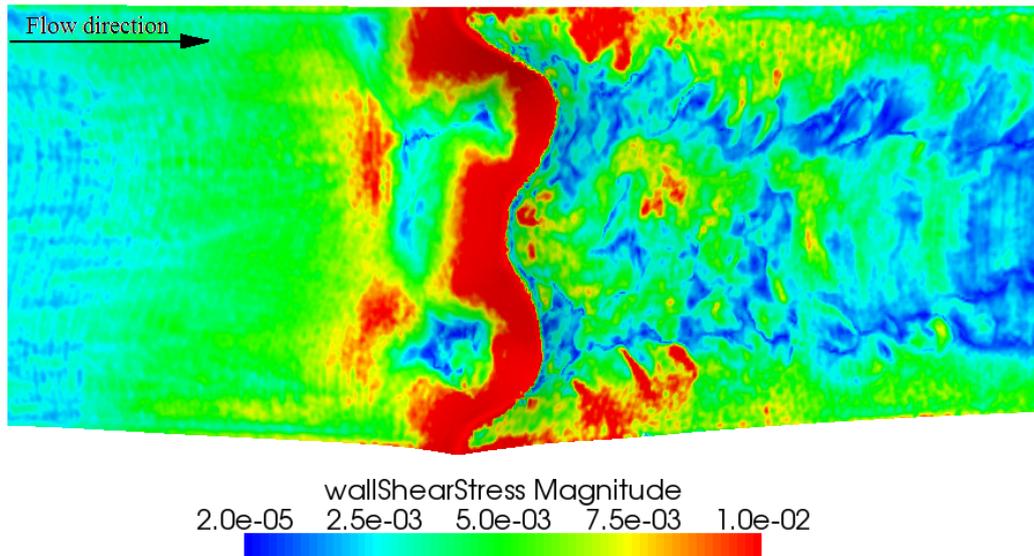
Figure 43: Wall shear stress of flow over a three-dimensional actual dune geometry

Knowing that separation and reattachment occur where the wall shear stress, and therefore velocity, is zero, makes it possible to identify where on the dune these flow features are present. By a closer inspection of the crest region a low wall shear stress presence can be identified following the crest line all along the dune. Another observation is the clear regions of low wall shear stress that are present behind the trailing crest edge causing separation and reattachment in this region. High wall shear stress, however, is visible behind the leading crest edge further motivating the observations made previously with regards to the effect of the crest line on the recirculation zone.

Furthermore, wall shear stress has a great effect on the transportation of particles. Firstly, since wall shear stress is directly related to velocity, it is possible to get a feel for the rate with which particles would be entrained in different regions along the surface. More importantly, high wall shear stress regions indicate regions of possible erosion while low wall shear indicate regions of possible particle deposition. This would mean that the windward slope would experience increasing erosion as one moves up the slope towards the crest. The depression regions near the crest experiences low wall shear stress and would therefore promote deposition of particles. On the lee-side more particles will deposit in the area behind the trailing crest edge than behind the leading crest edge due to the low wall shear stress in the region.

Looking at Figure 44 the velocity vectors can be seen for different sections through the dune. The idea of this image is to show the difference in the recirculation zone when moving from the trailing crest edge (Figure 44 (a)) to the leading crest edge (Figure 44 (b)). The trailing crest edge shows a large recirculation zone while the leading crest edge shows a small recirculation zone. This further confirms the flow characteristic explained in Figure 41 as well as the lee-side wall shear stress shown in Figure 43. Since the velocity vectors are displayed in vertical arrangement it is possible to observe changes in the velocity profile as it moves up the dune. From both sections flow acceleration up the windward slope is visible. This flow acceleration has the ability to fill the velocity profile near the surface as the flow accelerates. This flow acceleration is also

66

observed in literature (Parsons *et al.*, 2004a). Furthermore, it supports the observations in the two-dimensional simulations as well as the wall shear stress observed in the three-dimensional simulations.
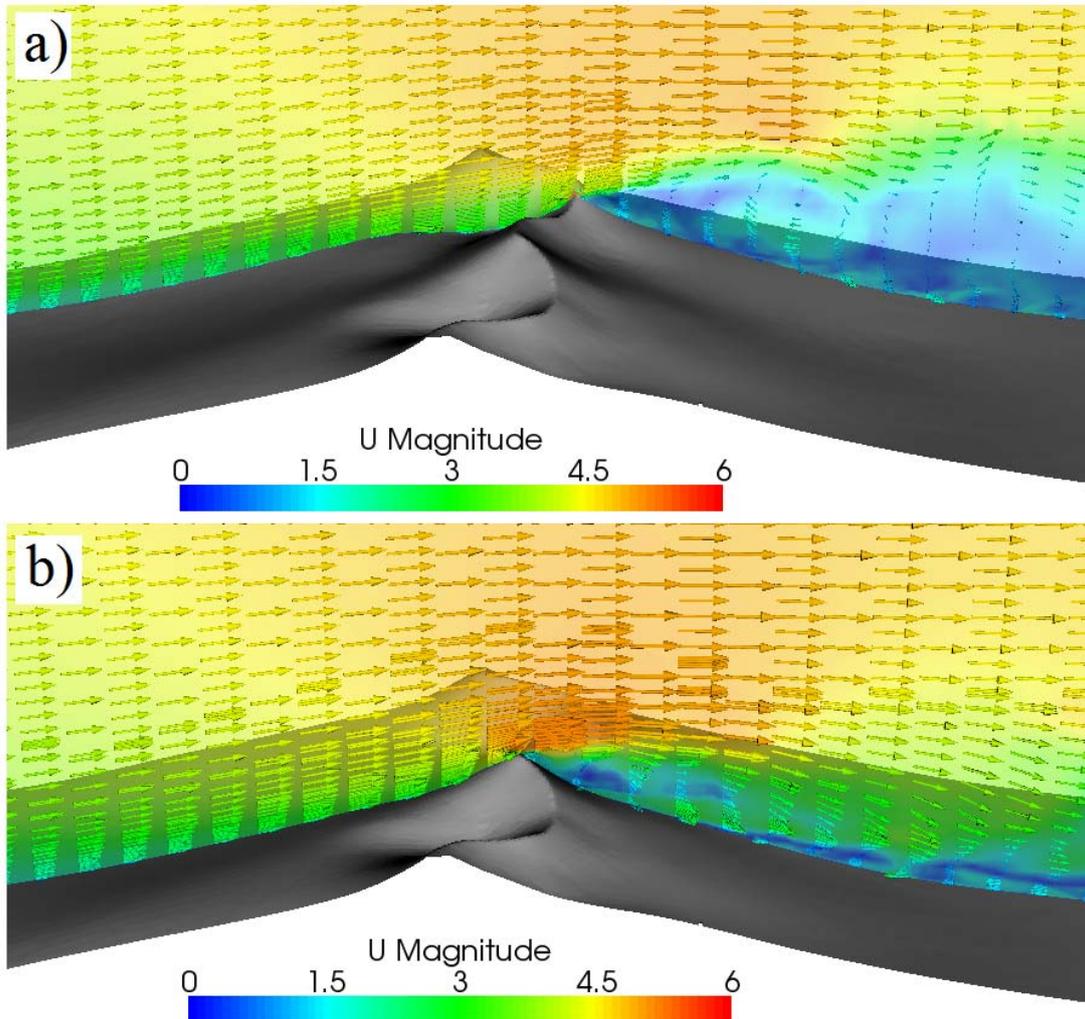
Figure 44: Recirculation zone difference: a) trailing crest edge section and b) leading crest edge

A better way to observe the different recirculation regions is to use streamlines. Streamlines show the path that air molecules would take through a given flow field. By looking at the general flow over the dune as shown in Figure 45 it can be seen how the orderly flow changes to disorderly flow as it crosses the dune crest. It is also visible how the flow crossing the dune at the leading crest edge is a lot faster at the crest than at the trailing crest edge. Furthermore, it can be noticed that the flow crossing the dune at the leading crest edge has a much lower arch than that of the flow crossing the trailing crest edge. This indicates the presence of recirculation vortex structures of different sizes. Lastly, it is can be seen that due to this difference in recirculation zone, cross flow occurs that forms the spiral flow structures away from the dune. Two spiral shaped flow structures are visible behind the trailing crest edge regions.

67
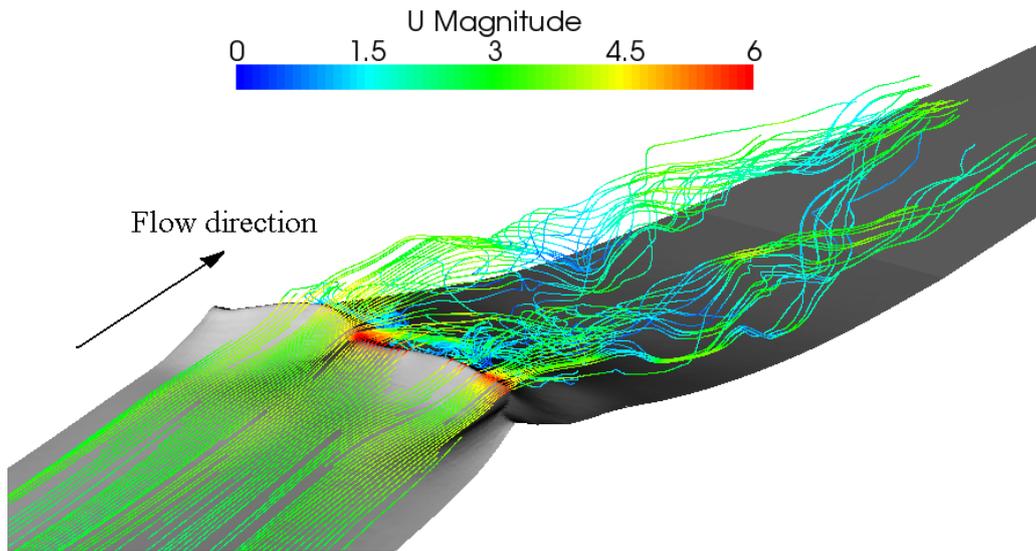
Figure 45: Streamline flow over a three-dimensional actual dune geometry

A closer inspection of the recirculation region in Figure 46 reveals two large recirculation zones behind the trailing crest edges of the dune. On the other hand the flow crossing the dune at the leading crest edge flows straight between the two vortex structures on either side. Further investigation of the flow behind the leading crest edge shows a smaller recirculation zone in that area. It can also be seen that the recirculation region looks almost continuous but of different shape and size depending on where on the dune it occurs.
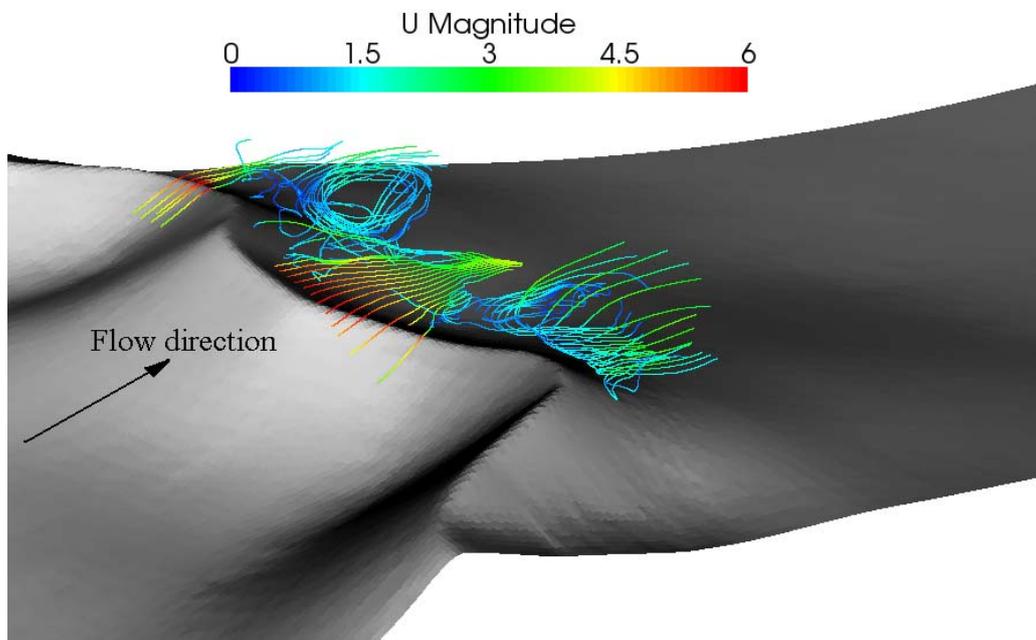
Figure 46: Streamlines of the near crest recirculation region

68

Streamlines also give a good indication of the path that very light particles might take. The streamlines are especially representative of the particle tracks since the particles in this study are very light weight and have large flight appendages that increase the drag. The streamlines show that almost weightless particles will have a greater chance of ending up in recirculation zones when crossing the dune at the trailing crest edge region than for the particles crossing at the leading crest edge.

The recirculation zone as seen from the streamline plot in Figure 46 can be depicted as in Figure 47. This vortex structure has a three-dimensional shape as a result from the crest-line curvature of the dune. The effect of the crest line curvature on the recirculating flow shows the importance of three-dimensional simulation. This three-dimensional recirculation zone effect is impossible to capture while looking only at the two-dimensional simulations.
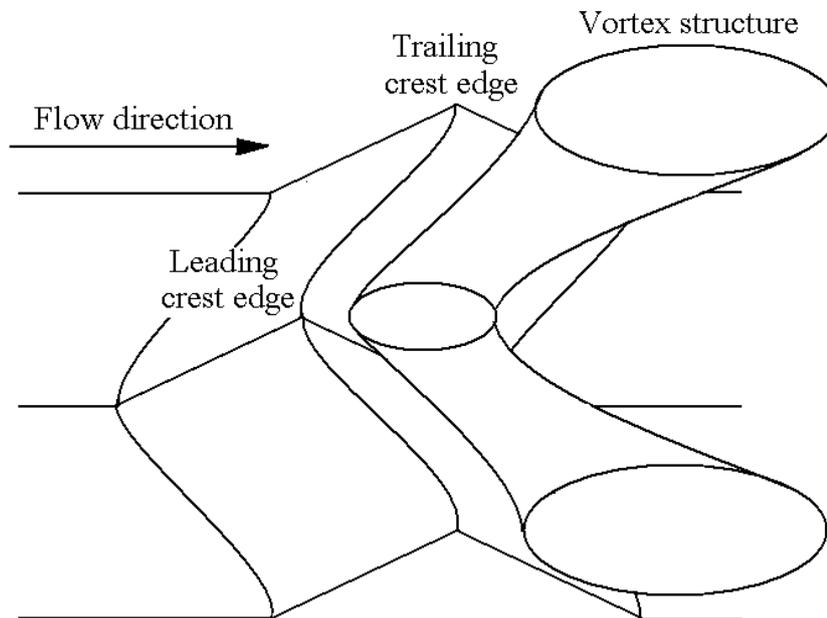
Figure 47: Three-dimensional near crest vortex structure

As mentioned earlier, continuous oscillations and changing flow fields that are suspected to be related to flow features that are inherently unsteady, motivates doing transient simulations.

4.2.3   Transient flow over an actual three-dimensional dune

The transient simulations in this section make use of LES turbulence model where the SGS is the one-equation eddy viscosity model. The one-equation SGS model is used since it was seen in literature that this model accounts for non-equilibrium effects (De Villiers, 2006) and provides good results for flows associated with unsteadiness (Fureby *et al.*, 1997).

The steady state simulations mesh, for which grid independence was motivated, is used as the starting point for the transient simulations. The mesh for the transient simulations using LES

69

turbulence models require finer boundary layers to be added. Six prism layers are used in the mesh with a larger growth rate to reduce the y^+ values. Furthermore, the refinement region on the lee-side is increased in height. More refinement is also introduced to improve simulation of the large eddies in the flow. Due to the small difference in appearance between the steady and transient meshes, the transient mesh is not displayed here. The steady state mesh is shown in Figure 36.

The results analysis process is again started by looking at the residuals for convergence. The residuals for the 50 second simulation period are shown in Figure 48. In this simulation the time step is kept low to ensure stability of the simulation. The time step is 0.005 second which ensures that the maximum Courant number stays below 1. The residuals are low and show very little change after the 50 second simulation period supporting convergence. The continuity shows a sharp decrease followed by a gradual increase that stables out after approximately 40 seconds. The low continuity values indicate that the simulation is stable and that conservation of mass principal is satisfied.
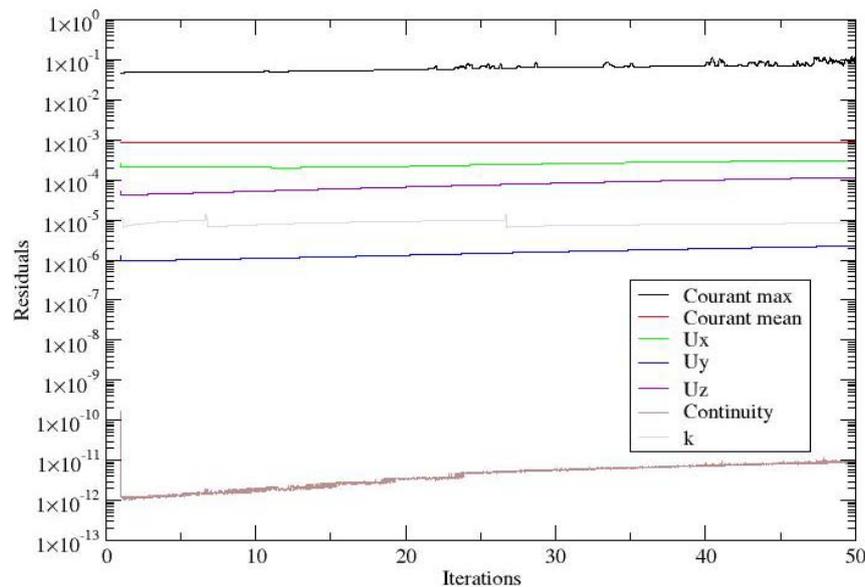
Figure 48: Residuals for transient three-dimensional actual dune simulation

For the transient simulations, as with the steady state simulations, wall functions are implemented to reduce the computational demand associated with extensive wall refinement. Since wall functions are implemented, the first cell centre next to the wall should fall within the logarithmic layer of the law-of-the-wall as shown in Figure 18. This relates to a y^+ values on the wall to be between 30 and 300 for the wall function to be most accurately applied.

Considering the y^+ values displayed on the dune surface in Figure 49 it can be seen that most of the values fall within the required range of 30 to 300. The range of flow velocities makes it difficult to apply the y^+ range perfectly. If the boundary layer is refined to reduce the high y^+ values at the crest, the y^+ values on the interdune will reduce as a result and so become too low. Not only will further refinement make the interdune y^+ values too low but also increase the

70

computational requirements significantly which will make pre- and post-processing even more difficult than it already is. The y^+ values in Figure 49 are therefore judged acceptable. It should be kept in mind that that every time step should conform to the y^+ requirements explained here. With a closer look this seemed to be the case. Only the final time step is displayed here for the purpose of the explanation.
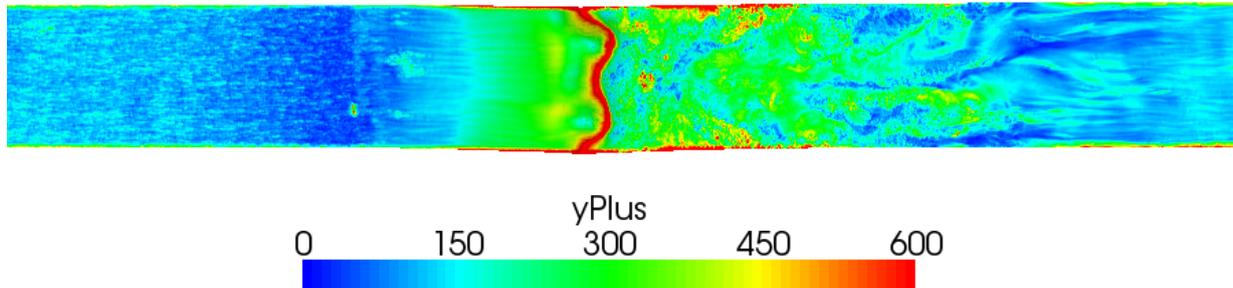
Figure 49: The y^+ values for transient simulation for latest time step

The results for the transient simulations show very similar flow features to that of the steady state simulations. These features include the characteristic pressure zones, flow acceleration up the windward slope, recirculation and more. These features were discussed in detail in section 4.2.2 and will therefore not be discussed again. In this section it is desired to rather discuss the flow features related to LES turbulence model as well as the transient nature of the flow. The transient flow results can be seen in Figure 50.

71
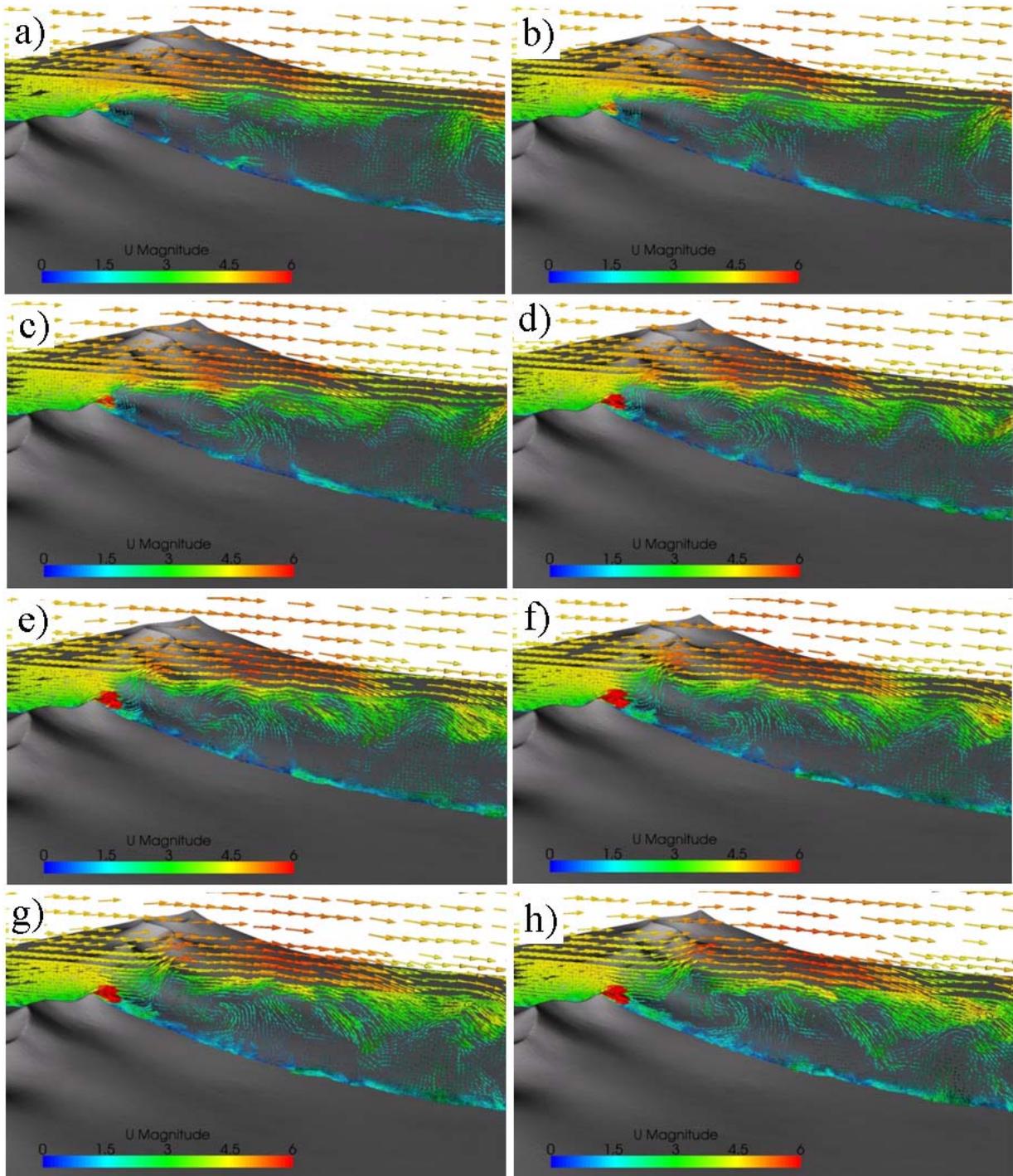
Figure 50: Transient flow results

By looking closely at the results it can be seen how the flow field changes over time. There are a number transient flow features visible. The first observation relate to vortex structures that form

72

near the crest, grow and move away from the dune in the general flow direction. Vortex structures roll in the flow and in so doing transport energy from high velocity region higher up to low velocity region near the surface. By observing the transition region between the recirculation zone and bulk flow it can also be seen how the bulk flow is diverted up or down due to the presence of vortex structures in the recirculation zone. The presence of vortex structures seems to increase the velocity magnitude of flow in the vicinity of the vortex perimeter. On the other hand, lower velocities are observed between vortex structures turning in the same direction.

Furthermore, the flow appears highly tree-dimensional as was reported in literature by Kim and Boysan (1999) and unsteady. This observation is supported by velocity vector distributions that show vortex structures that do not only occur in the two-dimensional plane along the general flow direction but in different shapes and orientations. Spiral vortex structures are also noticed in different areas of the lee-side recirculation zone. It should be noticed, however, that the maximum velocity near the crest change in magnitude as well as direction over time due to the vortex shedding effect.

It should be kept in mind that since the transient flow that is displayed in Figure 50 is highly three-dimensional means that the flow features at different sections of the dune differ. It also means there is a presence of flow along the dune length, even with the imposed flow perpendicular to the linear dune. Observing the flow along a two-dimensional section makes it easier to study what happens along a cross section of the dune but then limits the three-dimensional flow features that can be observed. Therefore, in some instances where vortex structures are not visible in the two-dimensional section, does not necessarily mean no vortex structures are present. With a closer look at the velocity vectors between vortex structures some velocity vectors indicate a three-dimensional component out of the plane showing the presence of vortex structures or general flow, that are unaligned to the studied section.

There are a number of ways to observe the presence of vortex structures in the flow. These methods are summarised by De Villiers (2006). The first method uses pressure to indicate the presence of vortex structures. The theory relates to the fact that vortex structures are associated with a low pressure at the point around which the vortex rotates. The local pressure minimum occurs due to centrifugal forces that pull the molecules away from the point of rotation. The low pressure and centrifugal forces in equilibrium indicate a stable vortex structure. This low pressure is observed in the results produced by the two-dimensional simulations shown in Figure 66 in Appendix I. Furthermore, Robinson (1991) showed that the minimum pressure method could indicate vortex structures. However, Jeong and Hussain (1995) showed that there are some cases where the minimum pressure method could be misleading. Two main factors result in misleading indications of local pressure minima. The first is low pressure regions that form due to unsteadiness in the flow. The second factor relates to how viscous effects smear out local pressure minima. The difficulty of indicating vortices with this method due to these factors as well as the locating local pressure minima amongst the general pressure regions makes this method ill suited for the three-dimensional simulations involved in this project.

The second method entails using streamlines to indicate vortex structures. Since streamlines indicate the path of an air molecule in the flow field, a closed loop or spiral path would indicate the presence of a vortex structure. This method is easy to implement and provides three-dimensional information of the flow field making it a very attractive method for this project. The

73

method was first proposed by Lught (1979). The main drawback of these methods is that they are not Galilean invariant and may therefore detect a vortex in one reference frame but not at another moving at a different speed (De Villiers, 2006). This method might therefore fail in turbulent flow where vortex structures are produced at different speeds. The streamline method is therefore attractive due to its simplicity and insight provided into the three-dimensional flow. However, it should be kept in mind that streamlines obscure some vortex structures moving at different speeds.

The third method is to use the vorticity magnitude. This method has been used with fair amount of success in free-shear flows but may not be suitable for wall shear flows. This is because the vorticity magnitude method fails to indicate vortex structures when the surrounding vorticity is of comparable magnitude which occurs at the wall in the wall-bounded flows (De Villiers, 2006).

Consequently Jeong and Hussain (1995) produced two criteria for the identification of vortex structures. The first criteria state that vortex structures should have a net vorticity and circulation so that potential vortices are excluded. Secondly, vortex structures should be Galilean invariant. Three alternative methods were proposed that are all Galilean invariant and make use of the velocity gradient tensor ($\nabla \mathbf{U}$).

The first method was proposed by Chong *et al.* (1990) and uses the complex eigenvalues of the velocity gradient tensor to indicate vortex structures with streamlines where the reference is frame independent. The second method was proposed by Hunt *et al.* (1988) and it indicates eddy structures with the positive second invariant (Q) of the velocity gradient tensor. The third method was proposed by Jeong and Hussain (1995) and it works on the principal of identifying local saddle points in the pressure field (local pressure minima) by taking the gradient of the Navier-Stokes equations. To remove local pressure minima that are unrelated to vortex activities specific terms related to unsteady irrotational straining and viscous effects are removed (De Villiers, 2006).

In a comparative study by Jeong and Hussain (1995) these alternative methods for identifying vortex structures are evaluated. These Galilean invariant methods were shown to be superior to the older pressure, streamline and vorticity magnitude methods. Due to the availability of the second invariant post-processing tool in OpenFOAM-1.5 this method is used to investigate the presence of vortex structures in the flow field. An isocontour plot of the second invariant of the velocity gradient tensor is displayed in Figure 51.
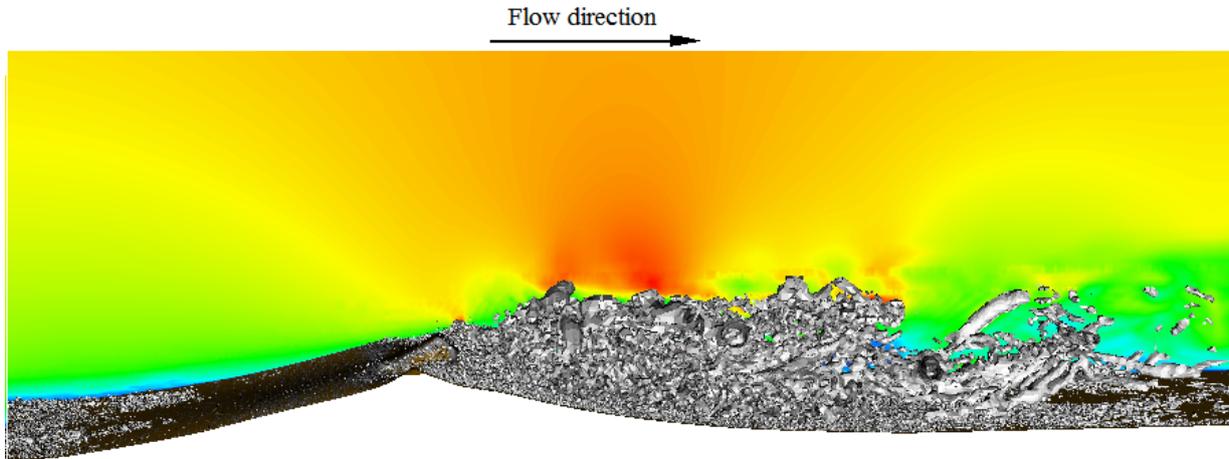
Figure 51: Vortex display with second invariant of velocity gradient tensor (Q = 0.0005) from the side

There are a number of observations that can be made by studying the vortex structures in the flow. The first observation is that there are in fact a large amount of vortex structures present most of which occur in the recirculation zone. The presence of vortex structures supports the use of a LES model to reproduce the turbulence in the flow field.

In the windward region vortex structures can be identified mainly along the wall boundary. This is to be suspected due to the no slip condition that imposes a velocity gradient and therefore a rolling action in the flow. Furthermore, the fact that vorticies are observed next to the wall supports the use of the second invariant method rather than the general vorticity magnitude method which is ill suited to locate vortex structures in near wall regions (De Villiers, 2006). The vortex structures on the surface occur in lines almost parallel to the crest line. These vortex tubes grow as the flow moves further along the surface. Vortex shedding is observed at the local depressions found in the upper slope of the dune geometry near the crest on the windward side. In this region the change in curvature is suspected to cause this early vortex shedding.

The recirculation zone on the other hand is dominated by vortex activity that originates from the crest region. Vorticies of different shapes, sizes and orientation can be seen. In some cases the vortex structures are tubes that lie parallel to the dune and in other cases balls of tumbling flow. It can be seen that most of the vorticies originate from the crest region. Near the crest the vortex structures are small and get larger as one move away from the dune. This is coherent with what was observed with the velocity vector plots. The sharp edges of some of the higher vortex structures are a result of coarse grid refinement for the higher flow regions used in the attempt to conserve the demand on computational resources.

4.2.4   Particle flow over an actual three-dimensional dune

Now that the steady and transient flow features have been investigated it is desired to look at how the flow features distribute particles in the flow field. As mentioned in the methodology, the solver used to simulate the particles in the flow uses a single time step of the flow field. The solver then calculates the motion of particles in the given flow field. The flow field is therefore

not affected by the particles and it stays constant. In reality seed particles will have a small effect on the flow. Therefore, assuming no influence on the flow is a simplification. The small size, mass and number of particles involved in this project make it possible to apply the simplification with a degree of confidence.

The second simplification is that the flow field stays constant over time as the particles move through the field. This simplification will have major effects on the motion of particles since it was observed in the transient results how vortex structures shed at the crest, grow and move away from the dune. The ideal would be to inject particles into a transient simulation employing the LES turbulence model. This is, however, not available in OpenFOAM-1.5 and would require more detailed programming knowledge of the code as well as more time to implement which is limited in this project. The solver used was only made available with the release of OpenFOAM-1.6 during the closing phase of this project which made it possible to produce the results presented here.

To reduce the effect of using a single time step it is decided to use a steady RANS simulation result. Since the steady state results resembles averaged flow features it provides the opportunity to observe what would happen to the average particle cloud as it travels over the dune and is influenced by a the given wind conditions. The RANS flow field contains the typical flow features including the flow acceleration up the windward slope as well as a recirculation zone. This particle motion solver is therefore accepted with regard to the scope and educational purpose of this study. The transient particle flow over the dune can be seen in Figure 52.

Particles are injected in the flow field at different heights to get a general idea of what particles will do as a result of the flow field. Figure 52 shows the particles, paths, the dune and applied flow field in the background. One observation that can be made is that particles, which fall to the surface before the dune slope, tend to stay at the toe region on the windward slope. On the other hand, particles that fall to the surface almost anywhere on the slope tend to bounce and roll up the slope, cross the crest and stay in the recirculation region near the crest. These particles that bounce and roll up the windward slope seem to have different velocities depending on where the particle rolls up. The different velocities are attributed to the three-dimensional shape of the windward slope. Furthermore, it can be noticed that particles accelerate up the slope due to the wind conditions.

Considering the height distribution of particles injected into the flow field it is possible to observe that particles starting from the surface to as high as 100 m above ground will all cross the dune close to the crest. This means the crest will have a high particle crossing density. These same particles will tend to lose momentum and fall to the surface once they enter the low velocity recirculation region. Most particles will recirculate up towards the crest. Some particles in recirculation zone seem to get caught up in a vortex and recirculate more than others before they drop to the surface. Particles in the recirculation zone move in all different directions and tempos showing the three-dimensional flow features present in the region. Of the particles in the recirculation zone a few may escape and move down the slope towards the interdune.

76
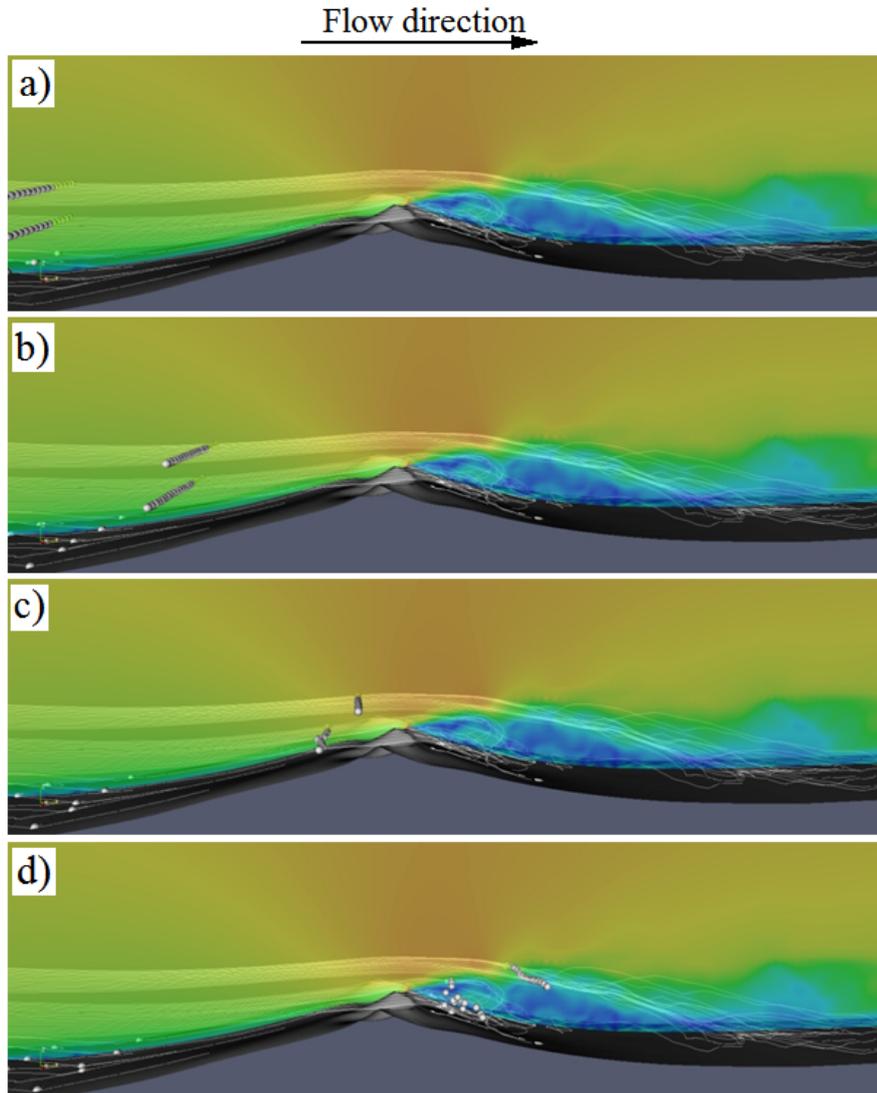
Figure 52: Transient particle motion

Particles starting from higher up in the atmosphere tend to miss the recirculation region and only drop to the surface on the opposite interdune. These particles generally move faster than the ones lower down showing the different speeds in the velocity profile. It is possible to observe that the particles higher up move up and down as they experience vertical components of the velocity vectors similar to which was studied in Figure 29. Once these particles fall to the surface they tend to bounce and roll away from the dune unaffected by the recirculation zone. In some cases particles on the interdune are influenced by trailing edge vortex structures that move them perpendicular with relation to the general approach flow direction.

From the observations it is clear that a great number of particles would bounce and roll along the surface. This observation is supported by the fact that any particles starting from the surface up to 100 m have a good chance of ending up on the windward slope. Also, particles ending up in the recirculation zone fall to the surface and also move back towards the crest due to the presence

77

of vortex structures in the flow. The large amount of particles that move along the surface is also observed in the field. Furthermore, measurements by Muller (2009) with nets are showed that most particles are captured along the surface of the dune and fewer with increasing height.

It is also observed that a higher number of particles would travel near the crest region since the particle paths seem to converge in this region due to the shape of the dune. This is also supported by the measurements by Muller (2009) where the most seeds and other plant material would be captured in nets at or near the crest region.

The important question is where these particles come to rest. It is observed that for the given flow field most particles that occur on the windward slope would come to rest in the recirculation zone where particles would stay due to the recirculation flow that drives them up the slope towards the crest. The flow velocities, particles in the recirculation zone experience, are, however, quite low. A point is therefore reached where the gravitational force pulling the particle down the dune and the low velocity forcing it up the slope are in equilibrium. This equilibrium point would form a line along the dune surface. For large number of particles in the flow field driven by a steady wind, conditions could result in particles coming to rest near this line. This would explain the occurrence of plant species growing in a line along the dune as observed in Figure 1.

Since the windward slope takes particles all the way up the slope and into the recirculation zone and the recirculation zone stretches almost half the way to the lee-side interdune means that a large particle capture area exists. In other words, all particles occurring within ¾ of the surface along the cross section are within the influence of flow promoting transportation towards the recirculation zone. In transient cases the vortex structures were observed to move even further away from the dune which would promote the transportation of particles up the lee-side slope from far away from the crest and even the lee-side toe region. The capture region may therefore be even larger when considering the transient flow features.

By looking at the recirculation zone more closely it is observed that particles deposits were greater behind the trailing crest edge than the leading crest edge. This supports the observations from the surface shear investigation in Figure 43. It also explains some plant growth observations in the Namib Desert as seen in Figure 1 where the seeds accumulate behind a large trailing crest edge region of the dune.

Other factors that need to be considered are obstructions along the dune surface. Since the majority of particles bounce and roll along the surface they are vulnerable to obstructions like existing plants or possible sand ridges on the dune. These obstructions would prevent particles to move further up the slope. This means that plants would most likely occur near existing plants or in lines due to ridges that prevented particles to move further up the dune.

4.3   Parallel Computations Performance

During this project it was desired to look at parallel performance by running a simulation over a range of multiple cores on the cluster. The reason for doing this was to look at factors that influence the parallel performance as well as to get a feel for the number of cores to use during simulations. The simulation selected for this study is two-dimensional air flow over a simple

78

dune obstacle similar to that explained in section 4.3.2. The two-dimensional simulation is selected for its simplicity and low memory requirements.

Through the experience of these simulations four main factors that influence the parallel performance were identified. All the factors are related to the amount of user traffic on the cluster. Firstly, large amounts of communication between cores on the same node can slow the simulation process. Secondly, excessive communication between cores on different nodes may increase simulation time. Thirdly, when large quantities of data is written to the storage disc, communication as well as writing speed can influence key steps in the simulation process when time dumps are stored. Lastly, simulations with high memory requirements can cause calculations to be delayed or even fail completely.

The cluster user should take these factors into account when conducting simulations. In the experience of this project it is suggested to avoid high traffic communication paths where possible. This can be done by allocating all cores needed for a simulation on a single node or processor where possible. The communication between cores on a processor or even processors on a node is faster than communication between nodes. Another factor to keep in mind is the amount of memory that would be needed. If more memory would be needed during any point in the simulation process a spread of cores over different nodes would be better. This is because using more nodes makes more memory available and would also avoid the possibility of using all the memory on one node which has been reported to cause failures in the past.

Throughout the project the cluster was found critical to the success of the project. However, due to the high usage of the cluster, associated queuing problems as well as simulation crashes because of other users or high memory demand it would be preferred to have a smaller but dedicated cluster for such projects in the future.

5. CONCLUSIONS

Mapping the dune with a differential GPS made it possible to get the necessary accuracy while still being time and cost effective. The final dune surface compared well with the dune mapped as well as with neighbouring dunes. This supported the choice of the site as well as mapping scheme.

The use of open source software played a major role in this project. On the one hand it provided the base for extensive parallel simulation without the cost of licensing which reduced simulation time. On the other hand delays due to using unfamiliar software that is less user friendly than commercial packages hampered progress at some stages of the project. OpenFOAM-1.5 provided most of the tools needed in this study including all the utilities, turbulence models and solvers but lacked some boundary conditions and particle tracking applications that were not available at the time of the study. Based on the experience of this project OpenFOAM is considered an exceptional educational tool and very competitive CFD software but requires some time to get use to. It is therefore recommended to attend training courses to speed up the learning process but it is even more important to establish a local OpenFOAM user group. Furthermore, it is concluded that to make use of the full potential of the software, a greater understanding of C++ programming as well as CFD is needed.

Two-dimensional simulations provided the opportunity to investigate the effects of various differencing schemes as well as turbulence models. The difference in results between first and second order accurate differencing schemes is noticed to be considerable even with extensive refinement. This leads to the decision to use second order differencing throughout the project. The differencing scheme used is the GAMMA switching/blending scheme which was found to provide a higher order differencing scheme while maintaining a good degree of stability. Comparing the different turbulence models showed less variation but still the realizable k-ε turbulence model was chosen due to its reported comparatively better performance in calculating the flow in recirculation zones.

The two-dimensional results could also be compared to previous studies by Parsons *et al.* (2004a and b). Even though Parsons *et al.* (2004a and b) made use of the upwind differencing scheme, similar flow features could be identified when comparing the results. Flow features include the high pressure at the dune toe and low pressure at the crest. The high pressure at the toe causes streamwise deceleration of the flow approaching the toe that result in a low velocity in the region. The difference between the high and low pressure zones form a pressure gradient on the windward face resulting in flow acceleration up this slope. The flow accelerates up the slope to a maximum at the crest. Clear recirculation is visible on the lee-side of the dune.

A LES turbulence model was used in the transient simulations to compensate for the difference between the large and small scale eddies. The transient simulations made it possible to look at how the flow changes over time. The transient results show clear separation with vortex shedding. It is also visible how vortex structures originate from the dune crest region, grow and move away from the dune in the general flow direction. Using the second invariant of the velocity gradient tensor it was possible to study three-dimensional vortex structures which would be difficult with velocity vectors and sometimes unclear with streamlines. It was clear that there

are a large number of vortex structures in the lee-side of the dune. Vortex structures of all sizes occur on the lee side as a result of vortex shedding near the crest. Further downstream from the dune the vortex structures seem to dissipate as a result of viscous damping.

By injecting particles into the steady state RANS turbulence results it was possible to observe how particles would move in an averaged flow field. The results showed that most particles would eventually end up in the recirculation zone. Since most particles fall to the dune surface at some point they tend to roll and bounce towards the recirculation zone. In this rolling motion they might get caught up in existing plants or sand ridges that might prevent the particles from moving further. This might explain some of the line groupings of plants that are visible on the dune slopes. Furthermore, most particles seem to cross the dune in the first few meters above the crest. This observation is supported by the work of Muller (2009) who captured most particles at or near the crest region of the dune.

Parallel computing played a vital role in the project. A number of factors were identified which all relate to traffic on the network, memory and storage. The speedup simulations at the time provided the opportunity to get a feel for the number of cores to be used for future simulation as well as a better understanding of high performance computing systems. It is recommended that future users conduct similar speedup simulation tests before conducting large scale simulations.

Considering the results it can be seen that all the objectives for this project have been achieved successfully and that this project is a step forward from the two-dimensional and first order accurate models of the past reported in the literature. There were, however, a number of areas that could be recommended for future studies.

One project that would provide valuable contribution to the local CFD group would be to look at a comparison of unsteady simulations between RANS and LES turbulence models in detail. In such a project a simplified three-dimensional geometry would be recommended to make it easier to identify the flow features that result specifically from the turbulence model. An investigation of the governing equations would be valuable to couple the sources of the flow features to the differences that might be observed.

It is also recommended that OpenFOAM be used for an MScEng study to investigate the differences between common turbulence models. OpenFOAM has a great number of turbulence models available and this type of project would provide the perfect opportunity to increase experience with the software as well as to shed some light on turbulence modelling choices. The project suggested is a steady state simulation of air flow over a simple bluff body in two- or three-dimensions. Air flow over bluff bodies would provide the necessary flow features to fully test turbulence models due to the presence of recirculation zones and vortex shedding. Furthermore, such an investigation would bring into view a large amount of literature available on the topic of turbulence modelling which would greatly benefit the local CFD group.

Due to the difficulties faced in this project with regards to quantitative and controlled measurements of the flow field it is recommended that future studies make use of simplified dune models or scaled actual dune models and wind tunnel measurements for more useful experimental data. Such data could be used to validate the simulations models.

REFERENCES

Bagleito E, 2009, Turbulence and Modelling, Lecture 1, CD-Adapco Aerotherm workshop, Johannesburg, South Africa, 13/10/2009

Blocken B, Stathopoulos T and Carmeliet J, 2007, CFD simulation of the atmospheric boundary layer: wall function problems, Atmospheric Environment 41(2), pp. 238-252

Bradbrook K F, Biron P, Lane S N, Richards K S, Roy A G, 1998, Investigation of controls on secondary circulation and mixing processes in simple confluence geometry using a three-dimensional numerical model, Hydrological Processes 12, pp. 1371-1396

Briggen P M, Blocken B and Schellen H L, 2009, Wind-driven rain on the facade of a monumental tower: Numerical simulation, full scale validation and sensitivity analysis, Building and Environment 44, pp. 1675-1690

CD-adapco, 2009, http://www.cd-adapco.com

Cebecim T and Bradshaw P, 1977, Momentum transfer in boundary layers, Hemisphere Publishing Corporation, New York

Chong M S, Perry A E and Cantwell B J, 1990, A general classification of three-dimensional flow field, Physics of Fluids A 2, pp. 765

Combrinck M L, 2008, A Computational Fluid Dynamic Analysis of the Air Flow over the Keystone Plant Species, Azorella Selago, on Sub-Antarctic Marion Island, MScEng Thesis, Department of Mechanical and Mechatronic Engineering, University of Stellenbosch, South Africa

De Villiers E, 2006, The Potential of Large Eddy Simulation for the Modeling of Wall Bounded Flows, PhD Thesis, Department of Mechanical Engineering, Imperial College of Science, Technology and Medicine, London

EnGits, 2009, http://engits.eu/cms

Flemmer R L C and Banks C L, 1986. On the drag coefficient of a sphere, Power Technology 48, pp. 217-221

Fureby C, Gosman A D, Tabor G, Weller H G, Sandham N and Wolfshtein M, 1997, Large eddy simulation of turbulent channel flows, Turbulent Shear Flows 11,

Gmsh, 2009, http://www.geuz.org/gmsh

Google Earth, 2009, http://maps.google.co.za, (Gobabeb, Namibia)

Hanjalić K, Kenjereš S, 2008, Some developments in turbulence modeling for wind and environmental engineering, Journal of Wind Engineering and Industrial Aerodynamics 96, pp. 1537-1570

Harris R I and Deaves D M, 1981, The structure of strong winds, Wind engineering in the eighties, Proc. Of the CRIRA Conference, 12 - 13 November 1980, Construction Industry Research and Information Association, London, Paper 4

Henschel J, Klintenberg P, Carole R and Seely M, 2007, Long-term ecological research from an arid, variable, draught-prone environment, Sécheresse 18(4), pp. 342-347

Hunt J C R, Wray A A and Moin P, 1988, Eddies, stream and convergence zones in turbulent flows, in Center for Turbulence Research Report S88, CTR, pp. 193

Igage, 2009, http://www.igage.com/mp/pm3/pm3 (ProMark 3 User Manual)

Issa R I, 1986, Solution of the implicitly discretised fluid flow equations by operator-splitting, Journal of Computational Physics 62, pp. 40-65

Jasak H, Weller H G and Gosman A D, 1999, High resolution NVD differencing scheme for arbitrarily unstructured meshes, International Journal of Numerical Methods in Fluids 31, pp. 431– 449

Jasak H, 2009, http://powerlab.fsb.hr/ped/kturbo/openfoam/slides/SMDI06.pdf

Jeong J and Hussain F, 1995, On the identification of a vortex, Journal of Fluid Mechanics 285, pp. 69-94

Kim S and Boysan F, 1999, Application of CFD to environmental flows, Journal of Wind Engineering and Industrial Aerodynamics 81, pp. 145-158

Lakes Environmental, 2009, http://www.weblakes.com/wrplot

Lancaster J, Lancaster N and Seely M K, 1984, Climate of the central Namib Desert, Madoqua 14 (1), pp. 5-61

Launder B E and Spalding D B, 1974, The numerical computation of turbulent flows, Computer Methods in Applied Mechanics and Engineering 3, pp. 269-289

Livingstone I, 1985, The Dynamics Of Sand Transport On A Namib Linear Dune, Hertford College, University of Oxford

Lugt H J, 1979, The dilemma of defining a vortex, in Recent Developments in Theoretical and Experimental Fluid Mechanics, U Muller, K Roesner, and B Schmidt, editors, Springer, p309-321

Mikkelsel A K and Livesey F M, 1995, Evaluation of the use of numerical k-ε model Kameleon II, for predicting wind pressure on building surfaces, Journal of Wind Engineering and Industrial Aerodynamics 57, pp. 375-389

Muller A A, 2008, Photograph taken of high dune near Gobabeb training and research centre

Muller A A, 2009, The Dynamics of Seed Bank Dispersal and Deposition Under Natural Environmental Conditions In The Central Namib and Kalahari Desert, MSc Thesis, Department of Environmental and Geographical Science, University of Namibia, Namibia

Nikuradse J, 1933, Strömungsgsetze in rauhen Rohren, Forschg. Arb. Ing.-Wes. No. 361

OpenCFD, 2009, http://www.opencfd.co.uk/openfoam/doc/snappyHexMesh.html

Paraview, 2009, http://www.paraview.org

Parsons D, Wiggs G F S, Walker I J, Ferguson R I and Garvey B G, 2004a, Numerical modelling of flow over an idealised transverse dune, Environmental Modelling & Software 19, pp. 153-162

Parsons D, Walker I J, Wiggs G F S, 2004b, Numerical modelling of flow over an idealised transverse dune of varying geometry, Geomorphology 59, pp. 149-164

Patankar S V and Spalding D B, 1972, A calculation procedure for heat, mass and momentum transfer in three-dimensional parabolic flows, International Journal of Heat and Mass Transfer 15

Richards P J, 1989, Computational Modelling of Wind Around a Low Rise Building Using PHOENIX, Report for the ARFC Institute of Engineering Research West Park, Silsoe Research Institute, Bedfordshire, UK

Richards P J and Hoxey R P, 1993, Appropriate boundary conditions for computational wind engineering models using the k-ε turbulence model, Journal of Wind Engineering and Industrial Aerodynamics 46&47, pp. 145-153

Robinson S K, 1991, Coherent motions in the turbulent boundary layer, Annual Review Fluid Mechanics 23, pp. 601-639.

Sharan M, Rama Krishna T V B P S and Aditi, 2003, On the bulk Richardson number and flux-profile relations in atmospheric surface layer under weak wind stable conditions, Atmospheric Environment 37, pp. 3681-3691

Sycode, 2009, http://www.sycode.com/products/terraincad

Tsoar H, 1978, The Dynamics of Longitudinal Dunes: Final Technical Report, European Research Office, U.S. Army, London, DA-ERO 76-G-072

Tsoar H, 1983, The dynamics acting on a longitudinal (seif) sand dune, Sedimentology 30, pp. 567-578

Versteeg H K and Malalasekera W, 2007, An Introduction to Computational Fluid Dynamics: The Finite Volume Method, Second Edition, Publisher: Pearson Prentice Hall, London, England

Waterson N P, 1994, Validation of Convection Discretisation Schemes, VKI Dep. Rep. 33, Von Karmen Institute for Fluid Dynamics, Rhode-Saint-Genese, Belgium, pp. 1-177

Watson A, 1987, Discussion: variation in wind velocity and sand transport on the windward flanks of desert sand dunes, Sedimentology 34, pp. 511-520

Wieringa J, 1992, Updating the Davenport roughness classification, Journal of Wind Engineering and Industrial Aerodynamics 41-44, pp. 357-368

Wiggs G F S, Livingstone I and Warren A, 1996, The role of streamline curvature in sand dune dynamics: evidence from field and wind tunnel measurements, Geomorphology 17, pp. 29-46

Yakhot V, Orszag S A, Thangam S, Gatshi T B and Speziale C G, 1992, Development of a turbulence model for shear flow by the double expansion technique, Physics and Fluids A 4, pp. 1510-1520

# APPENDIX A: Gobabeb Location and Project Contributions

A.1: Gobabeb Location
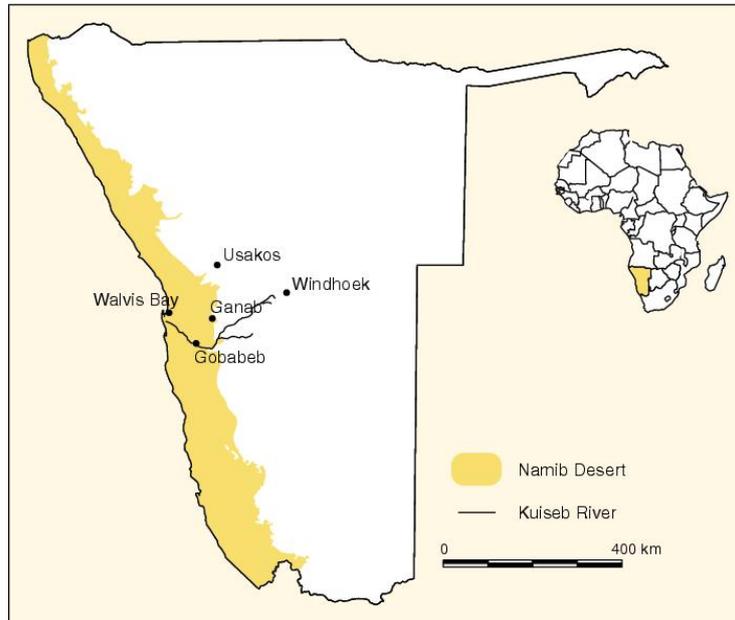
Figure 53: Location of Gobabeb training and research centre (23ʹ 33' S; 15ʹ 02' E) in Namibia (Henschel *et al.*, 2007)

A.2: Project Contribution

This project contributes to the greater understanding of deserts since wind plays such a key role. Understanding the wind helps to better understand the seeds and therefore the distribution of plants. The wind also defines the landscape since it transports sand. Furthermore, the wind has a strong effect on the water resources of the desert by influencing the distribution of rain and fog as well as to affect the rate water is evaporated from the surface of plants. Therefore improving the understanding of near surface wind patterns also provides insight in to the shape of the landscape, the arrangement of vegetation and in turn the distribution of animals throughout the desert.

The project may serve as a starting point for future projects looking to analyse the wind patterns on a larger scale. The simulation model can be expanded to analyse large scale wind patterns, seed movement as well as sand migration which will contribute to local weather prediction. Understanding the local weather patterns may give greater insight into desertification on the perimeter of the Namib Desert.

APPENDIX B: Classification of Terrain Roughness Length

Table 5: Davenport classification of aerodynamic terrain roughness length (Wieringa, 1992)

| y_0	Landscape description
0.0002 Sea	Open sea or lake, tidal flat, snow-covered flat plain, featureless desert, tarmac, concrete, with free fetch of several kilometres.
0.005 Smooth	Featureless land surface without any noticeable obstacles and with negligible vegetation; e.g. beaches, pack ice without large ridges, morass, and snow-covered or fallow open country.
0.03 Open	Level country with low vegetation (e.g. grass) and isolated obstacles with separations of at least 50 obstacle heights; e.g. grazing land without windbreaks, heather, moor and tundra, runaway area of airports.
0.1 Roughly open	Cultivated area with regular cover of low crops, or moderately open country with occasional obstacles (e.g. low hedges, single rows of trees, isolated farms) at relative horizontal distances of at least 20 obstacle heights.
0.25 Rough	Recently-developed "young" landscape with high crops or crops of varying height, and scattered obstacles (e.g. dense shelterbelts, vineyards) at relative distances of about 15 obstacle heights.
0.5 Very rough	"Old" cultivated landscape with many rather large obstacle groups (e.g. large farms and clumps of forests) separated by open spaces of about 10 obstacle heights. Also, low large vegetation with small interspecies such as bush land, orchards and young densely planted forests.
1 Closed	Landscape totally and quite regularly covered with similar-size large obstacles, with open spaces comparable to the obstacle heights; e.g. mature regular forests, homogeneous cities or villages.
≥ 2 Chaotic	Centres of large towns with a mixture of low-rise and high-rise buildings. Also, irregular large forests with many clearings.

APPENDIX C: Dune Mapping Site Outline
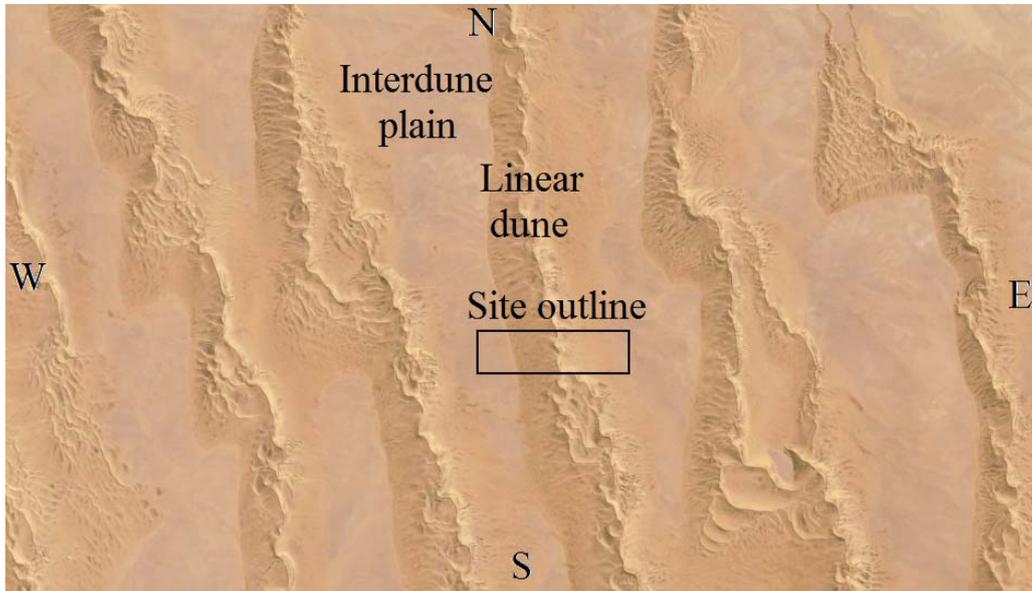
Figure 54: Close-up view of project site

APPENDIX D: Additional Dune Mapping Equipment and Procedure Information

D.1: The Differential GPS

Figure 55: Differential GPS ProMark 3

During mapping the transportability of the equipment had to be taken into account since it all would have to be carried by hand across the dune and back a number of times. This may seem like a simple task but high temperatures, dry air and sandy slopes makes it necessary to carry additional water and clothing as well. The differential GPS is connected to a pole which is light weight and easy to carry. The pole allows the antenna to be above the person operating it allowing for better reception of satellites. Furthermore, the pole makes it possible to leave the GPS unattended making it possible to take a rest and document coordinates without the GPS being left in the sand or being in the way. The large antenna disc improves the satellite reception signal strength as well as increasing the number of satellites in view. As a result the antenna improves the accuracy of the positioning.

Table 6: ProMark 3 GPS Accuracy Specifications (Igage, 2009)

Statistic Survey Performance	
Horizontal	0.005m + 1 ppm
Vertical	0.01m + 2 ppm
Azimuth	< 1 arc second
Observation time	4 to 40 minutes
Kinematic Survey Performance	
Horizontal	0.012m + 2.5 ppm
Vertical	0.015m + 2.5 ppm
Minimum Recommended Point Observation Time	15 seconds
Recommended Initializer Bar Occupation	5 minutes
Real-Time Performance	
SBAS (rms) Horizontal	< 1m
DGPS (rms) Horizontal	< 1m

D.2: Dune Mapping Procedure

Figure 56: Dune mapping procedure

Figure 57: Extended dune surface

APPENDIX E: Meshing in OpenFOAM-1.5

To use snappyHexMesh a surface file is necessary that defines the geometry involved in the meshing. For this project the surface refers to the generated dune surface that is explained in section 3.1.4. Prior to meshing it is also required to create a simple structured hexahedral mesh in such a way that the geometry is included within the boundaries of the mesh. The Hexahedral mesh may be created with the blockMesh utility in OpenFOAM. This hexahedral mesh forms the basis from which the final mesh is generated. The meshing process is illustrated in Figure 58.
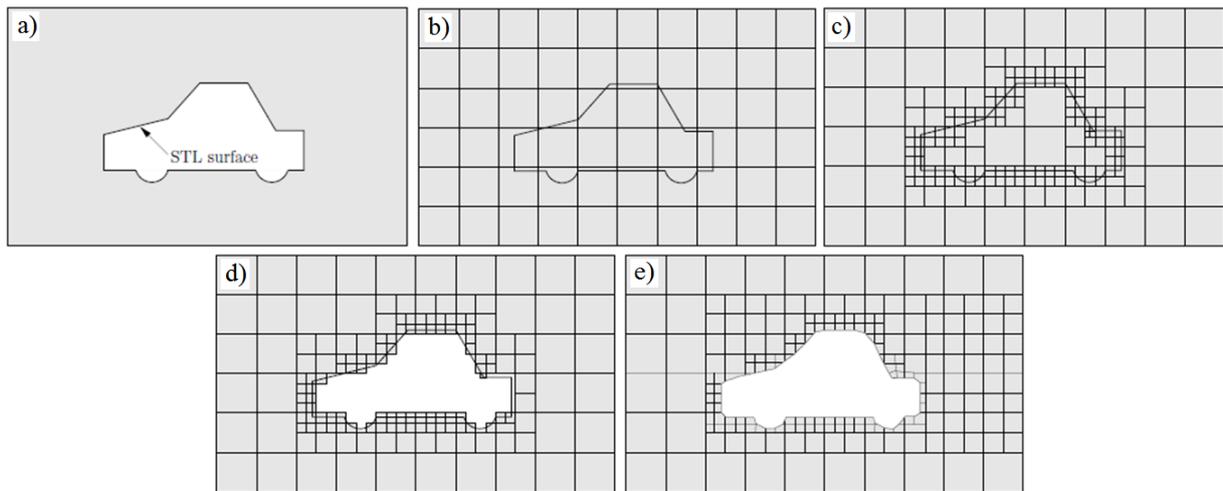

Figure 58: Meshing procedure: a) surface file, b) hexahedral mesh, c) refinement, d) cutting and e) snapping (OpenCFD, 2009)

During the first step the software refines the mesh in the region of the surface as shown in Figure 58 (c). Next the unnecessary elements are cut away as shown in Figure 58 (d). During this step the user has the ability to specify the region where the unnecessary elements are located. The final step is to snap the outlying points to the surface in order to smooth out the curves as shown in Figure 58 (e). Many parameters are available to modify the meshing process to the needs of the simulation. It is also possible to check the mesh and improve the quality by adjusting the required variables.

An optional step to the meshing process is to add boundary layer elements to the surface of the geometry. Boundary layer cells are created by extruding the geometry surface while the edges of the prism layer cells coincide with that of the snapped cells generated in the previous meshing process. The boundary layer elements are defined by specifying the amount of layers, where they have to be added as well as the expansion ratio. All the variables are contained in a dictionary file that serves as instructions for the software.

92
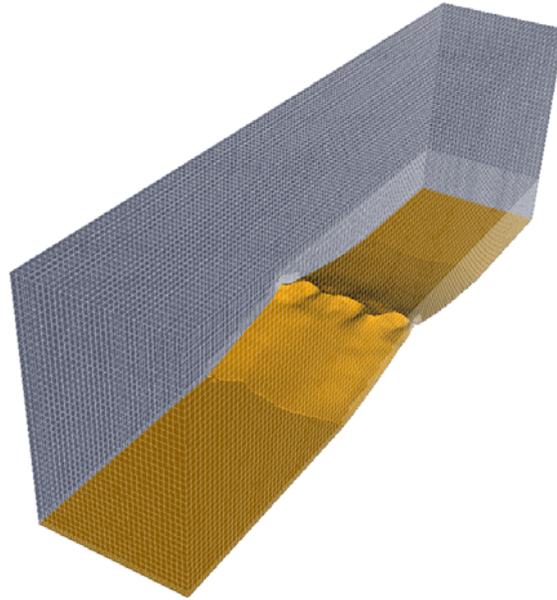
Figure 59: Volume mesh of atmosphere above the dune

Since the meshing tool in OpenFOAM-1.5 lacks feature line meshing capabilities, it is difficult to mesh the sharp crest edge often found on dunes. In Figure 60 (a) the sharp edge mesh is shown. One way to improve the crest meshing is to increase the refinement level. Since the refinement level is already very high increasing it even more will be very computationally expensive. On the other hand the sharp edge makes it very difficult to achieve a continuous prism layer over the crest. To facilitate continuous prism layer meshing, the crest region is smoothed. From Figure 60 it is clear that the difference in meshing the dune with a smooth edge makes very little difference while providing increased accuracy as well as allowing for reduced mesh refinement.
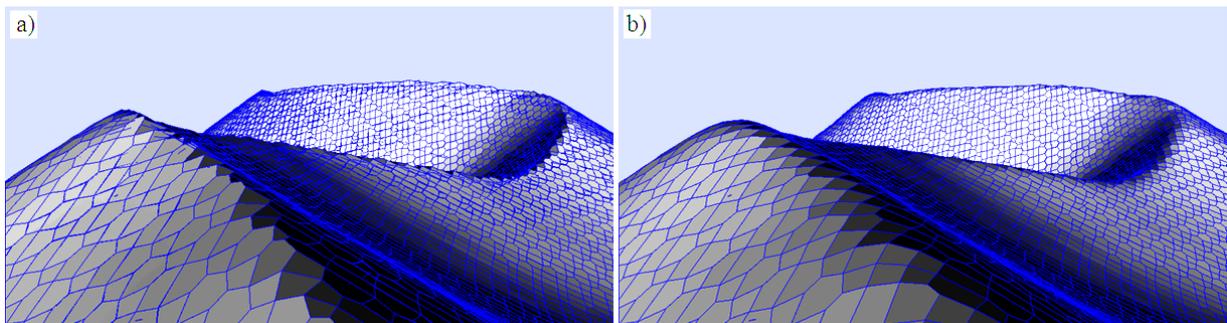

Figure 60: Crest meshing: a) sharp edge and b) smoothe edge

93

APPENDIX F: Wind Sensors Specifications

Table 7: Sensor calibration coefficients for logger - station1

Station ID	Channel	Type	Range	Offset	Multiplier	Height (m)	Sensor ID
Station1	1	Temp	6	0.6765	0.9707	2.5	1T
	2	Temp	6	0.3858	0.9716	5	2T
	9	Speed	1	0.38	0.1537	2.5	1S
	10	Speed	1	0.38	0.1537	5	2S

Table 8: Calibration coefficients for logger – station2

Station ID	Channel	Type	Range	Offset	Multiplier	Height (m)	Sensor ID
Station2	1	Temp	6	1.2395	0.9568	7.5	3T
	2	Temp	6	-0.0018	0.9817	10	4T
	7	Direction	8	0.3	0.992	6	-
	9	Speed	1	0.38	0.1537	7.5	3S
	10	Speed	1	0.38	0.1537	10	4S

Table 9: Datalogger specifications

Supplier	MCSystems
Model no.	MCS130M2
Analog channels	8
Digital channels	2
Communication	RS232
Battery	Sealed lead acid cell, 6volt,7amp/hr
Housing	IP65PVC with sealing gasket

Table 10: Wind temperature sensor specifications

Supplier	MCSystems
Model no.	MCS151
Output	Analog
Operating temperatures range	-20℃ to 70℃
Accuracy	+/-0.2℃ at 25℃
Resolution	+/-0.1℃
Power requirement	4.8 to 6.5 volts at 300μA
Dimensions	8mm diameter x 75 mm
Mass	50 g

94

Table 11: Wind direction sensor specifications

Supplier	MCSystems
Model no.	MCS176
Output	Analog
Operating temperatures range	-10̊C to 50̊C
Accuracy	+/-5̊
Angular span	350̊
Power requirement	1 to 2.5 Volts at 200 μA
Vane	Anodized aluminium
Housing	UV protected PVC
Vertical height	300 mm
Mounting requirements	25.4 mm inside diameter
Mass	500 g

Table 12: Wind speed sensor specifications

Suppliers	MCSystems
Model no.	MCS177
Output	Digital
Operating wind speed range	0.5 to 45 m/s
Operating temperatures range	-10̊C to 50̊C
Accuracy	+2 % full scale
Turning radius	150 mm
Cup size	70 mm diameter
Cups	Anodized aluminium
Power requirement	4 to 15 Volts at 20 μA
Vane	Anodized aluminium
Housing	UV protected PVC
Vertical height	300 mm
Mounting requirements	25.4 mm inside diameter
Mass	0.5 kg

APPENDIX G: Seed Species and Particle Model Calculations

In Figure 61 some of the different seeds found in the Namib are shown. It is possible to notice the large flight appendages that cause these seeds to be picked up by even the slightest winds.

Figure 61: Namib plant seeds: a) Stipogrostis Sabulicola, b) Centrapodia Glauca and c) Stipogrostis Gonatostachys

The effective radius of the particle seen in Figure 61 (a) can be calculated by rearranging the drag equation. The drag is given by the following equation:

$$C_D = \frac{D}{\frac{1}{2}\rho U^2 A} \qquad (C.1)$$

In equation (C.1) C_D is the drag coefficient, D is the drag force, ρ is the air density, U is the air flow velocity and A is the projected area. When the air velocity is taken as the terminal velocity, then the drag force, D equals the gravitational force on the particle. Therefore the drag force can be substituted with the following:

$$D = F = mg \qquad (C.2)$$

In equation (C.2) m is the particle mass and g is the gravitational constant. Furthermore, the area can be written as the cross sectional area of a sphere as follows:

$$A = \pi r^2 \qquad (C.3)$$

In this equation r is the radius of the sphere. By substituting equations (C.2) and (C.3) into (C.1) and rearranging to get the radius results in:

$$r = \sqrt{\frac{2mg}{\rho U^2 \pi C_D}} \qquad\qquad (C.4)$$

The first step calculate the particle radius with equation (C.4) by choosing the initial value of the drag coefficient, C_D, and then insert it along with the values of terminal velocity, U, air density, ρ and particle mass, m. The next step is to calculate the Reynolds number Re with the following equation:

$$Re = \frac{\rho U (2r)}{\mu} \qquad\qquad (C.5)$$

In this equation μ is the air viscosity. It is possible to approximate the drag on the particle by using an equation proposed by Flemmer and Banks (1986) which is based on the Reynolds number. The approximation is given by the following equations:

$$C_D = \frac{24}{Re} 10^E \qquad\qquad (C.6)$$

$$E = 0.261 Re^{0.369} - 0.105 Re^{0.431} - \frac{0.124}{1 + (log_{10} Re)^2} \qquad\qquad (C.7)$$

In order to adjust the initial value of the drag coefficient an error value is calculated as follows:

$$E = \left| C_D{}^i - C_D{}^{i+1} \right| \qquad\qquad (C.8)$$

97

APPENDIX H: Additional Wind Data

A similar wind rosette to what was shown in Figure 19 can be plotted for the wind measurements when the mast was located on the dune slope. This can be seen in Figure 62. The main wind directions for the slope measurements are south-south-east (11,1 %), south (18.9 %) and south-south-west (12.3 %). The rosette shows a greater directional spread for the time period than that of the interdune measurements. In this case the main wind directions account for only 42.3 % of the winds experienced. Again the wind class frequency distribution shows a normal distribution around the 2.1 - 3.6 m/s wind class. One noticible difference is that a higher percentage of wind is distributed in the higher wind classes for the slope measurements than for the interdune measurements. This is to be expected since wind flowing up the dune slope accelerates all the way to the crest.
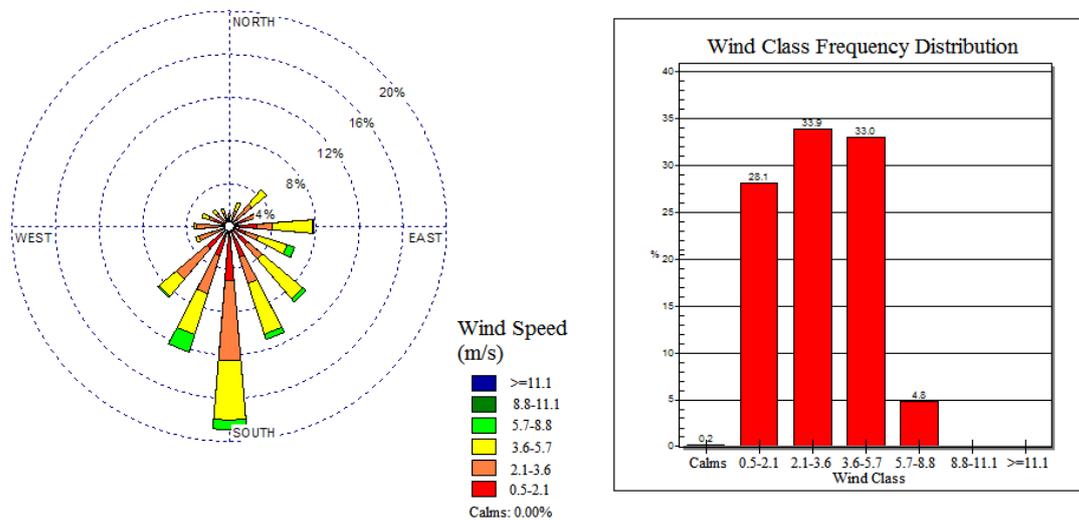
Figure 62: Wind data for mast positioned on the dune slope

The wind data for the measurement near the crest is displayed in Figure 63. For this period the wind is highly concentrated around the south direction (34 %). The other two most dominant wind directions are south-south-east (9 %) and south-south-west (10.1 %). The wind class frequency distribution shows a normal distribution this time around the 3.6-5.7 m/s wind class. The wind class frequency distribution again shows a larger percentage wind in the higher wind classes than the interdune and the slope measurements. This further confirms the expected behaviour that wind accelerates up the slope all the way to the crest.

98
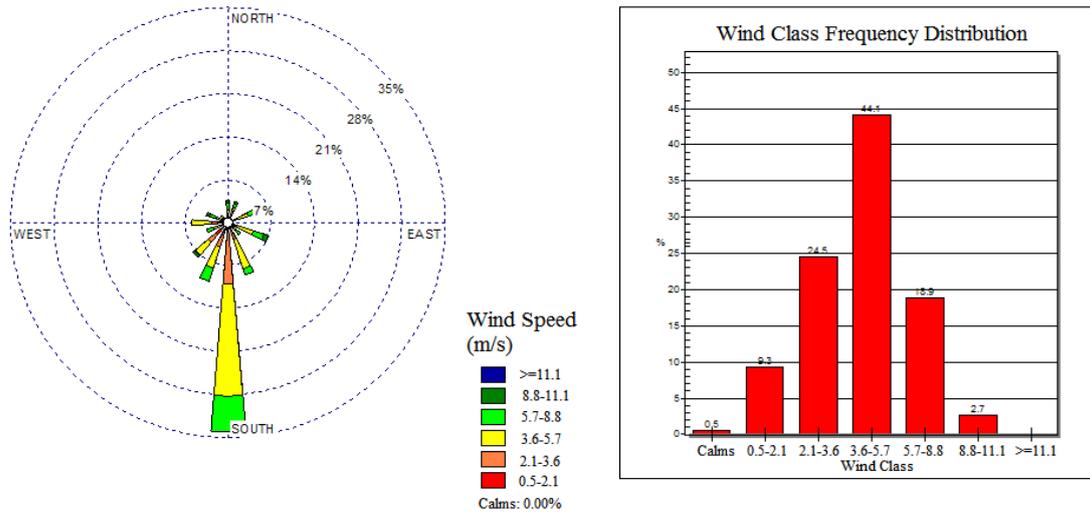
Figure 63: Wind data for crest

Another aspect that could be noticed is the frequency of calm wind speed that was recorded in the different locations. The interdune showed no calm wind periods, the slope showed 0.2 % calm wind periods and the crest showed 0.5 % calm wind periods. These calm periods might be related to recirculation flow that would be more present near the crest and steady flow that would be more present near the interdune area.

Considering the different frequency distributions for the sensors on the mast reveals some interesting information. In Figure 64 the different wind class frequency distributions for the interdune position are displayed.

Comparing the distributions it can be noticed that the higher positioned sensors have a larger percentage wind in the higher velocity classes. This makes sense since higher velocities are expected the higher one goes in the atmosphere. Furthermore, it can be seen that the sensors located higher on the mast have a greater spread among the velocity classes. This indicates a greater range of velocities and therefore more fluctuation in the wind for the higher sensors than for the lower sensors. This may be due to damping effect of plants and terrain on the wind measured by the sensors located lower on the mast.
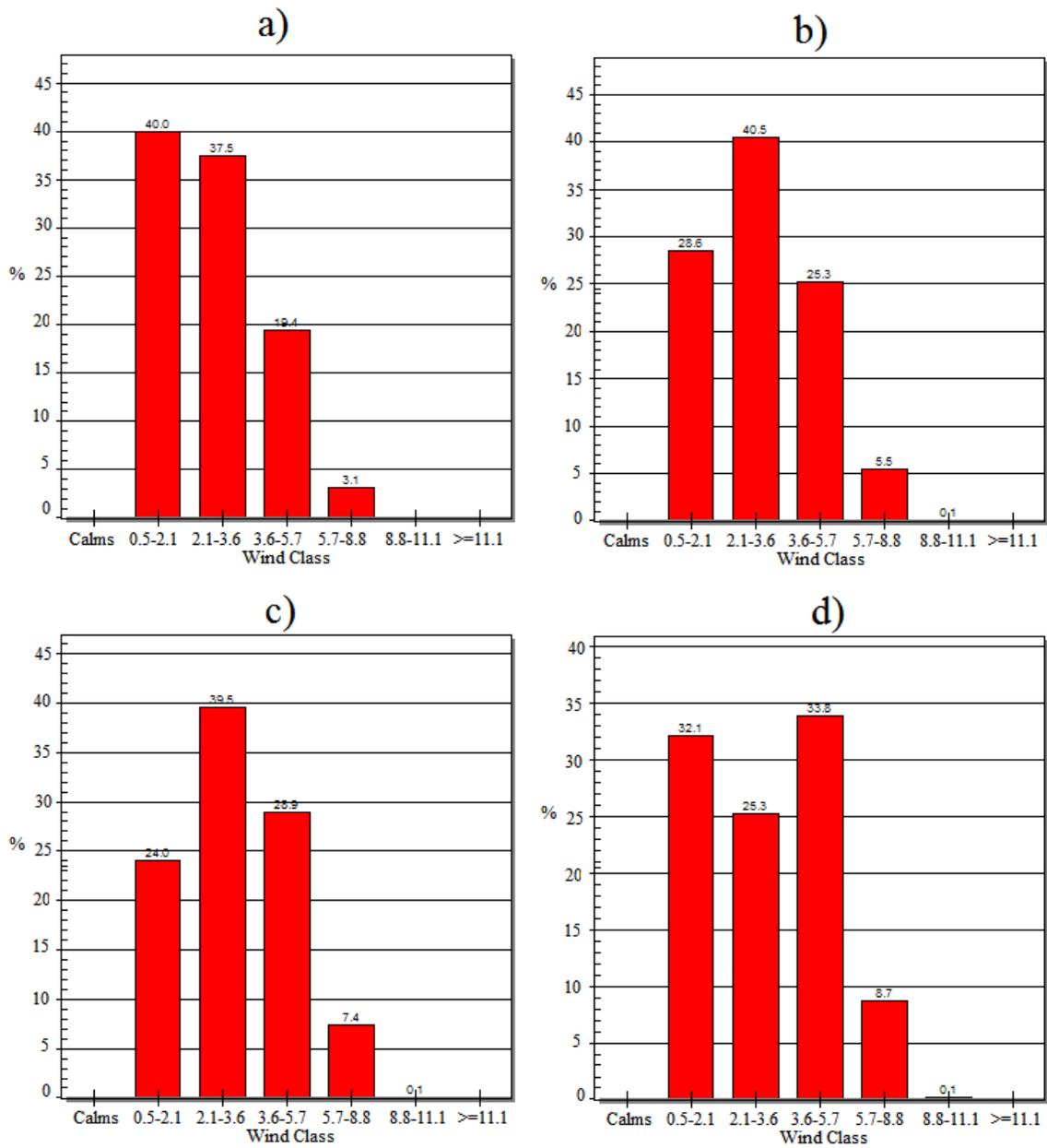
Figure 64: Wind class frequency distributions for different sensors on the mast: a) 2.5 m, b) 5 m, c) 7.5 m and d) 10 m above ground

APPENDIX I: Additional Two-dimensional Simulation Data

Table 13: Mesh statistics for steady state two-dimensional simulations

Total cells	581926
Total boundaries	6
Hexahedral	438693
Prism	0
Wedges	0
Pyramids	0
Tet-wedges	0
Tetrahedral	0
Polyhedral	143233
Max non-orthogonality	69.950
Average non-orthogonality	24.937
Max skewness	0.767
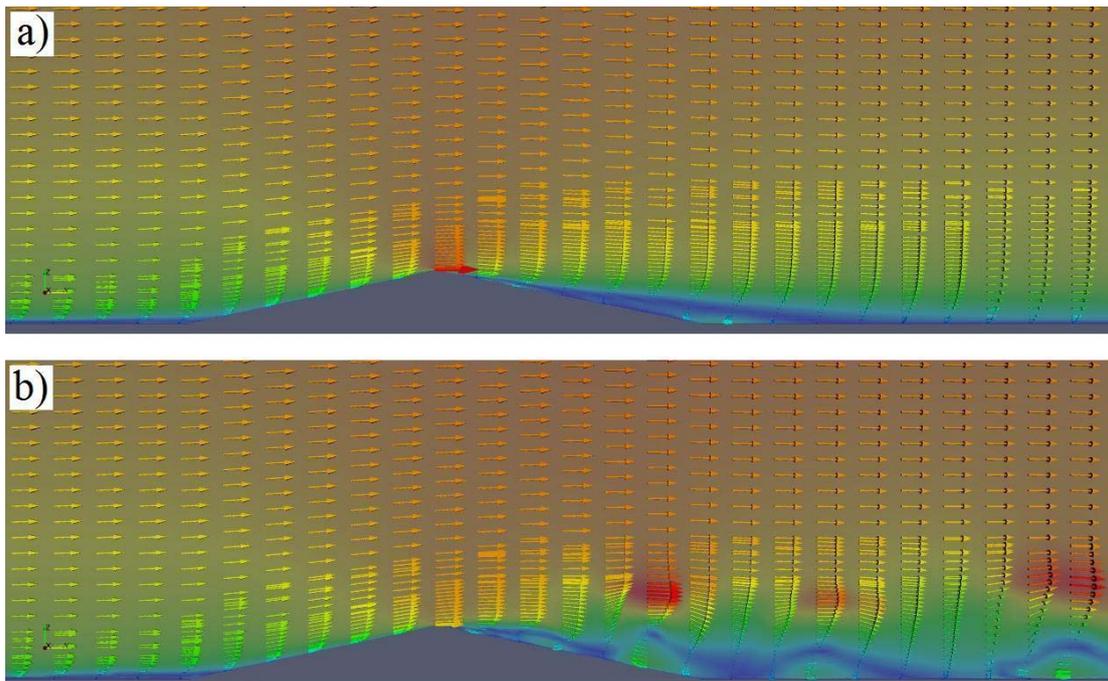
Figure 65: Velocity vector differecing scheme comparison: a) first order differencing and b) second order differencing

In Figure 66 the pressure field within the recirculation region can be seen. It is clear how the low pressure regions correspond to the separation point as well centres of vortex structures. On the other hand, high pressure regions match up with the areas between vortex structures where the outer perimeters collide. The low pressure at the centre of vortex structures relates to the outward pull of air due to inertial forces on air particles as a result of the rolling motion of the vortex structures. A stable vortex is therefore formed when the outward pull of the centrifugal forces are in equilibrium with the inward pull of the low pressure zone. Since local low pressure zones indicate the presence of vortex structures, it is possible to use pressure as a crude tool to locate vortex structures in the flow. However, it can also be seen that although the low pressure regions correspond to the general position (or presence) of a vortex in the region, they do not match up exactly. It is therefore not possible to identify the structure of a vortex clearly using the pressure method but rather to simply identify the presence or position of a vortex.
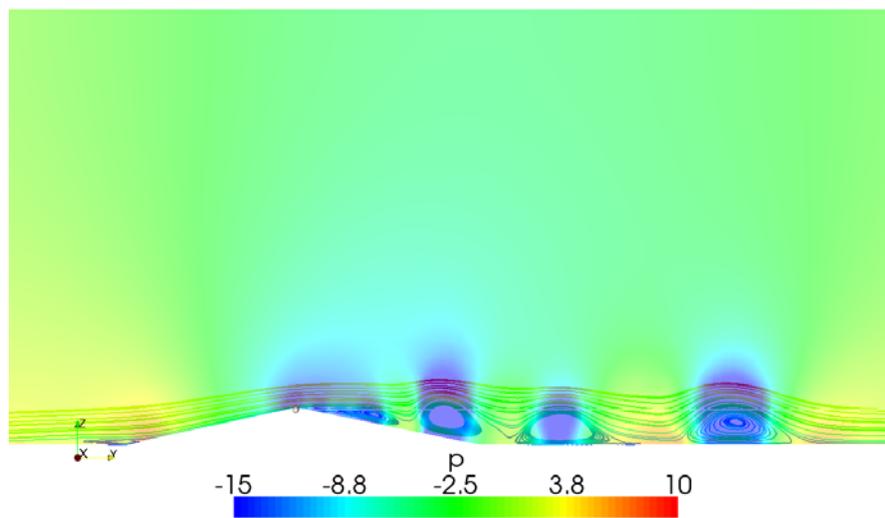

Figure 66: Pressure zones compared to recirculations zones of flow over a simple two-dimensional dune geometry

102

APPENDIX J: Additional Steady State Three-dimensional Simulation Data

Table 14: Mesh statistics for steady state three-dimensional simulations for the actual dune geometry

Total cells	7321854
Total boundaries	6
Hexahedral	6916109
Prism	16247
Wedges	0
Pyramids	0
Tet-wedges	29
Tetrahedral	0
Polyhedral	389469
Max non-orthogonality	64.174
Average non-orthogonality	7.530
Max skewness	1.007

Table 15: Discretization schemes for different terms for the RANS simulations as used in OpenFOAM case setup of fvSchemes library

| ddtSchemes	default	steadyState
gradSchemes	grad(p)	Gauss linear
	grad(U)	Gauss linear
divSchemes	div(phi,U)	Gauss Gamma 0.9
	div(phi,k)	Gauss Gamma 0.9
	div(phi,epsilon)	Gauss Gamma 0.9
	div(phi,R)	Gauss Gamma 0.9
	div(R)	Gauss Gamma 0.9
	div(phi,nuTilda)	Gauss Gamma 0.9
	div((nuEff*dev(grad(U).T())))	Gauss linear
laplacianSchemes	laplacian(nuEff,U)	Gauss linear corrected
	laplacian((1|A(U)),p)	Gauss linear corrected
	laplacian(DkEff,k)	Gauss linear corrected
	laplacian(DepsilonEff,epsilon)	Gauss linear corrected
	laplacian(DREff,R)	Gauss linear corrected
	laplacian(DnuTildaEff,nuTilda)	Gauss linear corrected
	laplacian(1,p)	Gauss linear corrected
interpolationSchemes	interpolate(U)	linear
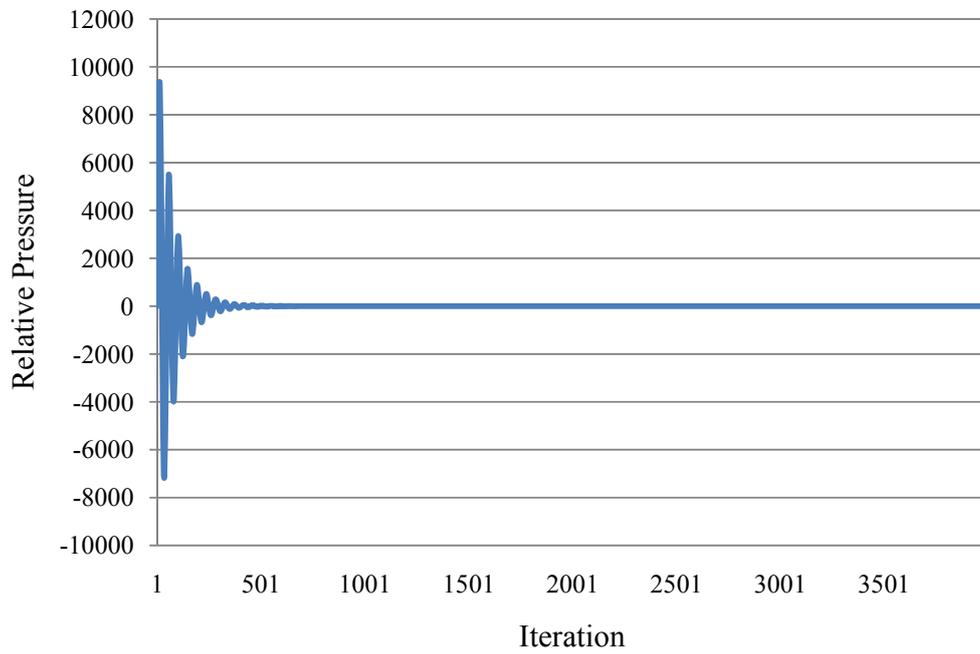
Figure 67: Relative pressure at monitoring point approximately 100 m before dune on windward side
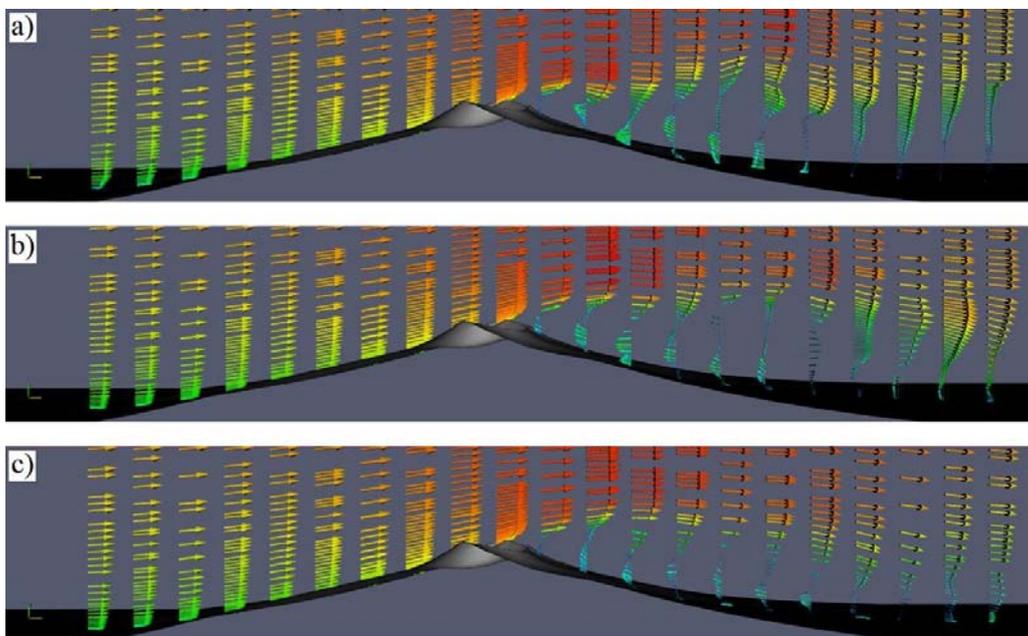

Figure 68: Grid independance velocity vectors flow results: a) fine, b) medium and c) coarse mesh

104
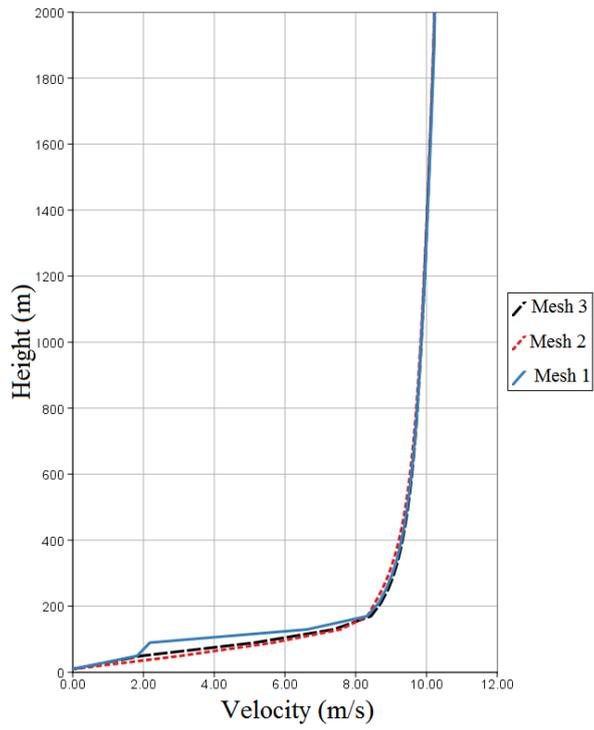
Figure 69: Velocity profile on lee-side of dune including the refinement

105
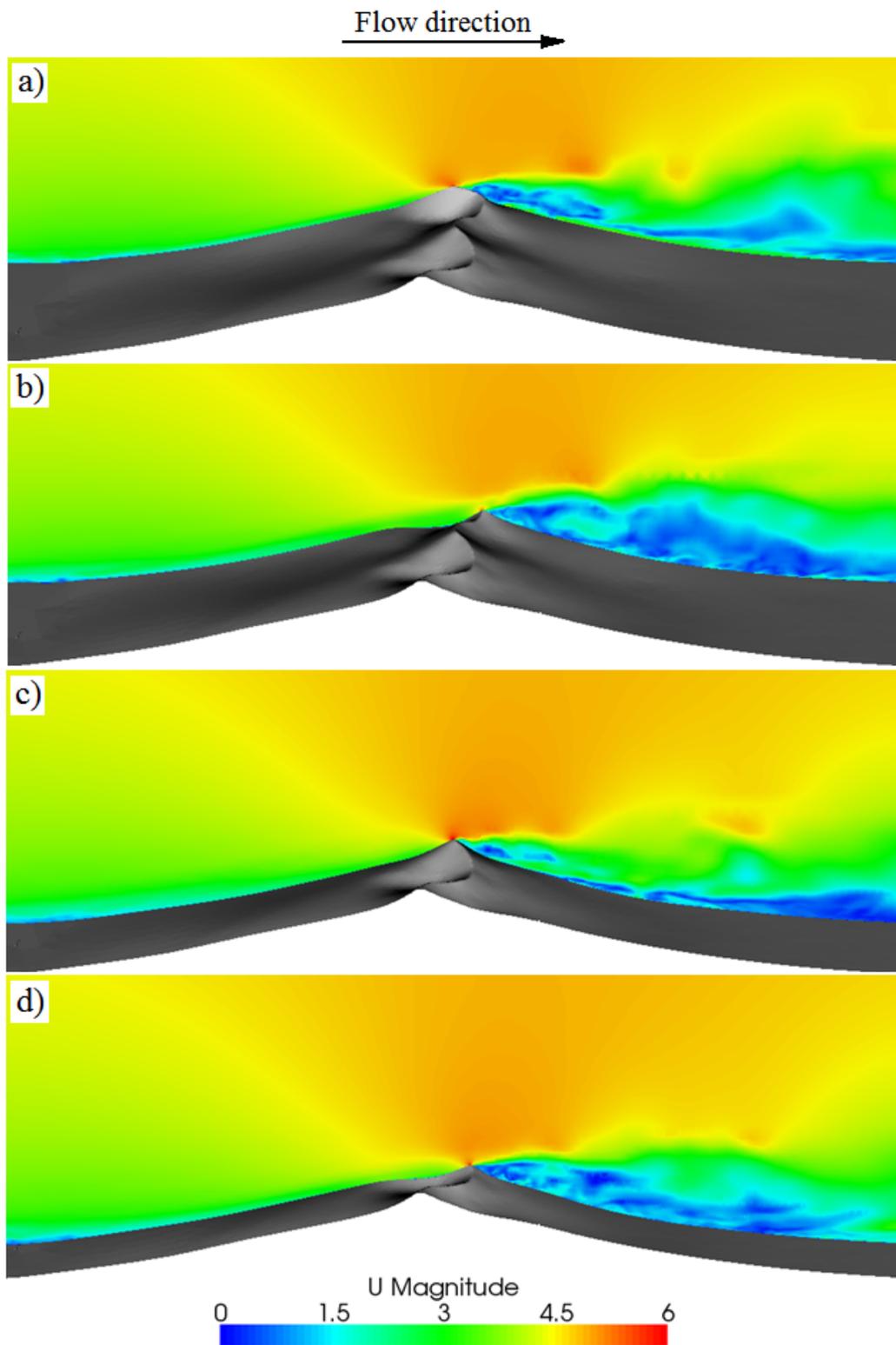
Figure 70: Velocity magnitude distribution for different cross sections

106

APPENDIX K: Additional Transient Three-dimensional Simulation Results

Table 16: Mesh statistics for transient three-dimensional simulations for the actual dune geometry

Total cells	7272639
Total boundaries	6
Hexahedral	6802258
Prism	16246
Wedges	0
Pyramids	0
Tet-wedges	29
Tetrahedral	0
Polyhedral	454106
Max non-orthogonality	63.509
Average non-orthogonality	7.859
Max skewness	1.017

Table 17: Discretization schemes for different terms for the LES simulations as used in OpenFOAM case setup of fvSchemes library

|		
ddtSchemes	default	backward
gradSchemes	grad(p)	Gauss linear
	grad(U)	Gauss linear
divSchemes	div(phi,U)	Gauss linear
	div(phi,k)	Gauss limitedLinear 1
	div(phi,B)	Gauss limitedLinear 1
	div(phi,nuTilda)	Gauss limitedLinear 1
	div(B)	Gauss linear
	div((nuEff*dev(grad(U).T())))	Gauss linear
laplacianSchemes	laplacian(nuEff,U)	Gauss linear corrected
	laplacian((1|A(U)),p)	Gauss linear corrected
	laplacian(DkEff,k)	Gauss linear corrected
	laplacian(DBEff,B)	Gauss linear corrected
	laplacian(DnuTildaEff,nuTilda)	Gauss linear corrected
interpolationSchemes	interpolate(U)	linear
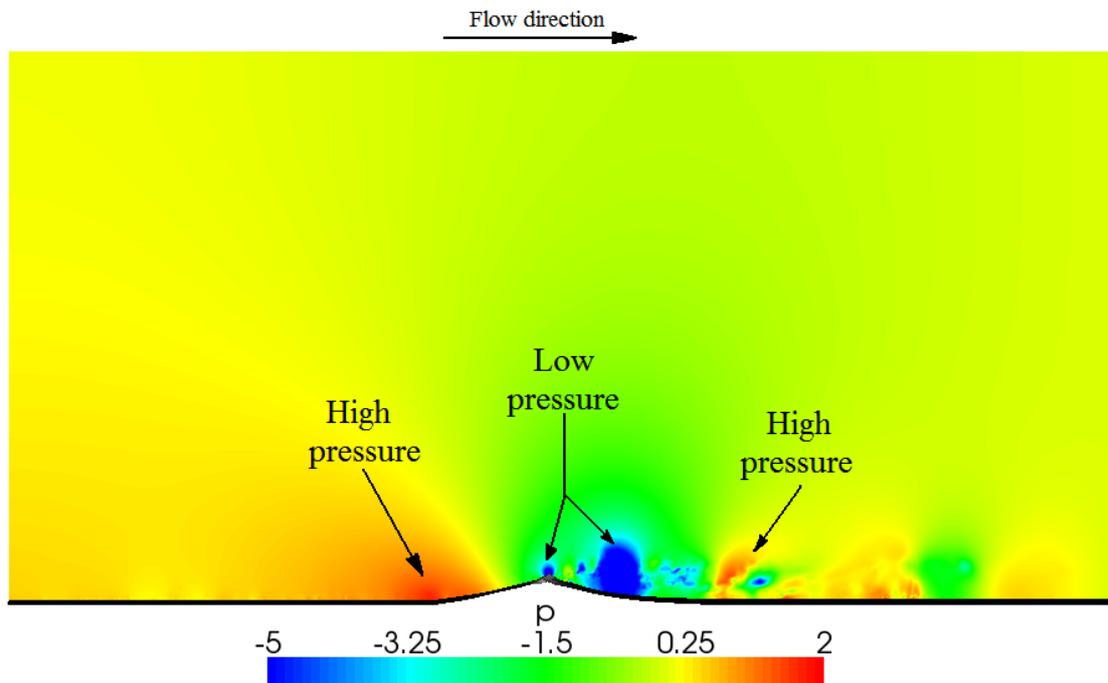
Figure 71: Pressure distribution for time dependant simulation results at time 50 seconds
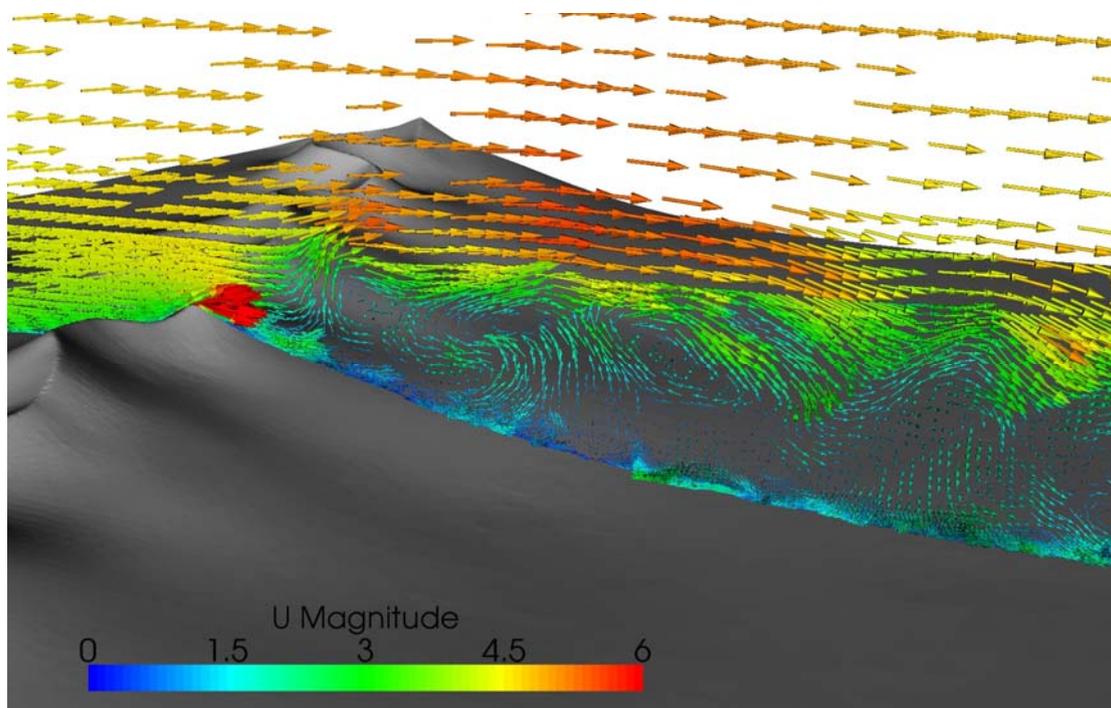

Figure 72: Velocity vector results for one time instant in transient simulations results
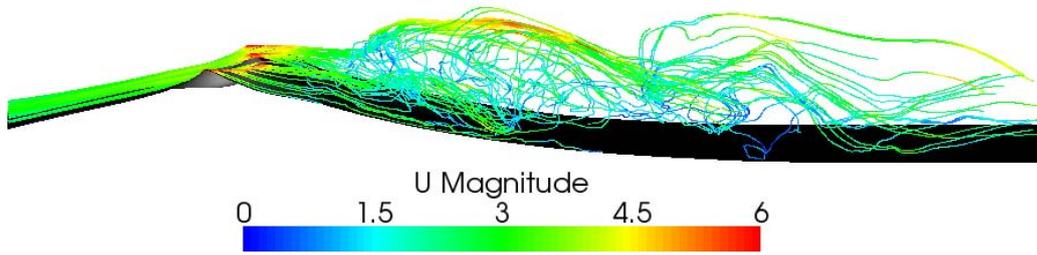
Figure 73: Streamline flow results of time dependant flow over actual three-dimensional dune geometry at time 50 seconds
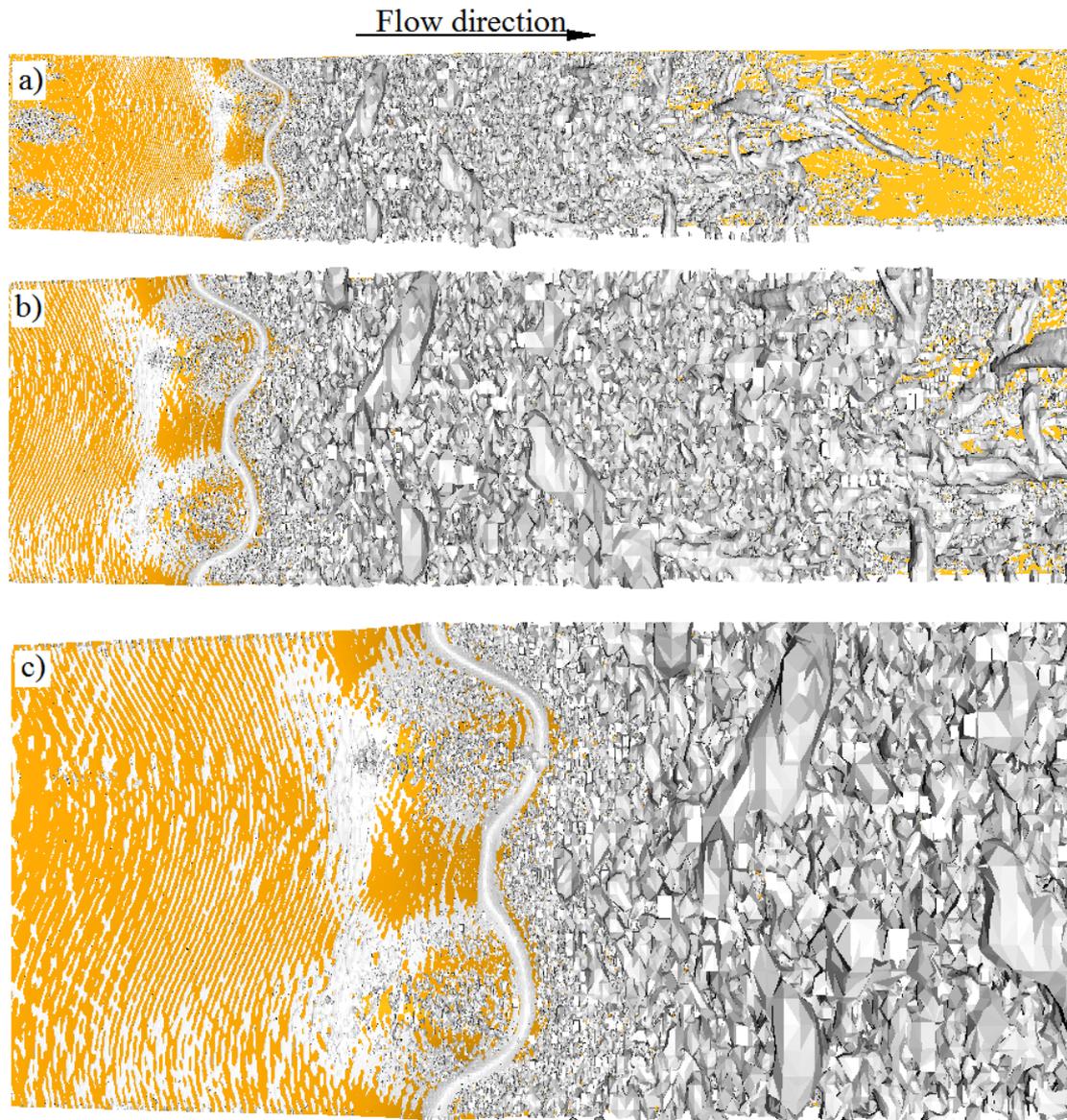
Figure 74: Second invariant of velocity gradient tensor (Q=0.0005) close up view of crest and recirculation region: a) far, b) medium and c) close-up view
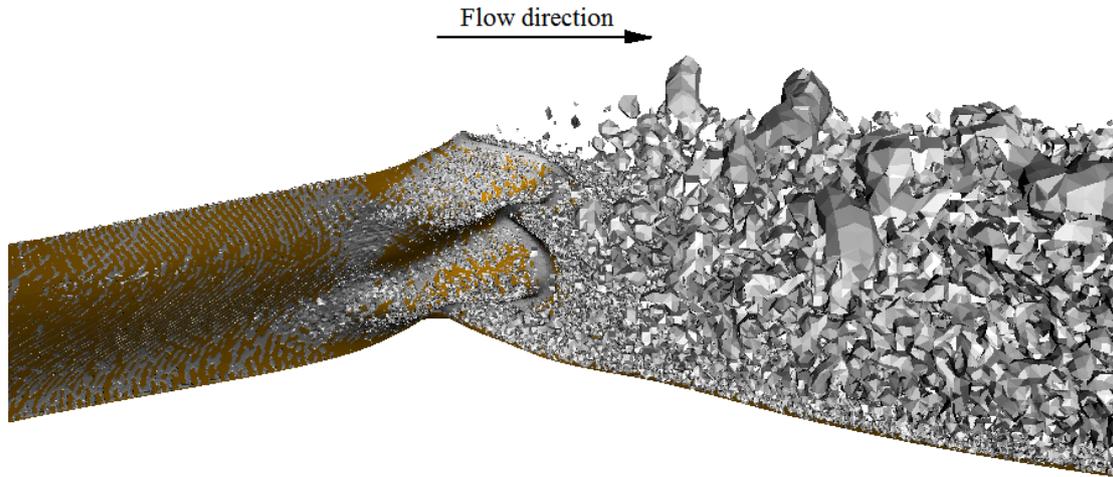
Figure 75: Second invariant of velocity gradient tensor (Q=0.0005) showing vortex shedding in recirculation zone

APPENDIX L: Additional Particle Simulation Results
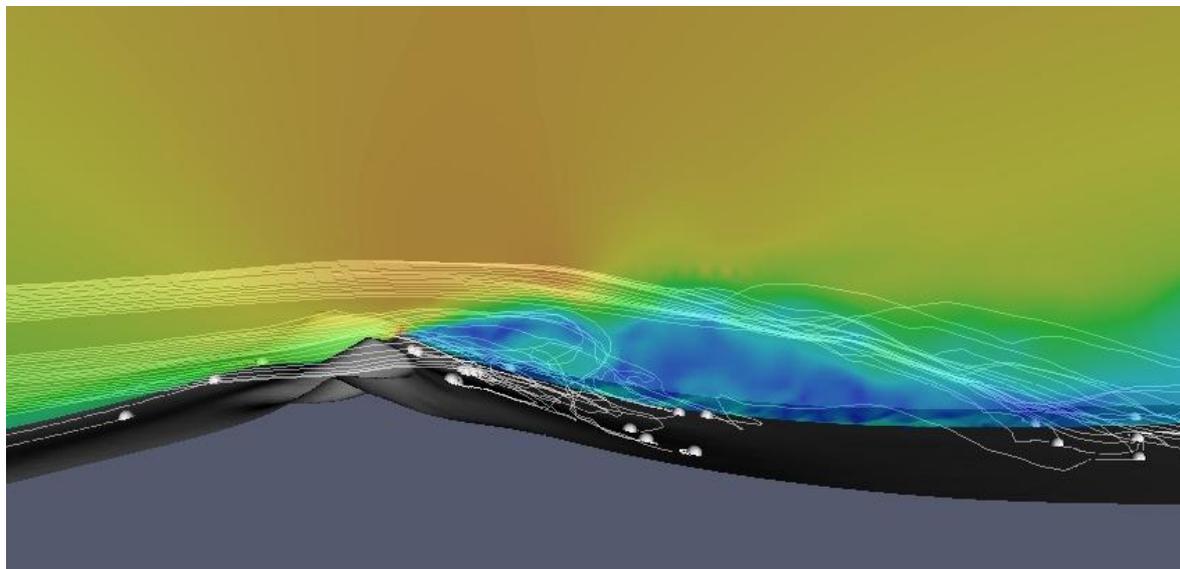

Figure 76: Close up view of recirculation zone
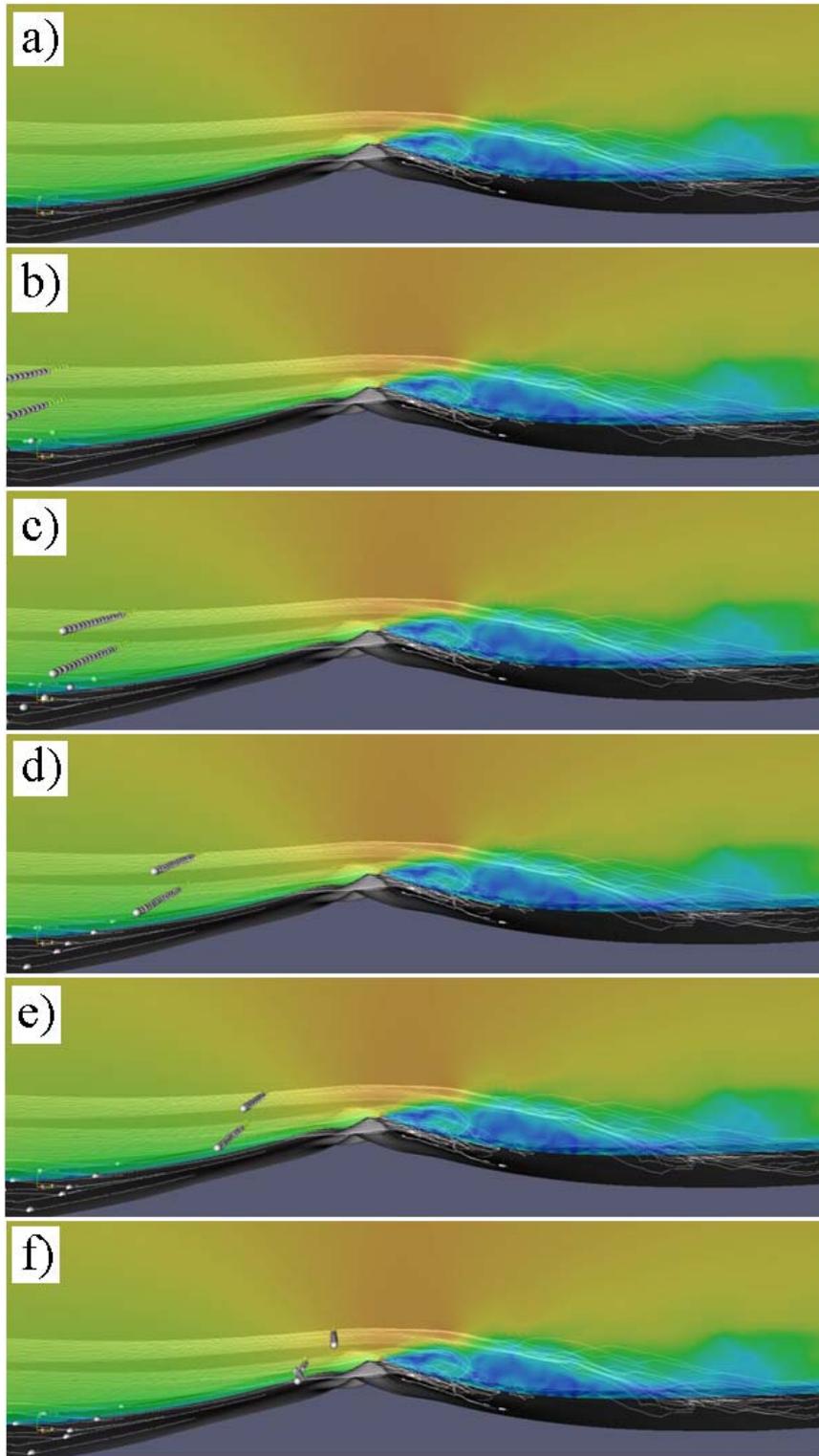
Figure 77: Transient particle flow time sequence (part 1)
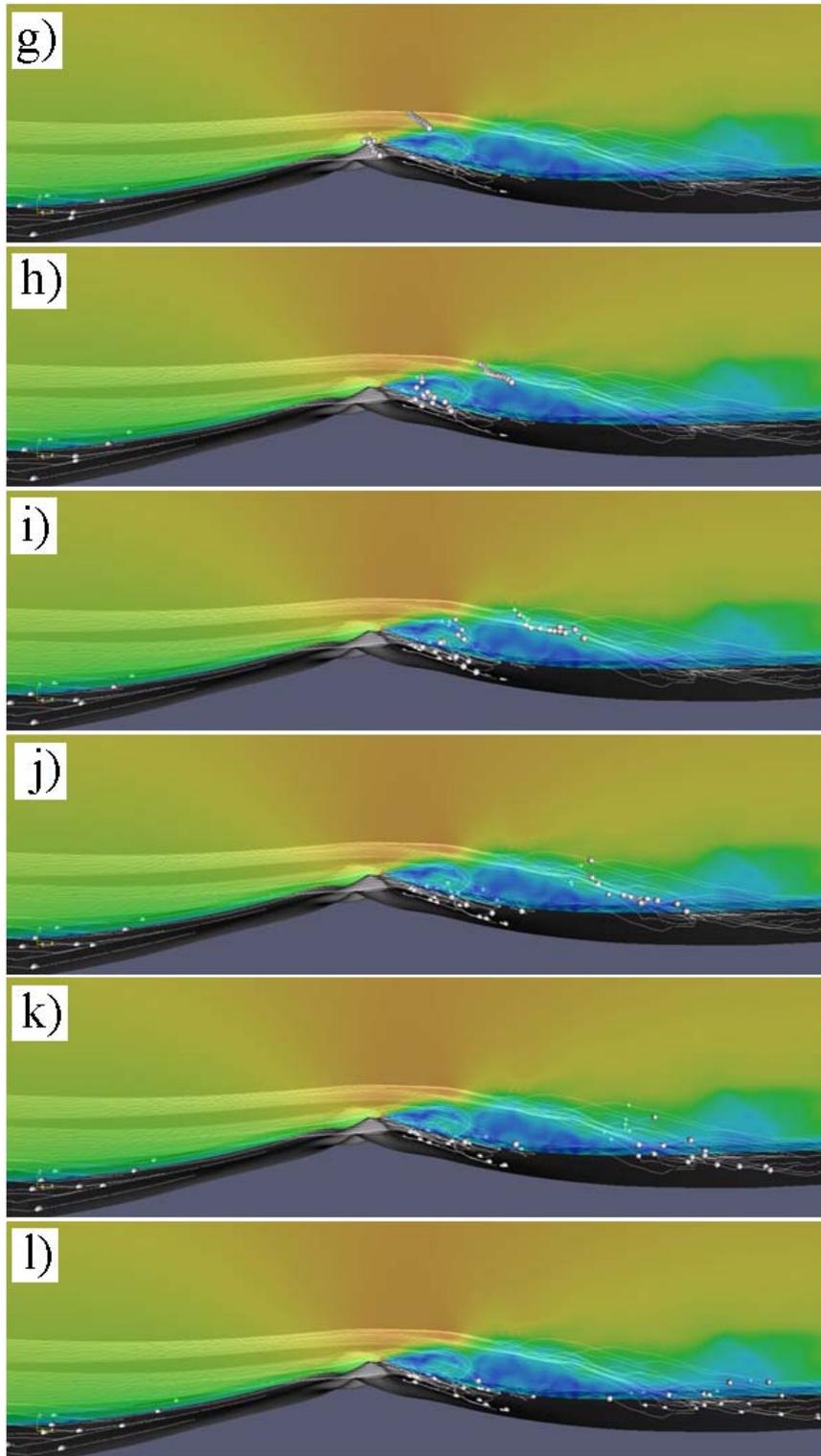
Figure 78: Transient particle flow time sequence (part 2)

APPENDIX M: Additional Parallel Performance Results

Table 18: Parallel performance parameters

Cores	Max cells per core	Sim time	Speedup
1	518926	7626.75	1
2	259463	7251.35	1.05
4	129732	5386.32	1.41
6	86488	2772.64	2.75
8	64866	1379.07	5.53
10	51893	1210.17	6.30
12	43244	1104.13	6.91
14	37066	994.16	8.08
16	32433	814.23	9.37
18	28829	668.97	11.40
20	25946	2001.34	3.81
22	23588	3810.74	2.00
24	21622	1278.08	5.97

APPENDIX N: Additional Photos of The Namib Desert

Figure 79: Namib linear dunes (looking west)

Figure 80: Namib linear dune

Figure 81: Mole's End dune

Figure 82: Dune field (looking south-west)

117

Figure 83: Linear dune (looking south)

Figure 84: Author with differential GPS

Figure 85: Linear dune end

Figure 86: Parallel linear dunes (looking west)

Figure 87: Ripples on linear dunes

Figure 88: Parallel linear dunes (looking south)